Spectral Study of Twenty-Three Type Ia Supernovae Using Principal Component Analysis

Alexander Erling Gude

ABSTRACT

We explore the diversity of type Ia supernovae near maximum light in the B band. We use a principal component analysis on twenty-three well observed type Ia supernovae in order to find a compact, numeric description for diversity. We find that the first component – which mainly controls color – accounts for 76% of diversity in the sample, and that by using only five eigenvectors we can account for 95.8% of diversity. We explore color diversity and find that very few of the supernovae follow a Cardelli Law for $E(B-V)$. We use the weights calculated for each of the supernovae to devise a method to lower despersion of type Ia supernovae around the Hubble line using only a single spectrum for each supernova, removing the need for multiband light curves.

1. Introduction

In the past ten years observations of type Ia supernovae have pointed to a universe that is not only expanding but accelerating (Riess et al. 1998; Perlmutter et al. 1999). Dark energy has been proposed as the cause, but very little is known about its exact form. Type Ia supernovae have been leading the study of dark energy since its discovery. Recent programs have yielded large data sets of spectra and light curves out to $z > 1$, and future programs will bring in even more data. As the total amount of data increase, programs are starting to become limited more by systematic errors than statistical error. We explore methods of reducing these errors using principal component analysis (PCA).

We perform a PCA on twenty-three high quality supernova spectra, twenty-one of which are backed by five band light curves, to come up with an empirical description of the variation of type Ia supernova spectra near maximum. PCA is the ideal tool to use for this analysis because it will allow a quantitative classification of supernovae and it will allow correlations to be found between spectral features. PCA will also allow quick analysis of large data sets, making it an excellent tool to prepare for future surveys.

2. Supernovae Cosmology

2.1. A History of Type Ia Supernovae as Standard Candles

Type I supernovae have been used as distance indicators for over forty years. They were first used by Kowal (1968) when he published a type I supernova Hubble diagram. Originally a type I supernova was defined as any supernova with a lack of hydrogen in their optical spectra (Minkowski 1941). It has since become clear that type I supernovae can actually be subdivided into two distinct classes: type Ib/c which are generated by massive stats that undergo a core collapse and type Ia which it is theorized are thermonuclear explosions of white dwarfs.

By the late 1980s it was becoming clear that most type Ia supernovae had similar spectral time series, light curves, and absolute magnitudes at maximum light. In 1992 a review by Branch & Tammann concluded that type Ia SNe were "the best standard candles known so far", with a dispersion in maximum B and V band magnitudes that was < 0.25 mag and likely even smaller.

The quality of data continued to improve over the next few years. The Calan/Tololo Supernova Search (CTSS) in 1990 obtained a set of high quality light curves and spectra of supernovae in the range $z = 0.01 - 0.1$ which allowed them to compare peak magnitudes while calculating their relative distance through their Hubble velocities (Hamuy et al. 1993). The search was difficult because as the appearance of a supernova is unpredictable, the team was unable to schedule follow up observations until after a supernova was found. Despite the challenges, CTSS was able to acquire thirty new type Ia light curves (Hamuy et al. 1995).

With the wealth of new data, several methods were devised to select the most easily calibrated type Ia supernovae from a set. Vaughan et al. (1995) developed $B-V$ color cuts that selected type Ia supernovae that had an observed dispersion of less than 0.25 mag. Phillips (1993) discovered a relation between absolute magnitude and $\Delta m_{15}(B)$, the amount the supernova decreased in brightness in the B-band over a 15 day period following maximum light.

Based on the success of the $\Delta m_{15}(B)$ parameter, Riess et al. (1996a) developed the multi-color light curve shape method (MLCS). This method parametrized light curves as a function of their absolute magnitude at maximum and fit for all colors simultaneously. By fitting all colors at once the MLCS method allowed color excess, $E(B-V)$ to be calculated. Traditionally this excess has been attributed to intervening dust which reddens the supernova, and so has been used to correct for extinction (Riess et al. 1996b).

Perlmutter et al. (1997 and 1999) developed their own method of parameterizing the B and V bands of a light curve. Using a stretch factor, a measure of the amount a canonical light curve needs to be stretched in time to match the observed light curve, they were able to more simply represent a light curve.

Type Ia supernovae can be used as standard candles because although they are not of a perfectly uniform luminosity, the above methods can be used to to calibrate them (Perlmutter

& Schmidt 2003). Further there are indications that there exists tight correlations between the spectral features of specific supernovae and their peak luminosity that should allow even more accurate calibration. It is already known that the ratio of the Si II feature at λ5750 to the feature at λ6150 increases with decreasing luminosity (Nugent et al. 1995). Likewise, the ratio of the two peaks on either side of Ca II H&K absorption share a similar relationship (Filippenko 1997).

3. Spectra of Type Ia Supernovae

Optical spectra are the means through which supernovae are classified (Branch et al. 2001). Type Ia spectra are characterized by a deep absorption feature near 6150 Å produced by blue shifted Si II λ6347, λ6371. The early spectrum exhibits broad features from lines of neutral and singly ionized intermediate-mass elements including O, Mg, Si, S, and Ca. There is some contribution from iron-peak elements, primarily Fe and Co near UV wavelengths. At this point the strongest features are those that arise from SI II λ6355 and Ca II H&K λ3934 and λ3968. As the spectrum evolves in time Fe II lines becomes prominent, and the evolution slows down.

The spectra of type Ia supernovae are rather homogeneous if compared at the same phase and can be used to estimate time of max if compared with spectral templates (Filippenko 1997). There are however differences in the spectra of type Ia supernovae. Line depths vary between different supernovae as does the velocity of ejecta.

One class of peculiar supernovae are the SN1991T-like supernovae. These supernovae are overly luminescent and bluer in B-V color than normal type Ia supernovae. They prominently feature a high excitation Fe III feature near maximum, with the characteristic type Ia features developing after maximum. These species of type Ia do not exhibit Si II or Ca II absorption lines in their early spectra.

A second peculiar class of supernovae are the SN1991bg-like supernovae. These supernovae are characteristically sub-luminous in V and B, and are particularly red in B-V color. After maximum they decline more quickly then the typical type Ia (Filippenko et al. 1992). These supernovae have a deep absorption feature at λ4200 from Ti II.

4. Principal Component Analysis

PCA is a mathematical technique to reduce sets of data to lower dimensions for analysis that was first described by Person (1901). PCA has proven effective in classifying quasar spectra (Suzuki 2005; Suzuki et al. 2005) and so we believe it will be similarly useful in analyzing type Ia spectra.

4.1. The PCA Formulation

A supernova spectrum is expressed as $\vec{s_i}(\lambda)$. We claim that this spectrum can be well represented by a reconstructed spectrum $\vec{r_i}(\lambda)$ which is the sum of the mean spectrum and m weighted principal component spectra as follows:

$$\vec{s_i}(\lambda) \approx \vec{r_{i,m}}(\lambda) = \vec{\mu}(\lambda) + \sum_{j=1}^{m} c_{ij}\vec{\xi_j}(\lambda)$$

where i refers to a particular supernova, $\vec{\mu}(\lambda)$ is the mean spectrum, $\vec{\xi_j}(\lambda)$ is the jth principal component spectrum (PCS), and c_{ij} is the real weight.

4.2. The Principal Component Spectrum

To find the principal component spectrum (PCS) we need to calculate the correlation of the fluxes at each wavelength in order to see how different parts of the spectrum are related. We compute a correlations matrix with elements:

$$\mathbf{R}(\lambda_m, \lambda_n) = \frac{1}{N-1}\sum_{i=1}^{N}\frac{[\vec{s_i}(\lambda_m) - \vec{\mu}(\lambda_m)][\vec{s_i}(\lambda_n) - \vec{\mu}(\lambda_n)]}{\sigma(\lambda_m)\sigma(\lambda_n)}$$

where N is the total number of spectra used in the analysis, σ_m and σ_n are the standard deviation of the flux in the wavelength bins corresponding to λ_m and λ_n respectively.

We then calculate the covariance matrix with elements:

$$\mathbf{V}(\lambda_m, \lambda_n) = \frac{1}{N-1}\sum_{i=1}^{N}[\vec{s_i}(\lambda_m) - \vec{\mu}(\lambda_m)][\vec{s_i}(\lambda_n) - \vec{\mu}(\lambda_n)]$$

We can then find the principal components by decomposing the covariance matrix $\mathbf{V}$ into the product of the orthonormal matrix $\mathbf{P}$ which consists of our eigenvectors, and the diagonal matrix $\mathbf{\Lambda}$ which contains the eigenvalues:

$$\mathbf{V} = \mathbf{P}^{-1}\mathbf{\Lambda}\mathbf{P}$$

The columns of $\mathbf{P}$ are our principal components. We order them by the amount of variance in the data set they are able to accommodate so that our first component accounts for the largest amount of variance.

4.3. Reconstructing Spectra

Once we have calculated our set of PCS we can reconstruct a given supernova spectrum $\vec{s}_i(\lambda)$. We must first calculate the weight c_{ij} for each of the jth as follows:

$$c_{ij} = (\vec{s}_i - \vec{\mu}) \cdot \vec{\xi}_j$$

We will later use normalized weights in our analysis, which are defined as:

$$c_{ij} = \lambda_i \sigma_{ij}$$

where λ_i is the standard deviation calculated for the weights of eigenvector i.

If we use m components then we can define the accumulated residual variance fraction as:

$$f_j = \frac{\sum_i^n \sum_j^m c_{ij}^2}{\sum_i^n \sum_j^N c_{ij}^2}$$

This quantity measures the importance of each eigenvector. It returns a number which is the percent of variation accounted for by simply adjusting the value of that eigenvector.

5. Data

For our analysis we used a data set consisting of twenty-three type Ia supernova spectra (Matheson et al. 2008; Nugent et al. 2002; Gomez et al. 1996), twenty-one of which have multicolor light curves (Jha et al. 2006; Riess et al. 2005).

With the exception of SN1991T and SN1991bg, all of the spectra come from Matheson et al.. The spectra provided by Matheson et al. were precessed in a uniform manner and were reduced before being released. With the exception of SN1991T and SN1991bg, for which we do not use light curves, and SN1998aq, whose light curve which comes from Riess et al. (2005), all of the light curves come from Jha et al. (2006). Jha et al. calibrated their photometry against standard stars in the field and then converted their filters to a standard system. The light curve for SN1998aq was processed in a similar manner to those taken by Jha et al..

5.1. SN1991T and SN1991bg Data

SN1991T and SN1991bg are peculiar supernovae. Their data were taken well before the other supernovae in the sample and so they were not taken with the above listed sources. SN1991T is

Table 1. Supernova Summary

Supernova	RA	DEC	Z	Z_{CMB}	MWEBV	Host Galaxy	Host Type
SN1991T	12:34:10.2	+02:39:56.0	0.0069	0.0058	0.095	NGC4527	SAB(s)bc
SN1991bg	02:25:03.7	+12:52:16.0	0.0035	0.0046	0.176	NGC4374	E1
SN1997dt	23:00:02.97	+15:58:50.4	0.0073	0.0061	0.057	NGC7448	Sbc
SN1998aq	11:56:25.87	+55:07:43.20	0.0037	0.0043	0.014	NGC3982	SAB(r)b
SN1998bp	17:54:50.73	+18:19:50.2	0.0104	0.0102	0.076	NGC6495	E
SN1998de	00:48:06.88	+27:37:29.9	0.0166	0.0156	0.057	NGC252	S0
SN1998dh	23:14:40.31	+04:32:13.4	0.0089	0.0077	0.068	NGC7541	Sbc
SN1998ec	06:53:06.10	+50:02:22.8	0.0199	0.0201	0.085	UGC3576	Sb
SN1998eg	22:39:30.34	+08:36:20.8	0.0248	0.0235	0.123	UGC12133	Sc
SN1998es	01:37:17.52	+05:52:50.2	0.0106	0.0096	0.032	NGC632	S0
SN1998V	18:22:37.40	+15:42:08.0	0.0176	0.0172	0.196	NGC6627	Sb
SN1999aa	08:27:42.15	+21:29:15.6	0.0144	0.0153	0.040	NGC2595	Sc
SN1999ac	16:07:15.05	+07:58:20.1	0.0095	0.0098	0.046	NGC6063	Scd
SN1999cc	16:02:42.04	+37:21:33.7	0.0313	0.0315	0.023	NGC6038	Sc
SN1999cl	12:31:56.03	+14:25:35.1	0.0076	0.0087	0.038	NGC4501(M88)	Sb
SN1999dq	02:33:59.71	+20:58:30.2	0.0143	0.0135	0.110	NGC976	Sc
SN1999ej	01:22:57.38	+33:27:57.4	0.0137	0.0128	0.071	NGC495	S0/Sa
SN1999gd	08:38:24.57	+25:45:33.8	0.0185	0.0193	0.041	NGC2623	N/A
SN1999gp	02:31:39.08	+39:22:52.4	0.0267	0.0260	0.056	UGC1993	Sb
SN2000cf	15:52:56.33	+65:56:13.2	0.0364	0.0365	0.032	MCG+11-19-25	N/A
SN2000cx	01:24:46.15	+09:30:31.1	0.0079	0.0069	0.082	NGC524	S0
SN2000dk	01:07:23.53	+32:24:23.4	0.0174	0.0165	0.070	NGC382	E
SN2000fa	07:15:29.87	+23:25:42.4	0.0213	0.0218	0.069	UGC3770	Sd/Irr

Table 2. Spectra summary

Supernova	MJD	Date	Phase	λ_{min}	λ_{max}	$d\lambda$
SN1991T*	48374.000	1991-04-28.00	0	1000.000	25000.00	10.00
SN1991bg**	48604.000	1991-12-14.00	1	3205.38	9062.79	0.63
SN1997dt	50788.090	1997-12-06.99	3	3720.00	7540.50	1.50
SN1998V	50891.500	1998-03-19.50	0.5	3720.00	7509.00	1.50
SN1998aq	50931.250	1998-04-28.25	1	3720.00	7510.50	1.50
SN1998bp	50936.441	1998-05-03.44	0.5	3720.00	7515.00	1.50
SN1998de	51026.398	1998-08-01.40	0	3720.00	7540.50	1.50
SN1998dh	51029.352	1998-08-04.34	0	3720.00	7540.50	1.50
SN1998ec	51086.488	1998-09-30.49	-1.5	3720.00	7521.00	1.50
SN1998eg	51110.141	1998-10-24.13	0	3720.00	7461.00	1.50
SN1998es	51142.211	1998-11-25.20	1	3460.00	7319.50	1.50
SN1999aa	51232.238	1999-02-23.24	1	3720.00	7540.50	1.50
SN1999ac	51249.520	1999-03-12.52	-0.5	3720.00	7540.50	1.50
SN1999cc	51315.391	1999-05-17.39	0.5	3720.00	7540.50	1.50
SN1999cl	51341.160	1999-06-12.16	-0.5	3527.50	7154.50	1.50
SN1999dq	51436.441	1999-09-15.43	1	3720.00	7540.50	1.50
SN1999ej	51481.262	1999-10-30.26	-0.5	3720.00	7540.50	1.50
SN1999gd	51520.512	1999-12-08.50	2.5	3720.00	7540.50	1.50
SN1999gp	51550.121	2000-01-07.12	0.5	3720.00	7540.50	1.50
SN2000cf	51675.340	2000-05-11.34	3	3720.00	7549.50	1.50
SN2000cx	51751.480	2000-07-26.48	0	3720.00	7540.50	1.50
SN2000dk	51813.371	2000-09-26.36	1.5	3720.00	7540.50	1.50
SN2000fa	51893.359	2000-12-15.35	1.5	3680.00	7541.00	1.50

Note. — * are spectra from Nugent et al. (2002). ** are spectra from Gomez et al. (1996). All other spectra are from Matheson et al. (2008).

Table 3. Lightcurve summary

Supernova	Redshift	Daymax	Color	Error	Stretch	B Band Max	Error
SN1997dt	0.007	50785.113	0.559	0.009	0.905	15.451	0.012
SN1998V	0.018	50891.151	0.036	0.004	0.969	15.042	0.005
SN1998aq*	0.004	50930.449	-0.124	0.002	0.922	12.244	0.002
SN1998bp	0.010	50936.159	0.270	0.005	0.740	15.337	0.006
SN1998de	0.017	51026.088	0.594	0.008	0.807	17.434	0.009
SN1998dh	0.009	51029.620	0.130	0.005	0.898	13.850	0.008
SN1998ec	0.020	51088.234	0.174	0.011	0.980	16.047	0.017
SN1998eg	0.025	51110.410	0.039	0.009	0.910	16.070	0.008
SN1998es	0.011	51141.549	0.068	0.005	1.047	13.795	0.006
SN1999aa	0.014	51231.719	-0.039	0.003	1.046	14.692	0.004
SN1999ac	0.009	51250.350	0.112	0.003	0.989	14.121	0.004
SN1999cc	0.031	51315.513	0.043	0.008	0.815	16.766	0.009
SN1999cl	0.008	51341.769	1.200	0.011	0.915	14.827	0.013
SN1999dq	0.014	51435.494	0.117	0.003	1.055	14.371	0.004
SN1999ej	0.014	51481.985	0.038	0.010	0.830	15.290	0.013
SN1999gd	0.018	51518.193	0.470	0.008	0.937	16.857	0.010
SN1999gp	0.027	51550.179	0.062	0.004	1.163	16.000	0.004
SN2000cf	0.036	51672.335	0.010	0.010	0.917	16.983	0.011
SN2000cx	0.008	51752.315	-0.068	0.008	0.834	13.062	0.008
SN2000dk	0.017	51812.609	0.067	0.004	0.766	15.349	0.004
SN2000fa	0.021	51892.118	0.077	0.005	0.966	15.790	0.006

Note. — * are from Riess et al. (2005). All others are from Jha et al. (2006).

an uncharacteristically luminescent type Ia with a $B - V$ color far bluer than normal. SN1991bg is under luminescent.

SN1991T only has spectra taken outside of the three day within maximum light range that we used to select supernovae, as its maximum coincided with the full moon. Even so we felt we had to include this supernova in our analysis as it was the first of its type discovered and is a prime example of one peculiar class of type Ia supernovae. We used the templates provided by Nugent et al. which is derived from the available spectra for SN1991T. Nugent corrected the supernova for extinction assuming a color excess $E(B - V) = 0.2$ using the methods described by Cardelli et al. (1989). We undid this correction to get back to the observed spectrum.

SN1991bg on the other hand has four spectra, two taken a day after maximum (Gomez et al. 1996; Turatto et al. 1996), and two taken two days after maximum (Turatto et al. 1996).

6. Processing

The light curves were fit using snfit with a SALT2 model. SALT2 is an empirical model of type Ia supernovae trained using a selection of light-curves and spectra from both nearby and distant type Ia supernovae (Guy et al. 2007). We provide the fitter with the redshift and day of B band maximum given by the source papers for each supernova. Day of B band maximum was fixed as we found SALT2 did a better job of fitting when this parameter was not allowed to float.

The spectra were selected such that the rest phase was within three days of maximum. When multiple spectra from one supernova satisfied this requirement we selected the spectrum closest to maximum. The phase of each spectrum was determined by subtracting the day of maximum from the light curve from the observed date of the spectrum.

We performed a flux calibration on each spectrum to adjust its color to match the color fit from the light curve. A model of each spectrum in the rest frame was created using SALT2 based on the light curve fit. As we only wanted to correct the general shape of the spectrum without distorting the features we re-binned each spectrum into 500Å bins and normalized by dividing each flux count by the total area under the spectrum. We then re-binned the SALT2 model and normalized it by dividing through by its area, although this time we only calculate the area using the part of the model the overlaps the data spectrum. We then calculated a difference between the model and the spectrum and fit a first and a second order polynomial to the differences. We then made corrected versions of the spectrum by using these polynomials to adjust the flux in each bin. We calculated the color for each of our three versions: uncorrected, first-order corrected, and second-order corrected, and selected the one whose color most closely matches the light curve. The corrections do not always improve the color, and so for some versions the uncorrected spectrum is used. We believe we were not always able to improve color with our corrections because we do not take into account where the filters overlap the spectrum when we re-bin them. This hypothesis will be tested, and other correction methods examined in future work. We then trimmed the spectrum

to only cover 3710Å to 7080Å as this was the largest range over which all the spectra overlapped.

Plots for each supernovae are included in Appendix A. These plots include the original normalized spectrum, the normalized flux calibrated spectrum, the 500Å binned spectrum and correction function that was finally used, and a light curve fit by SALT2 that was used to determine color.

For most of the spectra the binning size is 1.5Å in the observer frame. As the width of the spectral features of a type Ia supernova is on the order of 5000 $\frac{km}{sec}$ the spectra are oversampled. We therefore re-bin each flux calibrated spectra to 10Å to reduce noise. After the re-binning each spectrum is once again normalized by dividing through by the total area under the spectrum.

6.1. SN1991T and SN1991bg Processing

No processing was done on the SN1991T and SN1991bg spectra. Neither of these supernovae's light curves are properly fit with SALT2. Further, we require an artificial spectrum generated by SALT2 based on the light curve fit in order to properly flux calibrate the spectra, but the SALT2 spectrum template is not flexible enough to model these odd supernovae. Any correction we tried to make therefore would only bias our results by changing these peculiar spectra to be more normal.

As we had multiple spectra for SN1991bg, we had to make a selection of one to use for our analysis. The selection was made by comparing the color of each spectrum to the color reported by Turatto et al. (1996) of $(B-V)=0.74$. As we were unable to correct these spectra in any way we needed to select a spectrum already close to this in $(B-V)$ color. The spectrum supplied by Gomez et al. (1996) has $(B-V)=0.7397$. This value is closer than any of the spectrum provided by Turatto et al. (1996) which all fall within the range $1.1059>(B-V)>0.9323$. Therefore the Gomez et al. spectrum is the one used for SN1991bg in our analysis.

SN1991T had no spectrum near maximum, but we use a de-extinction-corrected version of the Nugent et al. template at maximum in place of an observed spectrum.

7. Analysis

7.1. PCA eigenvectors

We were successfully able to create a set of eigenvectors from the twenty-three supernovae. Using just three eigenvectors we are able to account for 91.3% of variation within the sample, and with five eigenvectors we account for 95.8% of variation.

The first eigenvector alone accounts for 76% of variation in the data set. While the other eigenvectors are relatively flat, the first eigenvector has a definate slope. This allows it to account for differences in the color of supernovae spectra in the data set, with positive coeffecients creating bluer spectra and negative coefficents creating redder spectra.

Table 4. First Five Normalized Weights for Each Supernova

Supernova	Class	Radius	θ	σ_1	σ_2	σ_3	σ_4	σ_5
SN1991bg	III	2.21	214.53	-1.82274	-1.25405	2.32927	-0.29614	-1.70822
SN1991T	IV	2.31	280.47	0.41972	-2.27191	-0.15796	-1.07779	0.64694
SN1997dt	III	1.16	182.43	-1.15496	-0.04904	-0.82824	-0.77541	0.52835
SN1998aq	IV	0.96	355.83	0.96126	-0.07014	0.00158	-1.12395	-0.39967
SN1998bp	II	0.76	133.35	-0.52207	0.55304	1.19854	-0.32893	1.80270
SN1998de	III	1.52	192.12	-1.48267	-0.31837	1.94749	2.10701	0.44297
SN1998dh	I	1.38	83.33	0.16048	1.37175	-0.32390	1.19359	-0.10991
SN1998ec	Zero	0.33	143.09	-0.26456	0.19873	-1.02778	1.51962	-0.65194
SN1998eg	I	1.25	55.73	0.70201	1.03018	0.34618	-0.38230	-0.43956
SN1998es	IV	0.78	309.59	0.49563	-0.59931	-0.26691	-0.40891	-0.86157
SN1998V	Zero	0.62	32.21	0.52586	0.33128	-0.05399	-0.24062	-1.10653
SN1999aa	IV	1.19	327.14	0.99893	-0.64514	-0.31026	-0.15829	-0.73372
SN1999ac	I	0.99	60.95	0.48125	0.86625	0.46076	0.15119	-1.02274
SN1999cc	I	1.02	67.86	0.38283	0.94092	-0.71142	1.05519	0.89260
SN1999cl	II	2.73	178.91	-2.72918	0.05201	-2.43622	-0.50893	-0.23464
SN1999dq	IV	0.95	294.66	0.39755	-0.86608	-0.22107	-0.20711	-0.53821
SN1999ej	Zero	0.20	19.25	0.18974	0.06626	-0.33475	-0.46655	1.59778
SN1999gd	II	1.15	152.48	-1.02299	0.53288	-0.30726	-1.34928	0.46196
SN1999gp	IV	1.11	321.67	0.86747	-0.68577	-0.40707	0.67967	-0.47576
SN2000cf	I	1.41	57.20	0.76164	1.18204	1.04556	-1.83399	-0.07544
SN2000cx	IV	2.35	295.33	1.00485	-2.12255	-0.21715	1.13353	1.76569
SN2000dk	I	1.33	82.33	0.17780	1.32041	0.81927	0.04584	1.39704
SN2000fa	Zero	0.64	42.76	0.47216	0.43659	-0.54467	1.27253	-1.17814

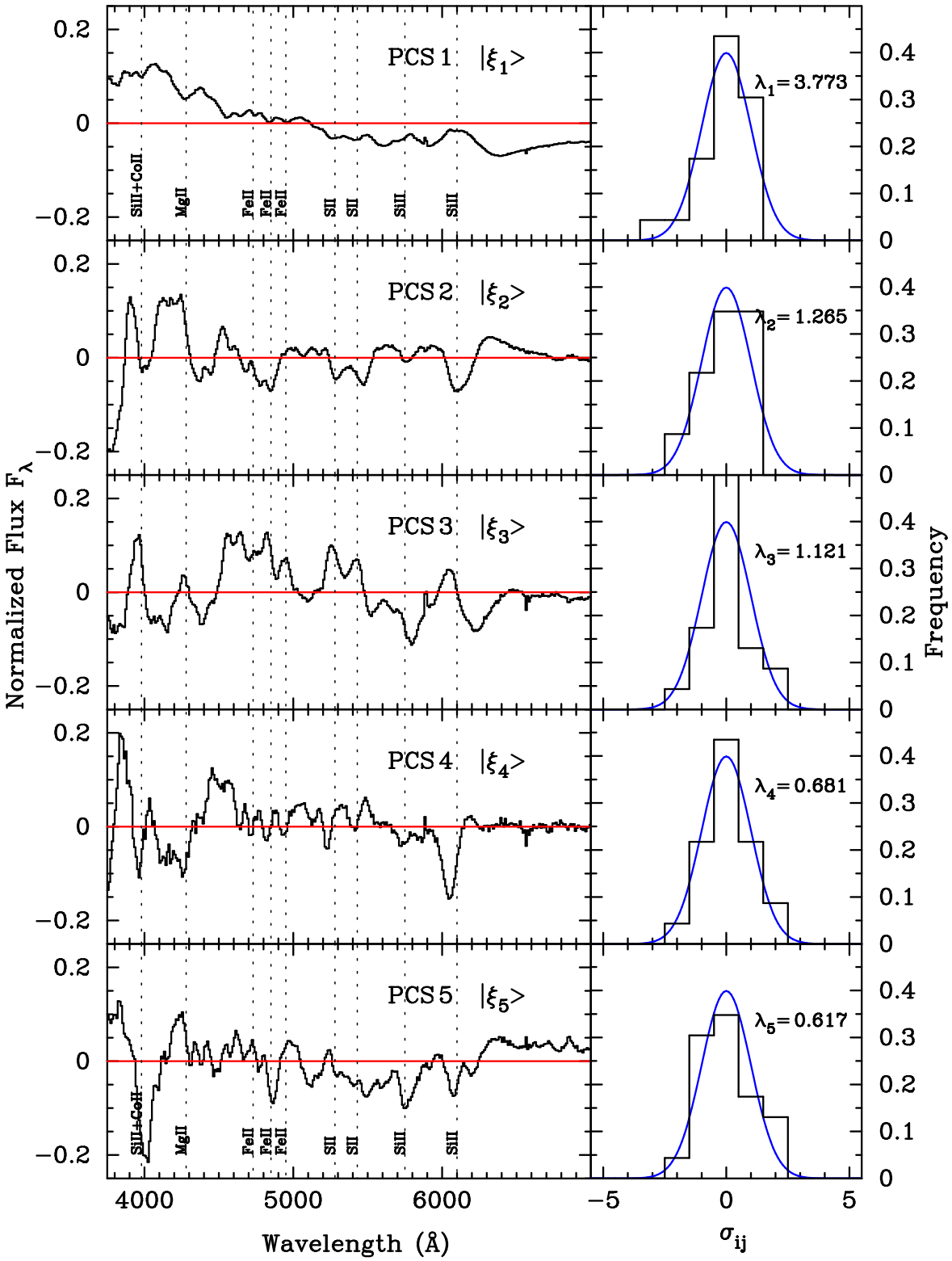

Fig. 1.— The first five eigenvectors, which account for 95.8% of variation in the sample. Note the slope of the first eigenvector.

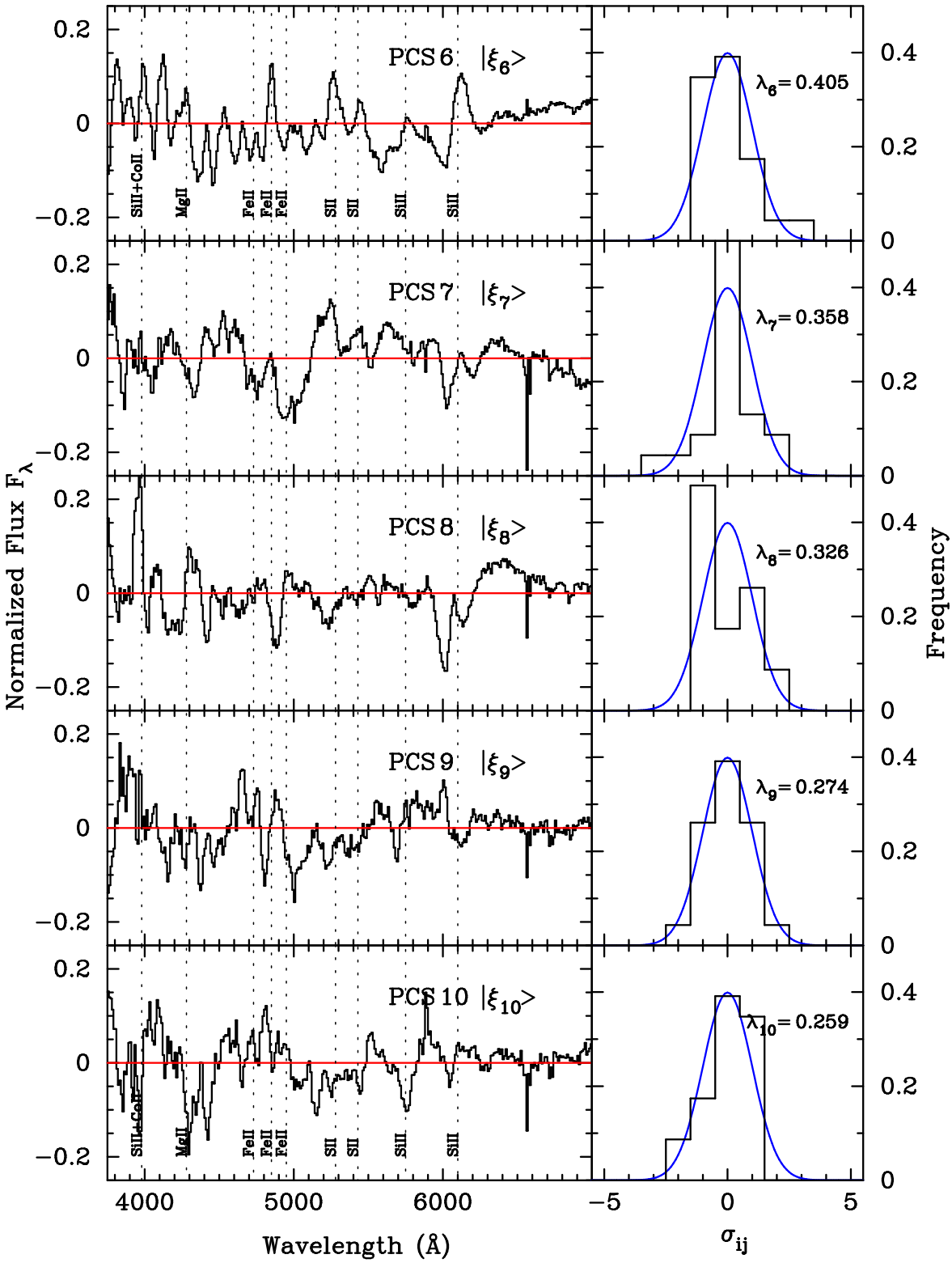

Fig. 2.— Eigenvectors six through ten, which account for 2.9% of variation in the sample.

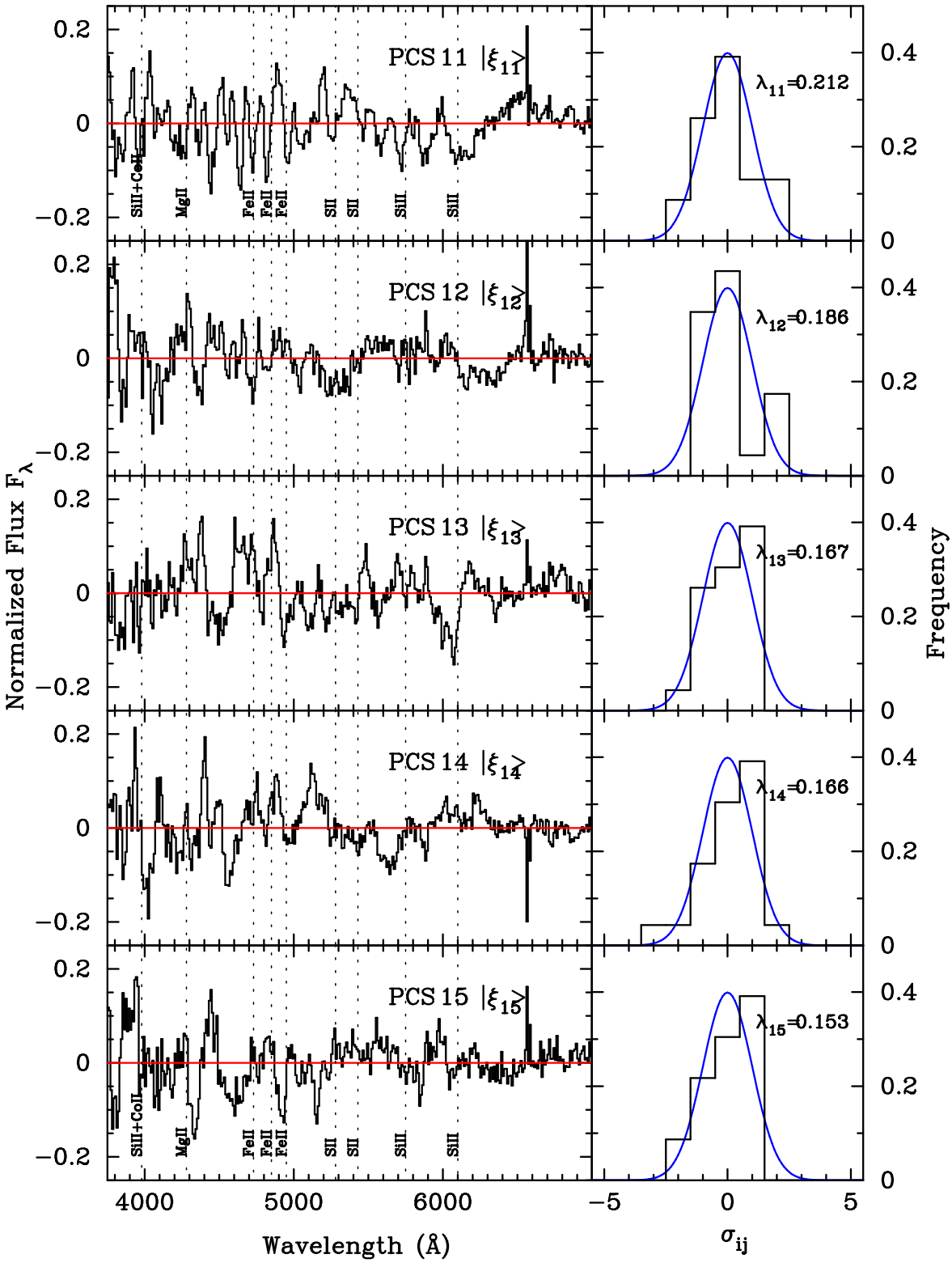

Fig. 3.— Eigenvectors eleven through fifteen, which account for 0.9% of variation in the sample.

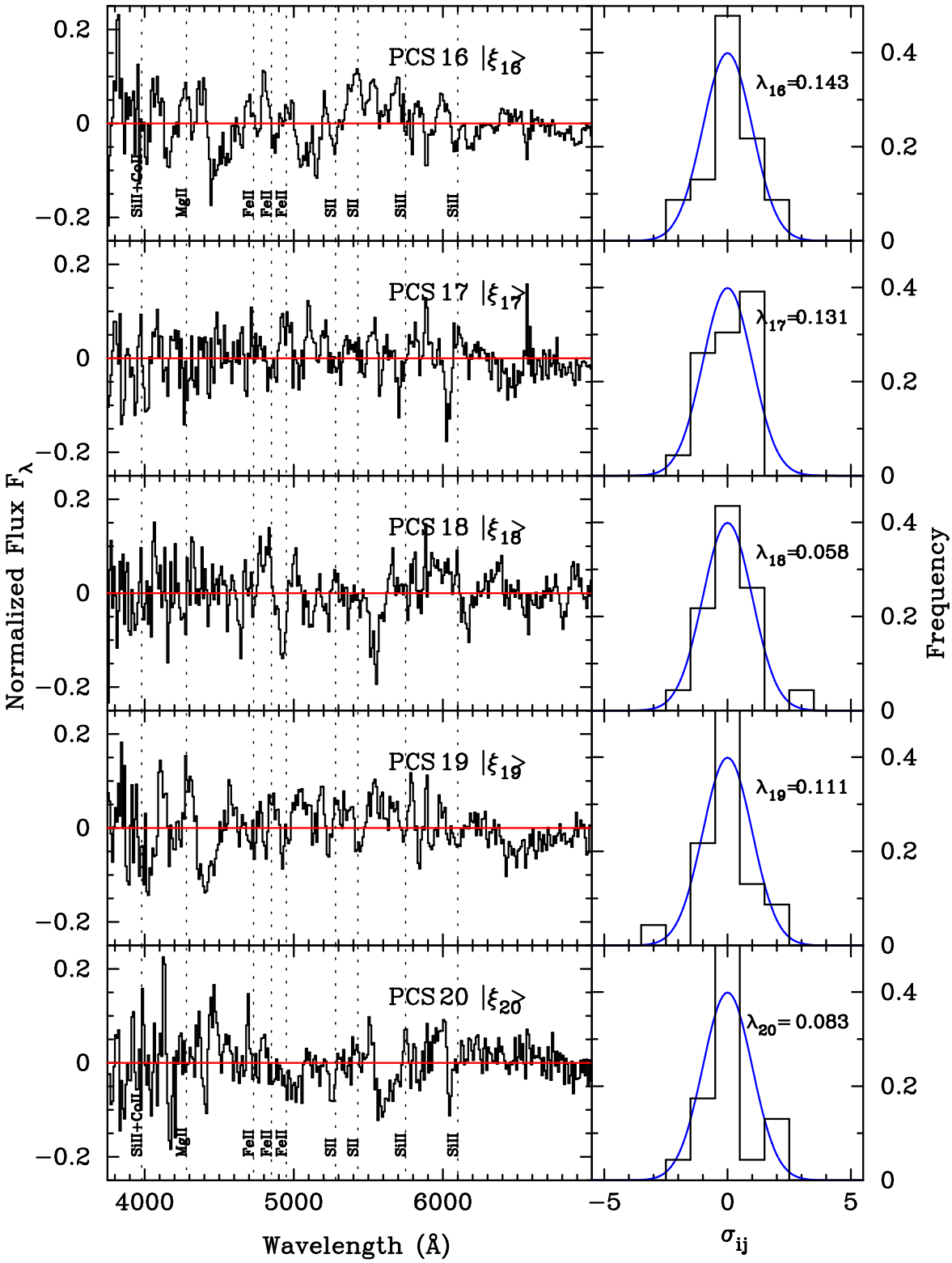

Fig. 4.— Eigenvectors sixteen through twenty, which account for 0.3% of variation in the sample.

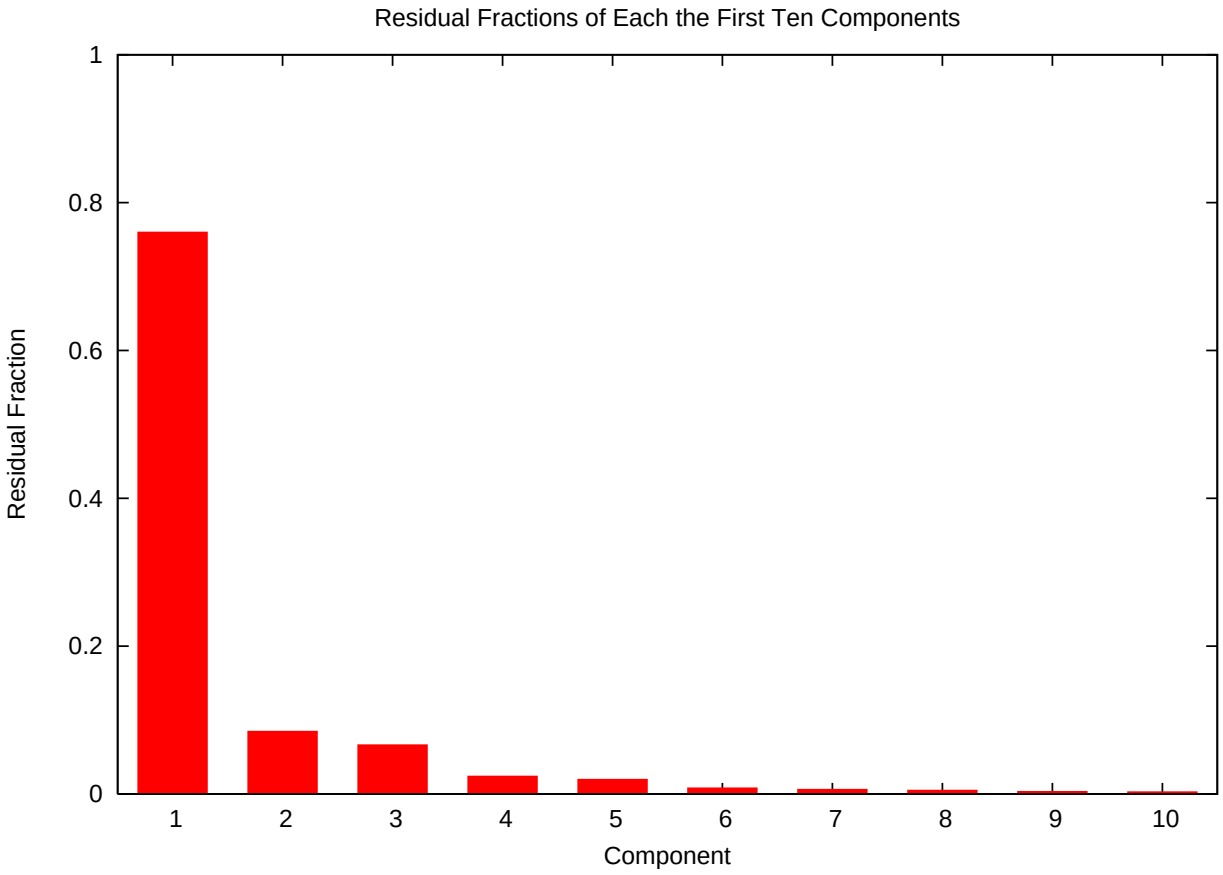

Fig. 5.— The residual fraction of the first ten components.

Table 5. Residual Fractions

Component	Eigenvalue λ_j^2	Eigenvalue$^{1/2}$ λ_j	Fraction	Comulative Fraction
1	14.2425	3.7739	0.7606	0.7606
2	1.6013	1.2654	0.0855	0.8461
3	1.2576	1.1214	0.0672	0.9132
4	0.4647	0.6817	0.0248	0.9380
5	0.3816	0.6177	0.0204	0.9584
6	0.1645	0.4056	0.0088	0.9672
7	0.1284	0.3583	0.0069	0.9740
8	0.1069	0.3269	0.0057	0.9798
9	0.0755	0.2747	0.0040	0.9838
10	0.0674	0.2596	0.0036	0.9874
11	0.0452	0.2126	0.0024	0.9898
12	0.0347	0.1862	0.0019	0.9916
13	0.0282	0.1679	0.0015	0.9931
14	0.0277	0.1664	0.0015	0.9946
15	0.0237	0.1539	0.0013	0.9959
16	0.0205	0.1432	0.0011	0.9970
17	0.0173	0.1314	0.0009	0.9979
18	0.0035	0.0590	0.0002	0.9981
19	0.0124	0.1112	0.0007	0.9988
20	0.0070	0.0839	0.0004	0.9991
21	0.0083	0.0913	0.0004	0.9996
22	0.0079	0.0891	0.0004	1.0000

Eigenvectors two through five, which combined account for 19.8% of variation, are all relatively flat. They primarily control the depths of different lines as well as the ratio of lines.

Eigenvectors six through twenty-two combined account for only 4.2% of variation in the data set. They primarily appear to represent noise in the spectra, and so do not appear to be useful in classifying or categorizing supernovae.

7.2. Classification of Supernovae

σ_1 is primarily responsible for the color of a supernova. Supernova with $\sigma_1 > 0$ are blue, while those with $\sigma_1 < 0$ are red. σ_2 and σ_3 control the ratio of various absorption features. We have divided the supernovae into classes based on the values of their σ_1 and σ_2 normalized weights.

We define a coordinate system such that:

$$r_i = \sqrt{(}\sigma_{i1}^2 + \sigma_{i2}^2)$$
$$\tan\theta_i = \frac{\sigma_{i2}}{\sigma_{i1}}$$

Using this system, classes I-IV are defined by the the four quadrants. We define a class zero centered on the origin with a radius r_0 defined so that the probability of a supernova lying within it are $P = 0.2$. We solve for r_i using:

$$P(r \leq r_0) = \int_0^{r_0} re^{-r^2/2}dr = 1 - e^{-r_0^2/2}$$

Class zero supernovae are the 20% of the sample closest to the mean spectrum. Class I are those supernovae with $\sigma_1 > 0$ and $\sigma_2 > 0$. Class I are blue with sharp peaks and deep absorption lines. Class II supernovae are defined by $\sigma_1 < 0$ and $\sigma_2 > 0$. The have deep lines, but are red. Class III is defined by $\sigma_1 > 0$ and $\sigma_2 < 0$. These supernovae are red, with a spectrum that is more flat with less defined features. SN1991bg is a Class III supernova, nearly two standard deviations from the mean in both of its normalized weights. Class IV are those supernovae with $\sigma_1 > 0$ and $\sigma_2 < 0$. They are blue with less pronounced features. SN1991T is a Class IV supernova.

In order to visualize how σ_1 and σ_2 effect the shape of a type Ia spectrum, we have provided a plot of the mean spectrum (figure 6), as well as the mean spectrum plus the first two components set so that we create a spectrum within each class, I through IV (figure 7). For each of these four demonstration spectra the weights are one standard deviation from the mean.

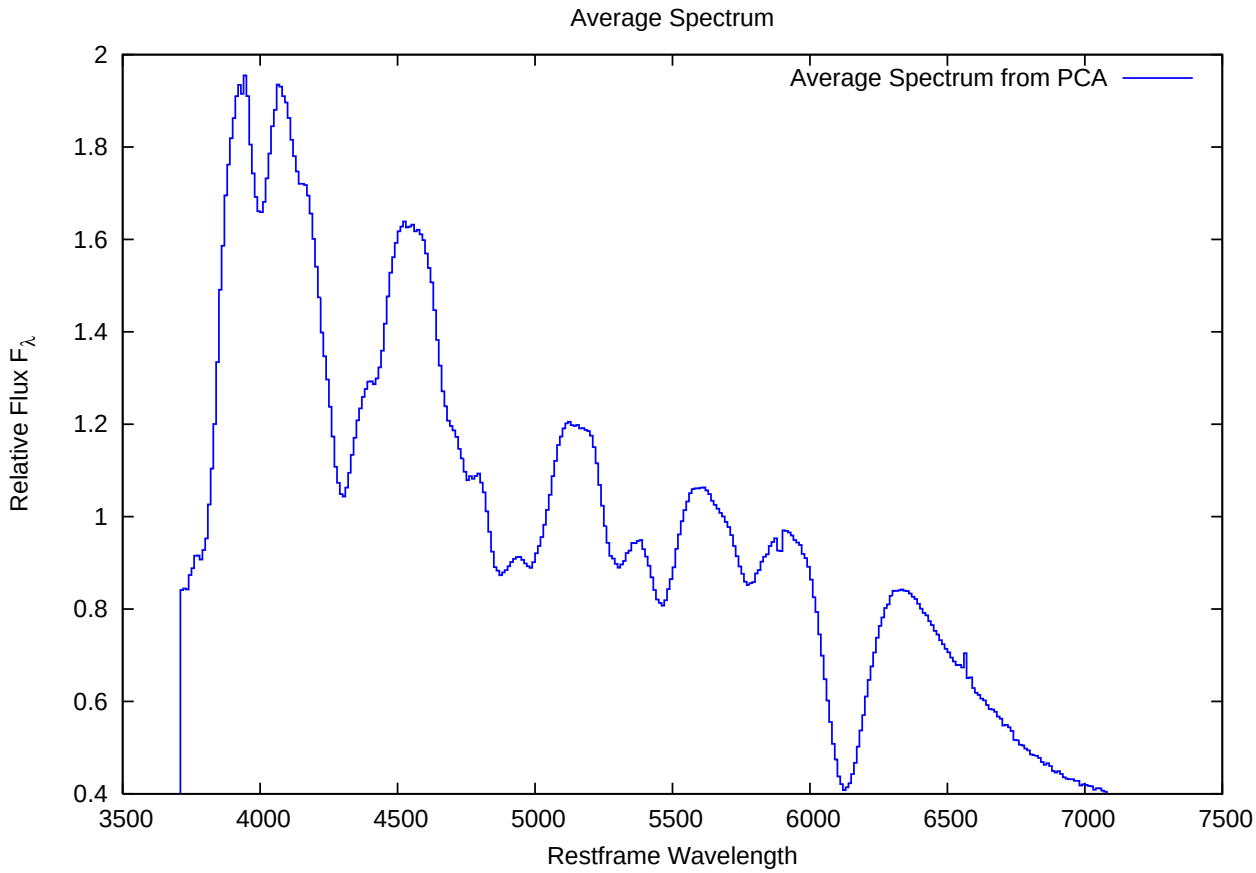

Fig. 6.— The mean spectrum, $\vec{\mu}$. Class zero are the 20% of supernovae that are closest to this

7.3. Color: Cardelli Law or Intrinsic?

Although $E(B-V)$ has traditionally been attributed to extinction, recent work has suggested it may not be. For example, recent work by Conley et al. (2008) has indicated that single parameter functions, such as dust laws, are in general unable to reproduce the variation in color seen in supernovae. They further find that the $U-B$ vs. $B-V$ relation found for their type Ia supernovae do not follow the relation one would expect for Milky-Way like dust.

In line with the results of Conley et al. the first eigenvector suggests that color is partially an intrinsic quantity, and not simply due to extinction. If color is purely an extinction related-effect we would expect this eigenvector to be nearly featureless so that line ratios would be completely uncorrelated with color. However, we observe deviations from the first eigenvector that align with the MgII feature, the FeIII features and the SiII features. This suggests that color is, to some extent, correlated with spectral features and is therefore not entirely extinction but is intrinsic to

each individual supernova.

If the color excess observed in type Ia spectra was purely due to extinction then we should be able to use the Cardelli law (Cardelli et al. 1989) to account for it. We therefore attempt to warp the Hsiao template (Hsiao et al. 2007), a template created by taking the mean spectra of over 100 type Ia supernovae near maximum light, with the Cardelli law. We fix $R_V = 3.1$ and vary A_V until we find a minimum in the χ^2 overlap between the warped Hsiao spectrum and the observed spectrum.

While many of the spectra appear to be able to be fit by a simple Cardelli law applied to the Hsiao template, nine supernovae fail. As expected the peculiar SN1991T and SN1991bg are not well fit. SN1998de, SN1998bp, SN1999cl, SN2000dk, and SN2000cx have spectral features that can not be matched with only a Cardelli law. SN1998aq and SN1999aa seem to fit well at first glance, but both have nonphysical preferred values of A_V, -0.031 for SN1998aq and -0.062 for SN1999aa. This suggests that for some of the supernovae Cardelli's law does not account for the observed color if $R_V = 3.1$ is fixed, however we can not say anything about the effects of letting R_V float. This is something that we would like to explore in future work.

Warping Hsiao's template with a Cardelli law provides a qualitative indication that color is not entirely due to extinction, but it does not provide us with a quantitative method of determining the amount of color excess due to extinction. For this we turn to the eigenvectors.

In figures 9, 10, and 11 we plot the normalized weight functions of the supernovae against each other. Supernovae with similar features will cluster. Further, it is possible to calculate a extinction vector in this space which allows us to observe exactly how much color excess is due to extinction. We plot the extinction vector by using the Cardelli law to warp the mean spectrum from the PCA. We fix $R_V = 3.1$ and increment A_V by 0.2. We then normalize this spectrum by its area again and subtract off the mean spectrum. We then dot this with an eigenvector which gives us a weight. Mathematically this is:

$$c_j^{CCM} = \vec{\xi_j} \cdot \left[\frac{\vec{\mu} \cdot CCM(R_V = 3.1, A_V)}{Normalization} - \vec{\mu} \right]$$

Where $\vec{\mu}$ is the mean spectrum, $CCM(R_V = 3.1, A_V)$ is the Cardelli factor, and $\vec{\xi_j}$ is the jth eigenvector.

Only if a supernova lies near the extinction line, in all three plots, is its color due to Cardelli like dust. It is worth nothing that very few supernovae lie close to the extinction vector in all three plots. This suggests that the variation we see in color from most type Ia supernovae is due to intrinsic properties of the supernovae and not extinction.

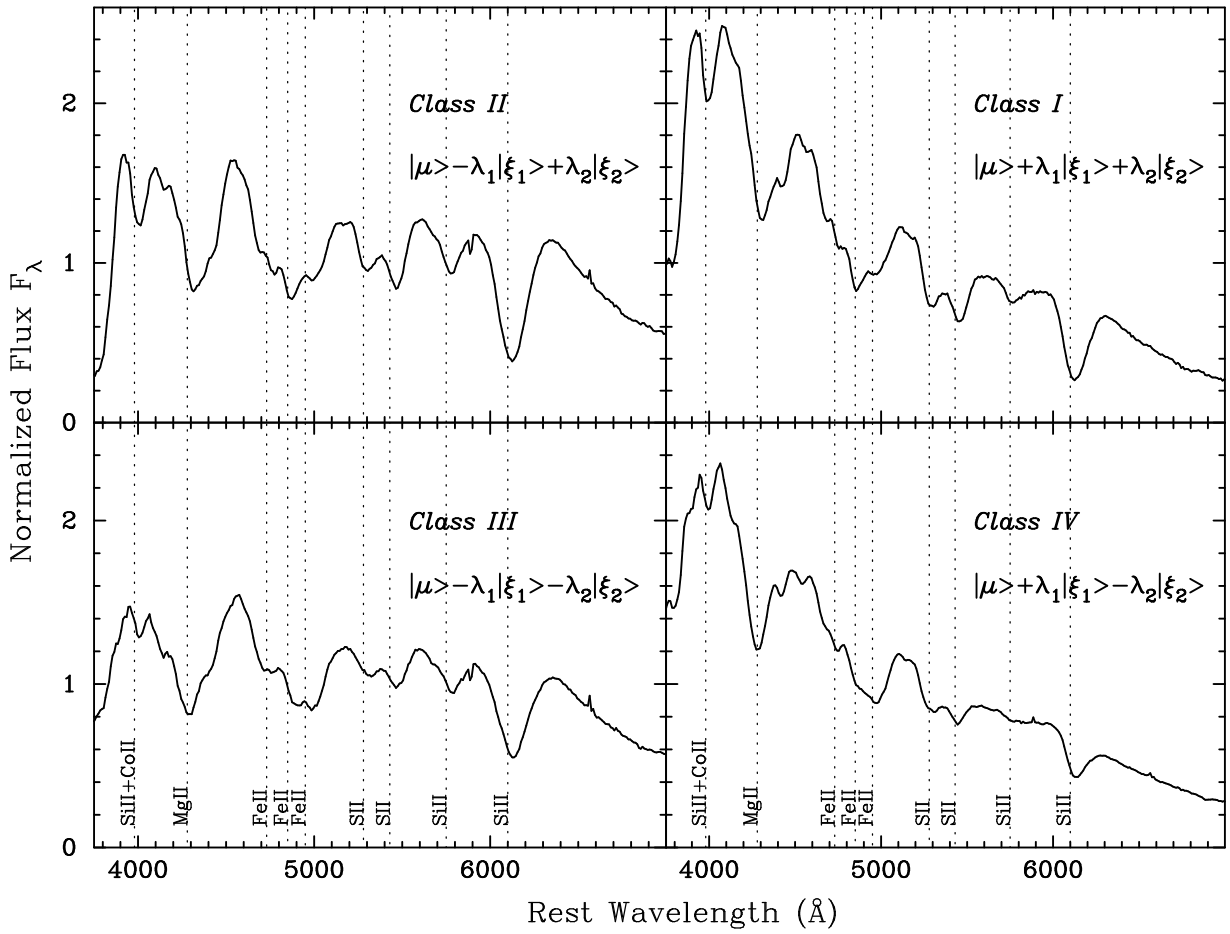

Fig. 7.— Four spectra demonstrating Class I through Class IV, with the normalized weights set so that each one is one standard deviation from the norm.

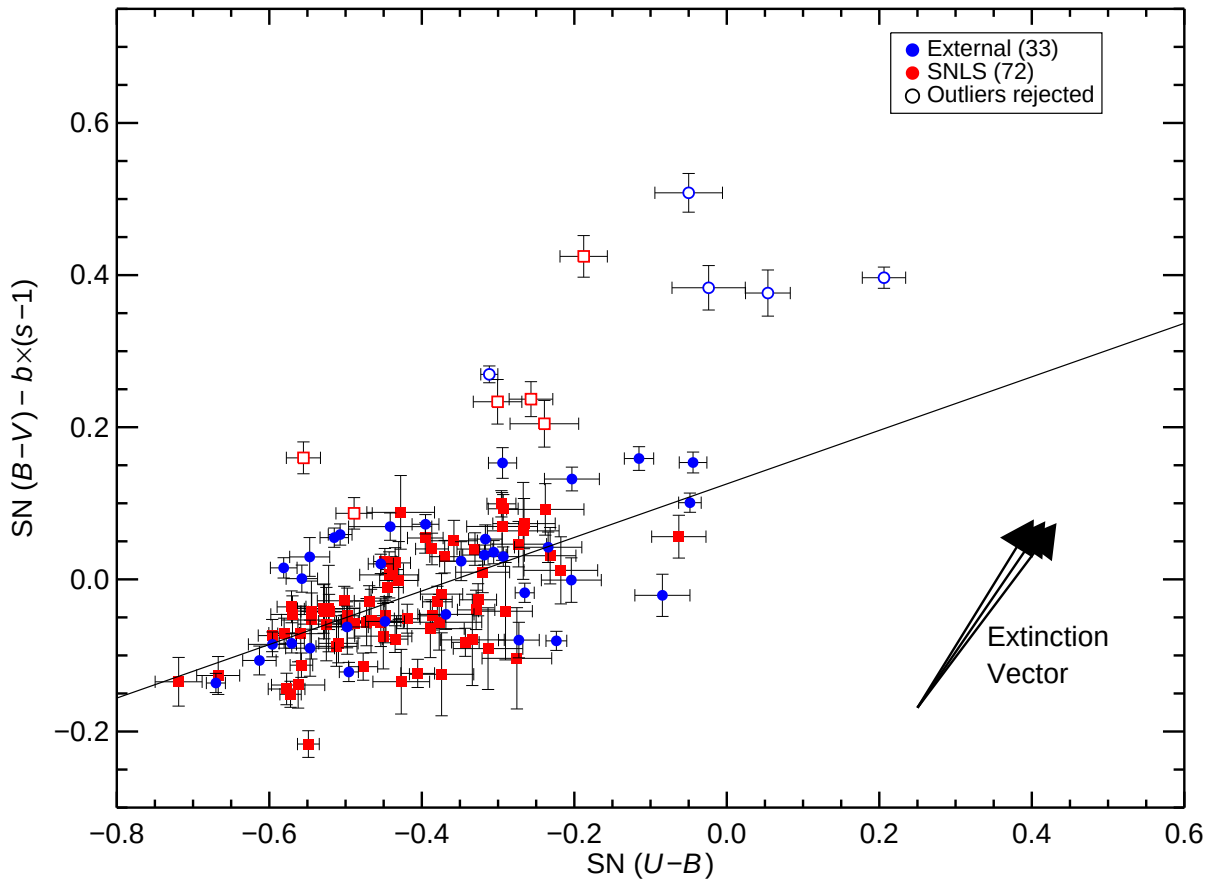

Fig. 8.— The derived $U - B$ vs. $B - V$ relation found by Conley et al. (2008). The best fit to the sample is the solid line. The arrow is the relation one would expect from Milky-Way like dust ($R_v = [1.6, 3.1, 4.6]$). Figure courtesy of Conley et al. (2008).

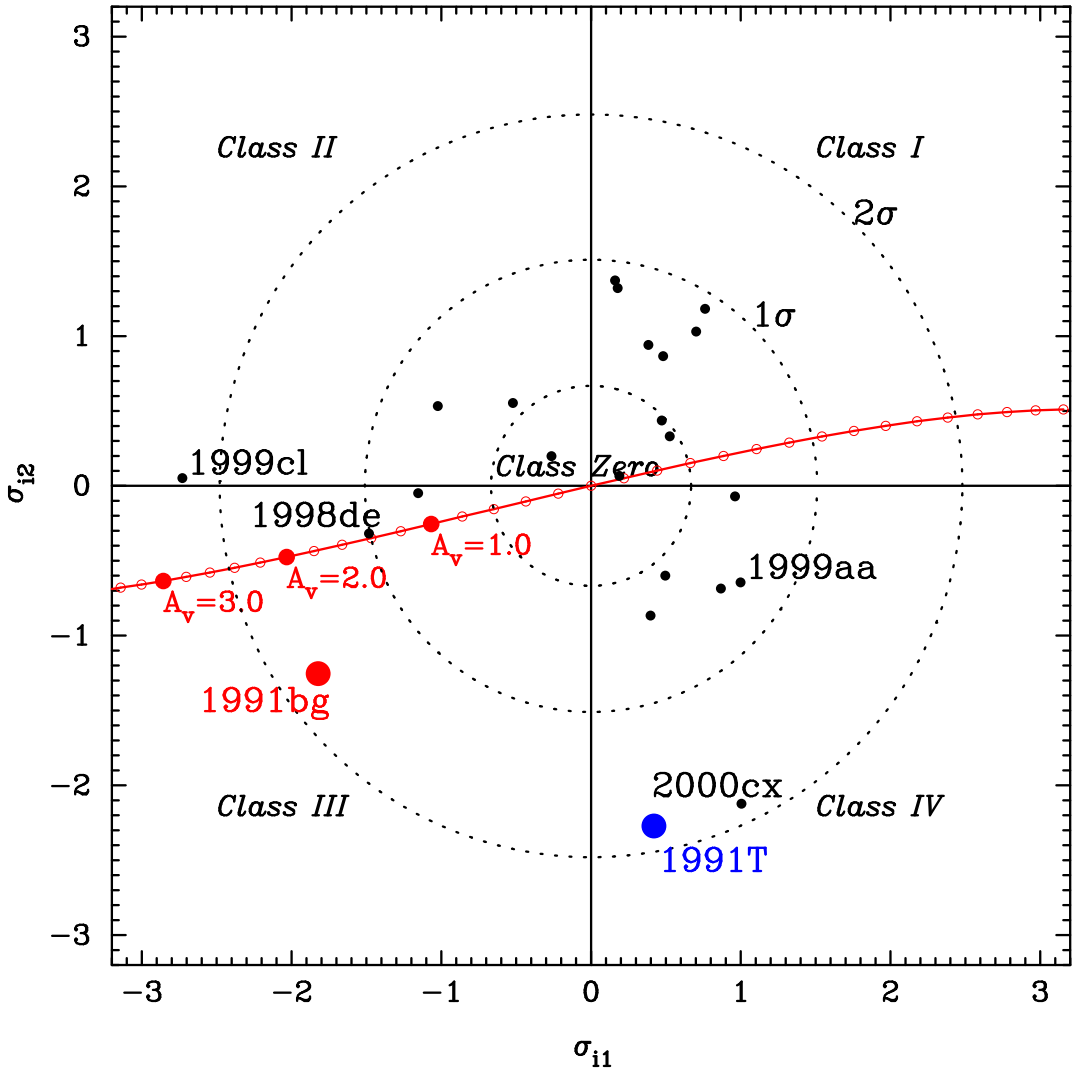

Fig. 9.— Supernovae plotted by their first and second normalized weight. Supernovae with $\sigma_1 > 0$ are blue, while those with $\sigma_1 < 0$ are red. The red line marks the expected extinction vector for Cardelli law extinction, with each open circle marking a step in A_V of 0.2.

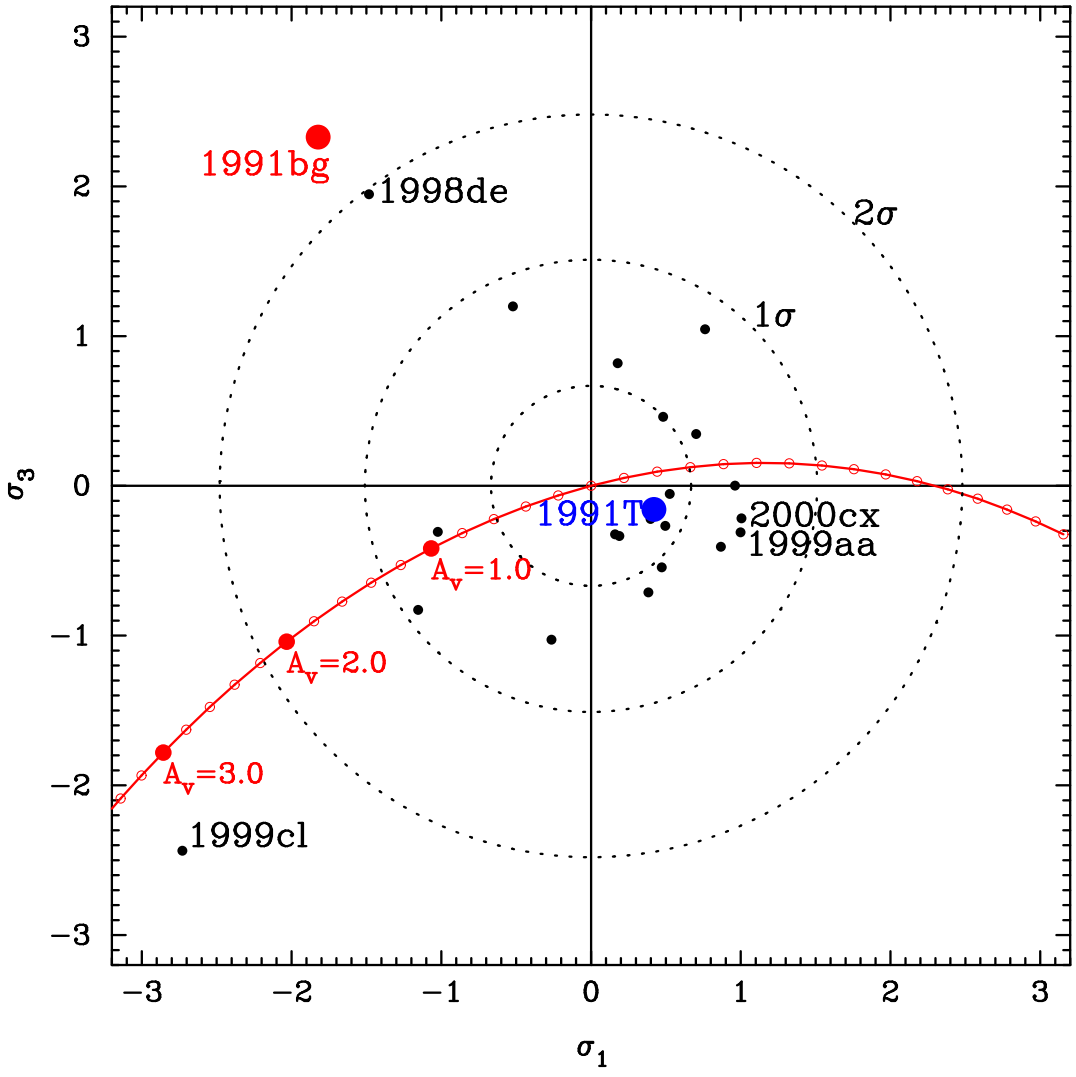

Fig. 10.— Supernovae plotted by their first and third normalized weight. Supernovae with $\sigma_1 > 0$ are blue, while those with $\sigma_1 < 0$ are red. The red line marks the expected extinction vector for Cardelli law extinction, with each open circle marking a step in A_V of 0.2.

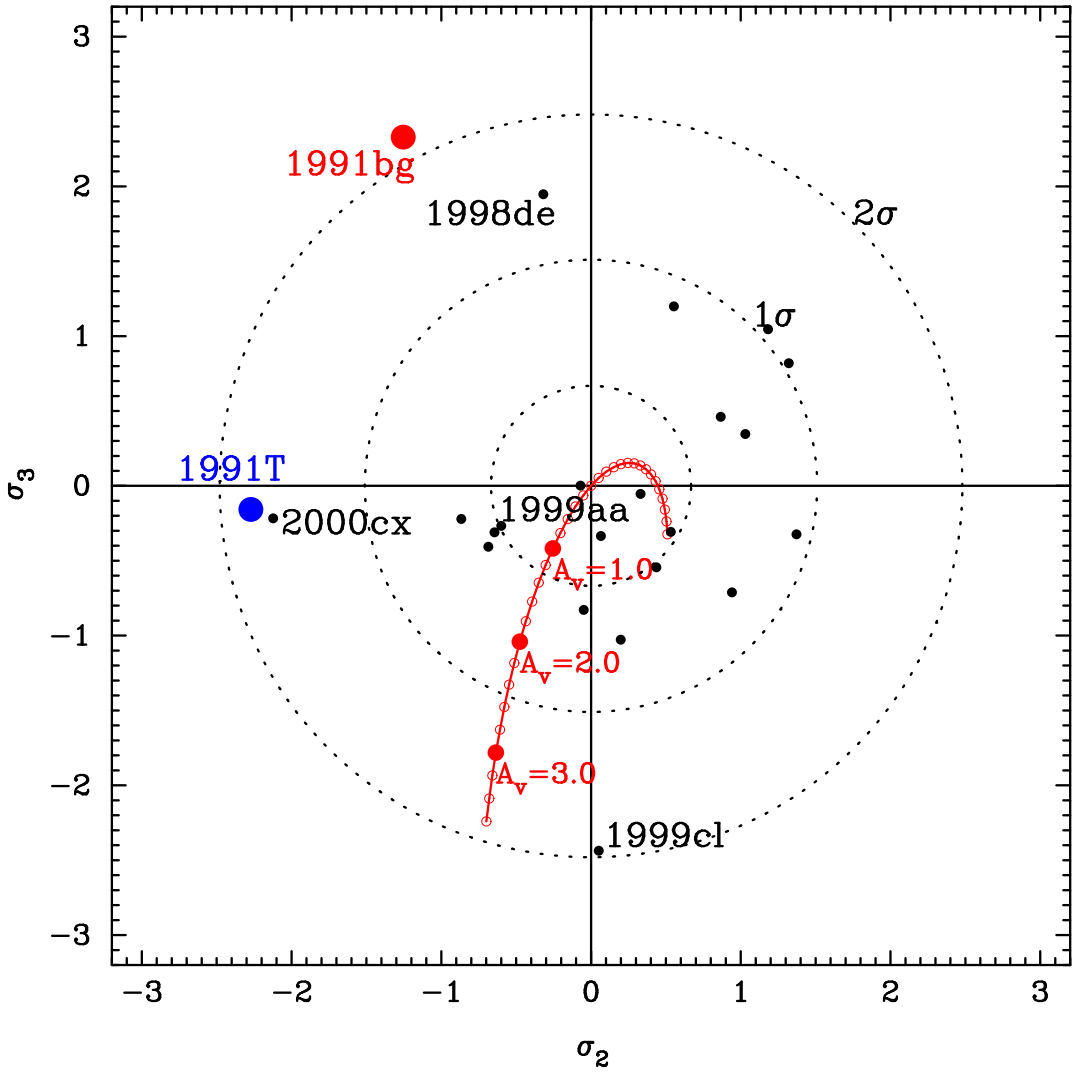

Fig. 11.— Supernovae plotted by their second and third normalized weight. The red line marks the expected extinction vector for Cardelli law extinction, with each open circle marking a step in A_V of 0.2.

7.4. Applications to the Hubble Diagram

We hope the PCA eigenvectors will assist in future cosmology research involving type Ia supernovae. In order to get an idea of their usefulness, we create a series of Hubble diagrams with the supernovae from the data set, except for SN1991T and SN1991T as they do not have light curves and SN1999cl which was such an outlier that it badly pulled the fit. We plot cz of the host galaxies of each of the supernovae against their maximum B band magnitude. Because the supernovae are nearby, they have peculiar velocity that must be corrected for. We used the cz calculated relative to the cosmic microwave background (Fixsen et al. 1996). We plot the Hubble law using $H_0 = 71.9km/s/Mpc$ as reported by Hinshaw et al. (2008).

We also make Hubble diagrams using color corrections (Astier et al. 2006; Sullivan et al. 2003), stretch corrections (Perlmutter et al. 1997; Perlmutter et al. 1999; Knop & The Supernovae Cosmology Project 2003), and both color and stretch corrections combined. For these corrections we fit for α and β iteratively, seeding with values of $\alpha = -1.24$ and $\beta = 2.28$ as determined by Kowalski et al. (2008). We find that for this sample, $\alpha = -2.084$ and $\beta = 3.610$. In order to find a fit that would correct most of our supernova, we removed by hand a single outlier with color > 1.

We then attempt to find a correlation between the normalized weights and dispersion around the Hubble line. While we'd like to be able to measure the effect on intrinsic dispersion, we do not have accurate enough error bars to do so. We plot the first normalized weight, σ_1 against $mag_B - Model$ and fit for a correction using weighted least squares. We then apply this correction and plot σ_2 against $mag_B - Model - A_1 * \sigma_1 - B_1$ where A_1 and B_1 are the slope and intercept of the correction. We continue to do this for the first five normalized weights. We then create Hubble diagrams using only the σ_1 correction, using σ_1 and σ_2, and so on until we use all of the corrections up to σ_5.

We then attempt to combine color, stretch, and the normalized weights into one correction. We use the same method as before, except we start by plotting σ_1 against $mag_B - Model - \alpha(S - 1) - \beta C$ which is the magnitudes already corrected with color and stretch. We repeat the above process, subtracting off corrections for each normalized weight found previously, before fitting a new correction for the next normalized weight.

We now have fourteen Hubble diagrams. Four were made with the uncorrected data, with color corrections, with stretch corrections, and with color and stretch corrections. Five were made with just using the normalized weights, and five were made combing color, stretch, and then using the normalized weights. For each of these Hubble Diagrams we calculate the dispersion, and then use this dispersion to remove any supernovae that are more than two standard deviations from the Hubble line, what we call a 2σ-cut dispersion. The supernova cut are marked by an * on table 6.

While table 6 seems to indicate that without using the 2σ-cut, we are able to achieve a lower dispersion with just our first weight than with color, stretch, or color and stretch combined corrections, this is without outlier rejection. If we reject SN1999cl, a four σ outlier, and then

perform the analysis, we find that the weight correction only improves the dispersion more than color alone, while stretch corrections and color with stretch corrections combined improve it more than using on the first weight. Using more than just the first weight increases dispersion, which is unexpected as PCA is guaranteed to lower dispersion. We see this increased dispersion though because we do not use the exact corrections determined by the PCA, but used a shortcut of fit for the corrections (the A_1 and B_1 mentioned above). Future analysis will be done with the PCA determined corrections.

If we apply the 2σ-cut after rejecting SN1999cl, we find that only using the first normalized weight gets us a dispersion that is lower than using a color correction alone or a stretch correction alone, but is worse than using a stretch correction and color correction combined. Again using more than just the first normalized weight increases the dispersion. Using color, stretch, and the first normalized weight increases dispersion as compared to using just color and stretch alone.

Table 6. Distance From The Hubble Line In Magnitudes

Supernova	Uncorrected	C	S	CS	W1	W2	W3	CSW1
SN1997dt	2.734*	2.537*	0.716	0.519	1.169*	0.487	-0.062	1.185*
SN1998V	0.074	0.010	-0.054	-0.118	-0.294	-1.130*	-1.446*	-0.217
SN1998aq	0.286	0.123	0.732	0.569	0.227	-0.448	-0.747	0.272
SN1998bp	1.503	0.962	0.530	-0.012	0.389	-0.536	-0.476	0.367
SN1998de	2.678*	2.275*	0.535	0.132	0.880	0.305	0.590	0.947
SN1998dh	0.628	0.414	0.158	-0.055	-0.001	-1.256*	-1.653*	0.013
SN1998ec	0.741	0.700	0.111	0.070	-0.190	-0.973	-1.581*	0.331
SN1998eg	0.424	0.236	0.282	0.094	0.180	-0.937	-1.133	-0.084
SN1998es	0.093	0.191	-0.154	-0.055	-0.297	-0.758	-1.139	-0.140
SN1999aa	-0.022	0.074	0.119	0.215	-0.054	-0.497	-0.890	-0.099
SN1999ac	0.374	0.351	-0.030	-0.054	-0.027	-1.078	-1.239	-0.132
SN1999cc	0.484	0.098	0.328	-0.058	0.013	-1.068	-1.581*	-0.092
SN1999cl	1.339	1.161	-2.992*	-3.169*	-1.346*	-2.069*	-3.100*	-1.787*
SN1999dq	-0.071	0.044	-0.493	-0.378	-0.530	-0.884	-1.251	-0.418
SN1999ej	0.964	0.610	0.826	0.473	0.356	-0.373	-0.773	0.527
SN1999gd	1.638*	1.506*	-0.058	-0.190	0.168	-0.749	-1.141	0.416
SN1999gp	0.134	0.475	-0.088	0.252	0.009	-0.418	-0.840	-0.001
SN2000cf	0.381	0.208	0.346	0.173	0.180	-0.998	-0.984	-0.033
SN2000cx	0.077	-0.269	0.321	-0.026	0.049	0.201	-0.164	-0.342
SN2000dk	0.471	-0.017	0.230	-0.258	-0.145	-1.379*	-1.433*	-0.198
SN2000fa	0.307	0.236	0.031	-0.041	-0.100	-0.978	-1.441*	-0.114
Dispersion	0.779	0.709	0.737	0.711	0.471	0.562	0.697	0.552
2σ-cut	0.419	0.341	0.319	0.237	0.291	0.464	0.497	0.322

Note. — C has been color corrected, S has been stretch corrected, CS has been color and stretch corrected, W1 has had a correction from the first normalized weight, W2 uses a correction from the first and second normalized weights, W3 uses a correction from the first, second, and third normalized weights. CSW1 uses a color and stretch correction, as well as corrections from the first normalized weight. The Dispersion is calculated as the standard deviation of the entries. 2σ-cut is the dispersion recalculated with supernovae that are more than two standard deviations from the Hubble line dropped. Entries marked with a * were dropped for the 2σ-cut calculation.

Table 7. Distance From The Hubble Line In Magnitudes

Supernova	Uncorrected	C	S	CS	W1	W2	W3	CSW1
SN1997dt	2.734*	2.537*	0.716*	0.519*	1.169*	0.487	-0.062	1.185*
SN1998V	0.074	0.010	-0.054	-0.118	-0.294	-1.130*	-1.446*	-0.217
SN1998aq	0.286	0.123	0.732*	0.569*	0.227	-0.448	-0.747	0.272
SN1998bp	1.503	0.962	0.530	-0.012	0.389	-0.536	-0.476	0.367
SN1998de	2.678*	2.275*	0.535	0.132	0.880*	0.305	0.590	0.947*
SN1998dh	0.628	0.414	0.158	-0.055	-0.001	-1.256*	-1.653*	0.013
SN1998ec	0.741	0.700	0.111	0.070	-0.190	-0.973	-1.581*	0.331
SN1998eg	0.424	0.236	0.282	0.094	0.180	-0.937	-1.133*	-0.084
SN1998es	0.093	0.191	-0.154	-0.055	-0.297	-0.758	-1.139*	-0.140
SN1999aa	-0.022	0.074	0.119	0.215	-0.054	-0.497	-0.890	-0.099
SN1999ac	0.374	0.351	-0.030	-0.054	-0.027	-1.078*	-1.239*	-0.132
SN1999cc	0.484	0.098	0.328	-0.058	0.013	-1.068*	-1.581*	-0.092
SN1999dq	-0.071	0.044	-0.493	-0.378	-0.530	-0.884	-1.251*	-0.418
SN1999ej	0.964	0.610	0.826*	0.473	0.356	-0.373	-0.773	0.527
SN1999gd	1.638*	1.506*	-0.058	-0.190	0.168	-0.749	-1.141*	0.416
SN1999gp	0.134	0.475	-0.088	0.252	0.009	-0.418	-0.840	-0.001
SN2000cf	0.381	0.208	0.346	0.173	0.180	-0.998*	-0.984	-0.033
SN2000cx	0.077	-0.269	0.321	-0.026	0.049	0.201	-0.164	-0.342
SN2000dk	0.471	-0.017	0.230	-0.258	-0.145	-1.379*	-1.433*	-0.198
SN2000fa	0.307	0.236	0.031	-0.041	-0.100	-0.978	-1.441*	-0.114
Dispersion	0.785	0.713	0.319	0.237	0.371	0.493	0.551	0.396
2σ-cut	0.374	0.283	0.247	0.187	0.224	0.451	0.461	0.254

Note. — The same as table 6, but SN1999cl has been removed before any calculations.

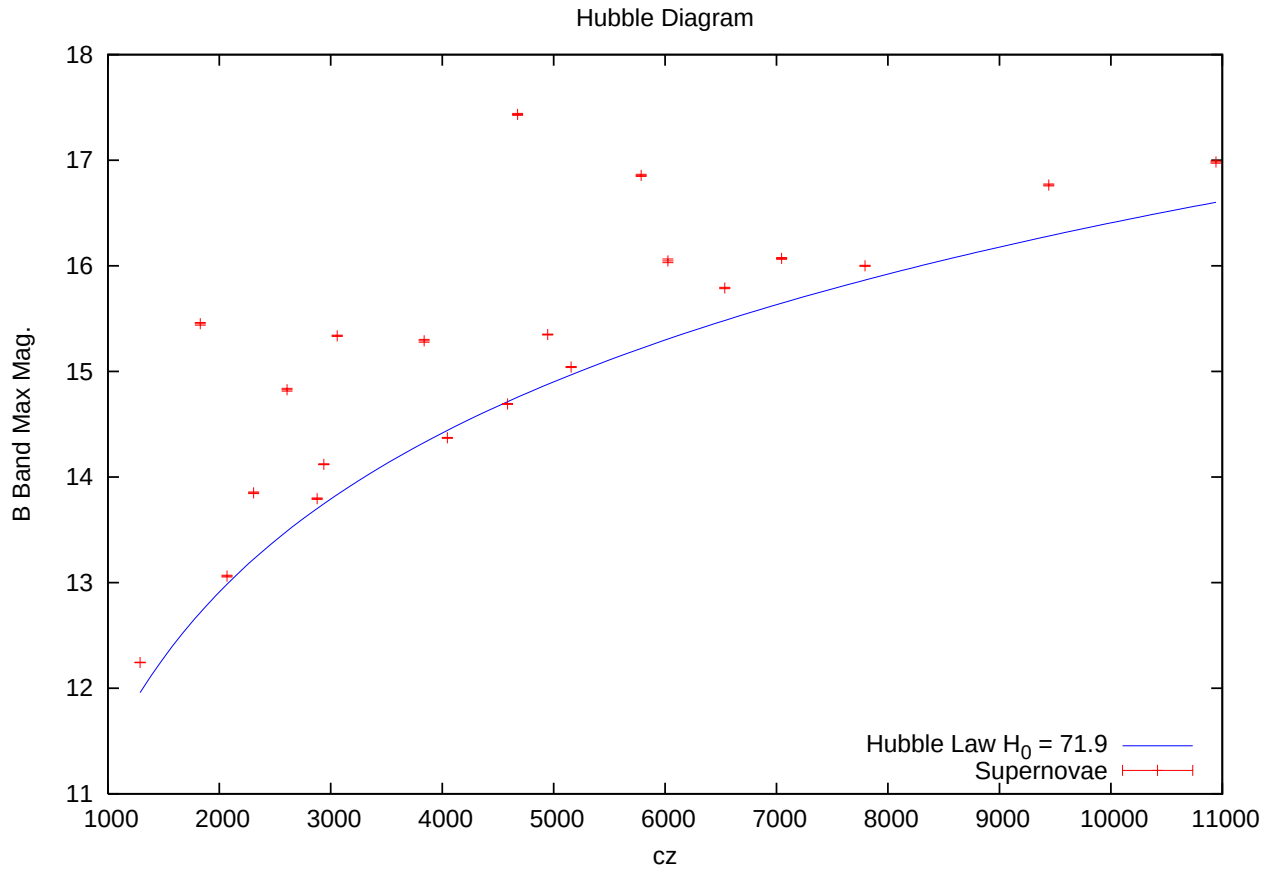

Fig. 12.— Hubble diagram of uncorrected supernovae.

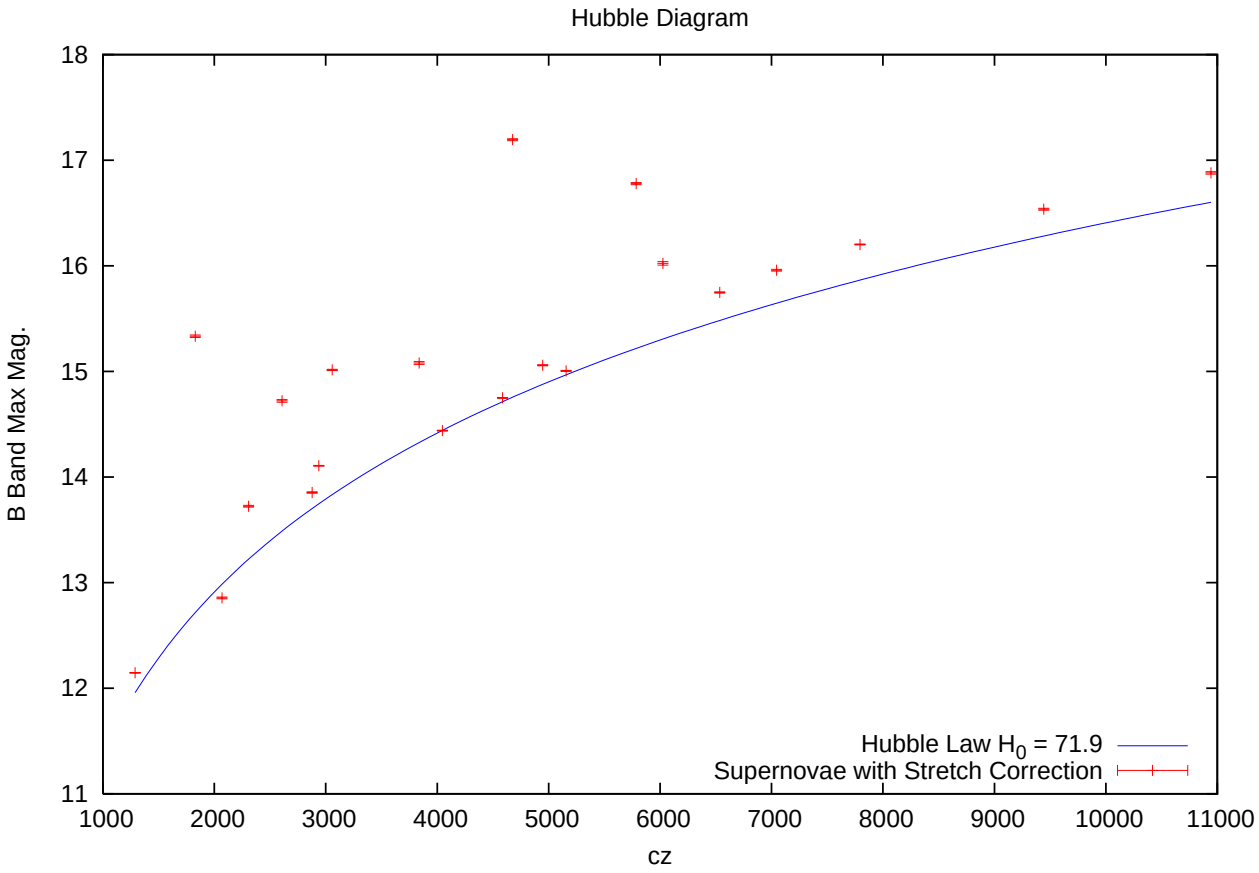

Fig. 13.— Hubble diagram of stretch corrected supernovae.

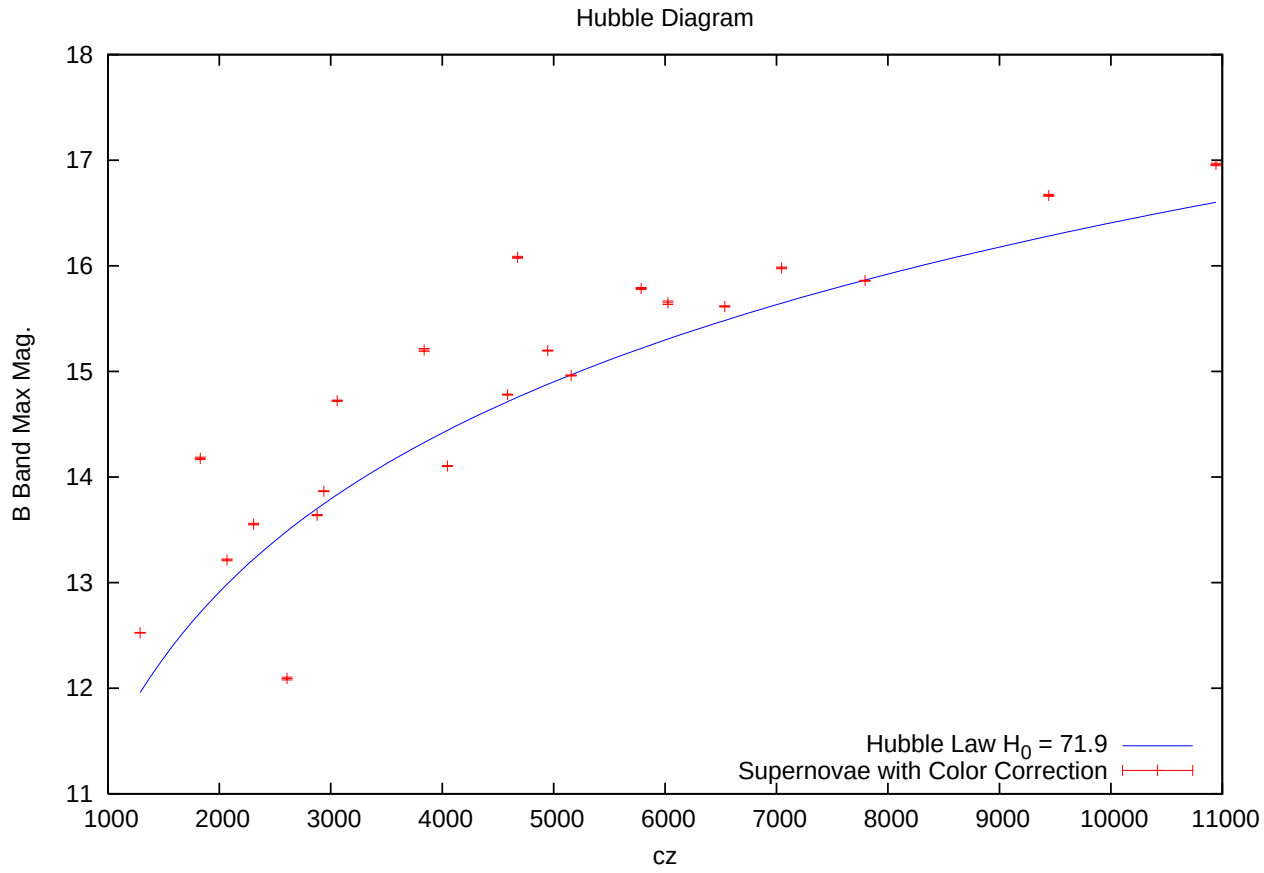

Fig. 14.— Hubble diagram of color corrected supernovae.

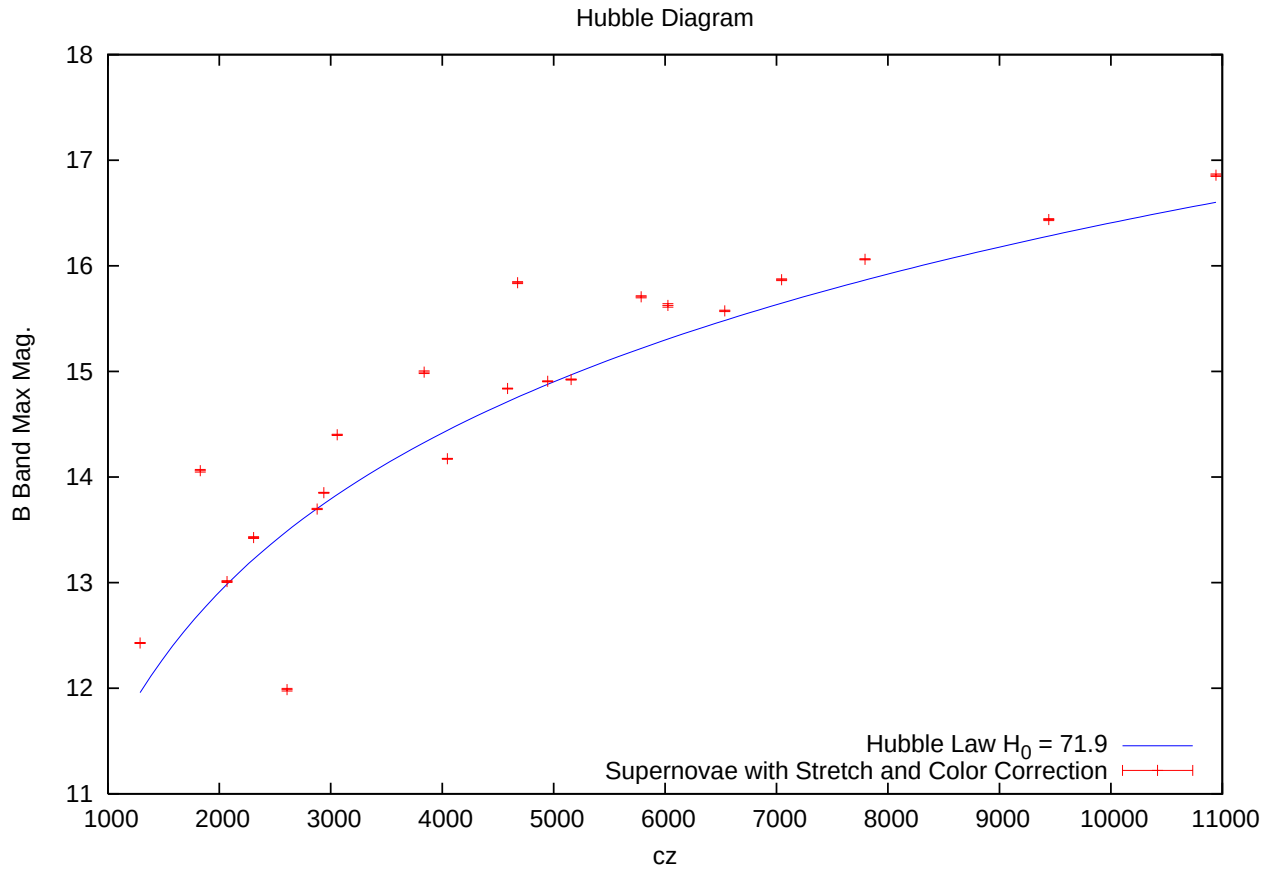

Fig. 15.— Hubble diagram of color and stretch corrected supernovae.

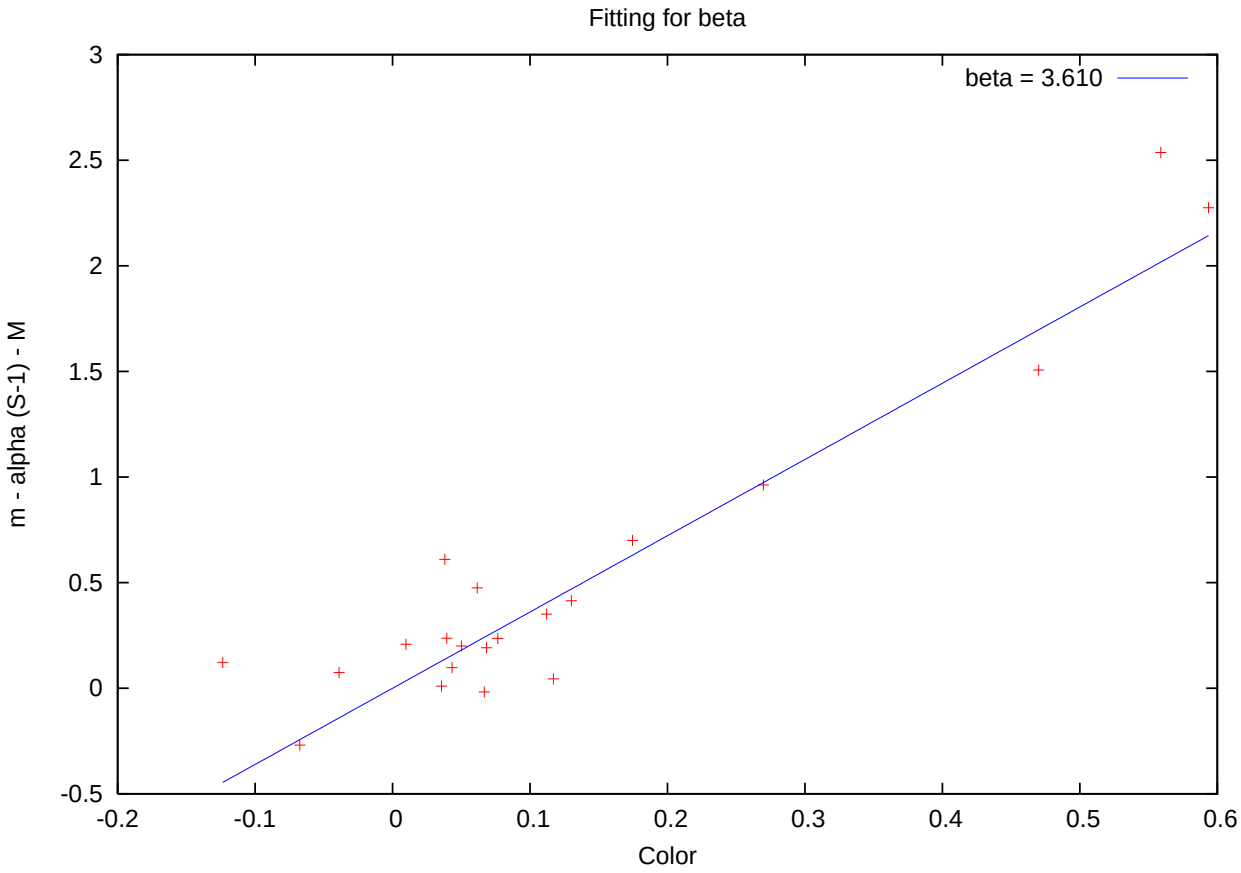

Fig. 16.— $\beta = 3.610$, and the supernovae.

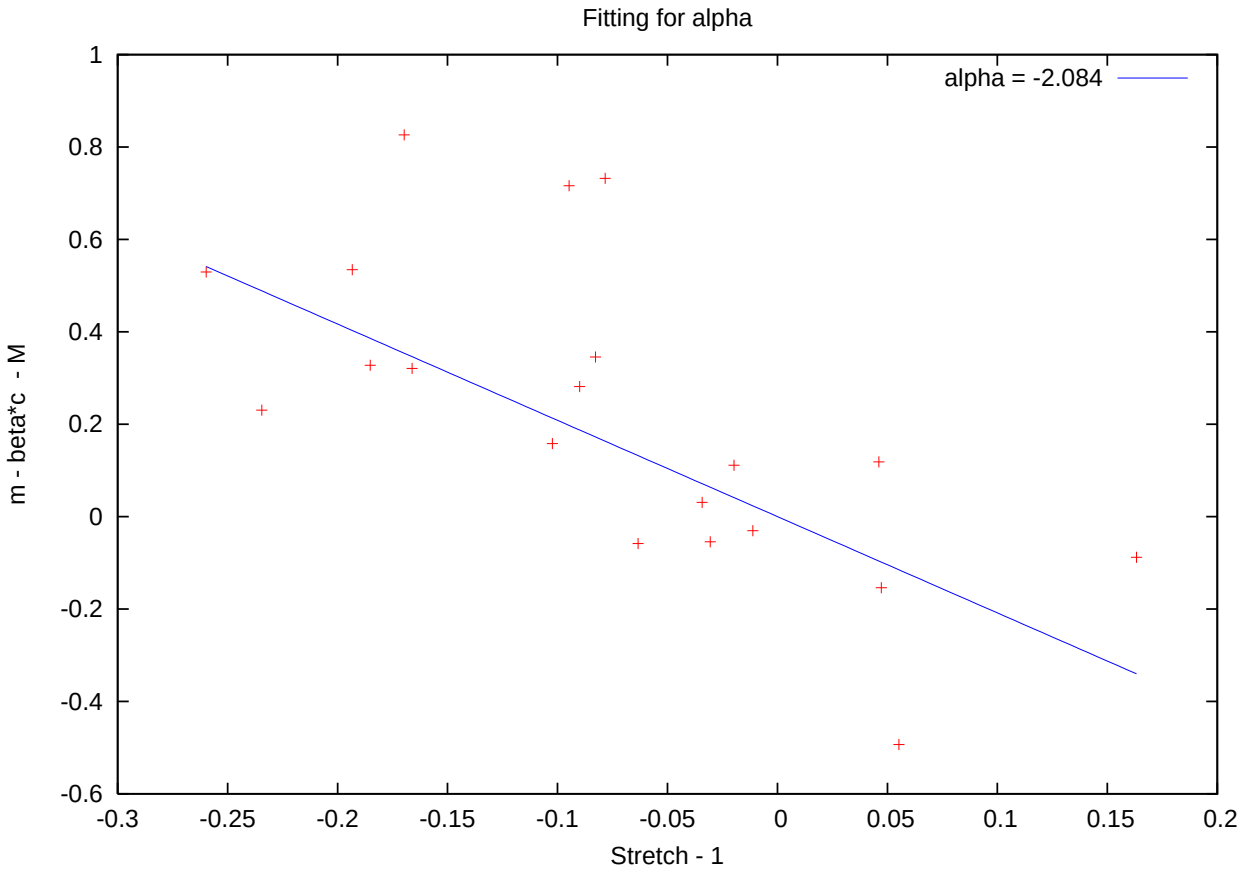

Fig. 17.— $\alpha = -2.084$, and the supernovae.

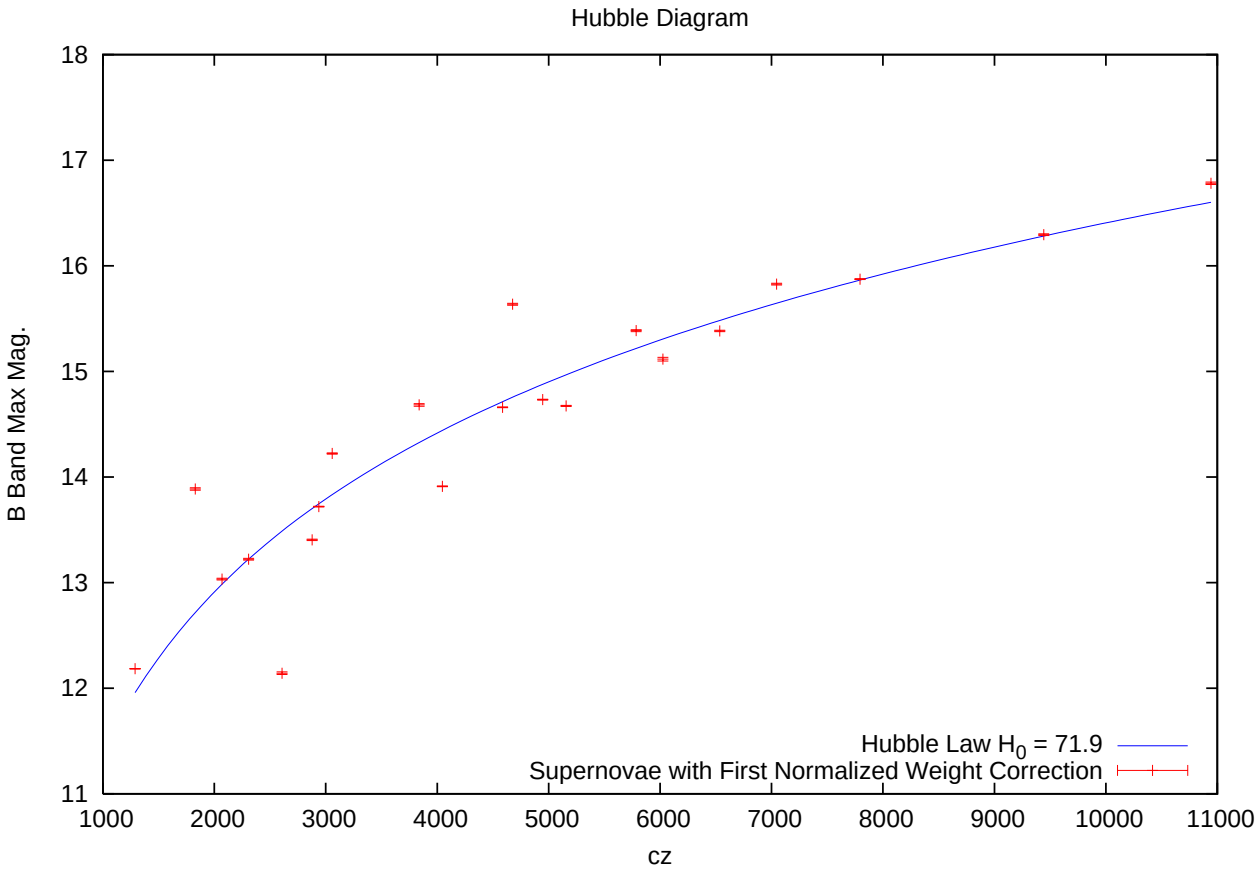

Fig. 18.— Hubble diagram of first normalized weight corrected supernovae.

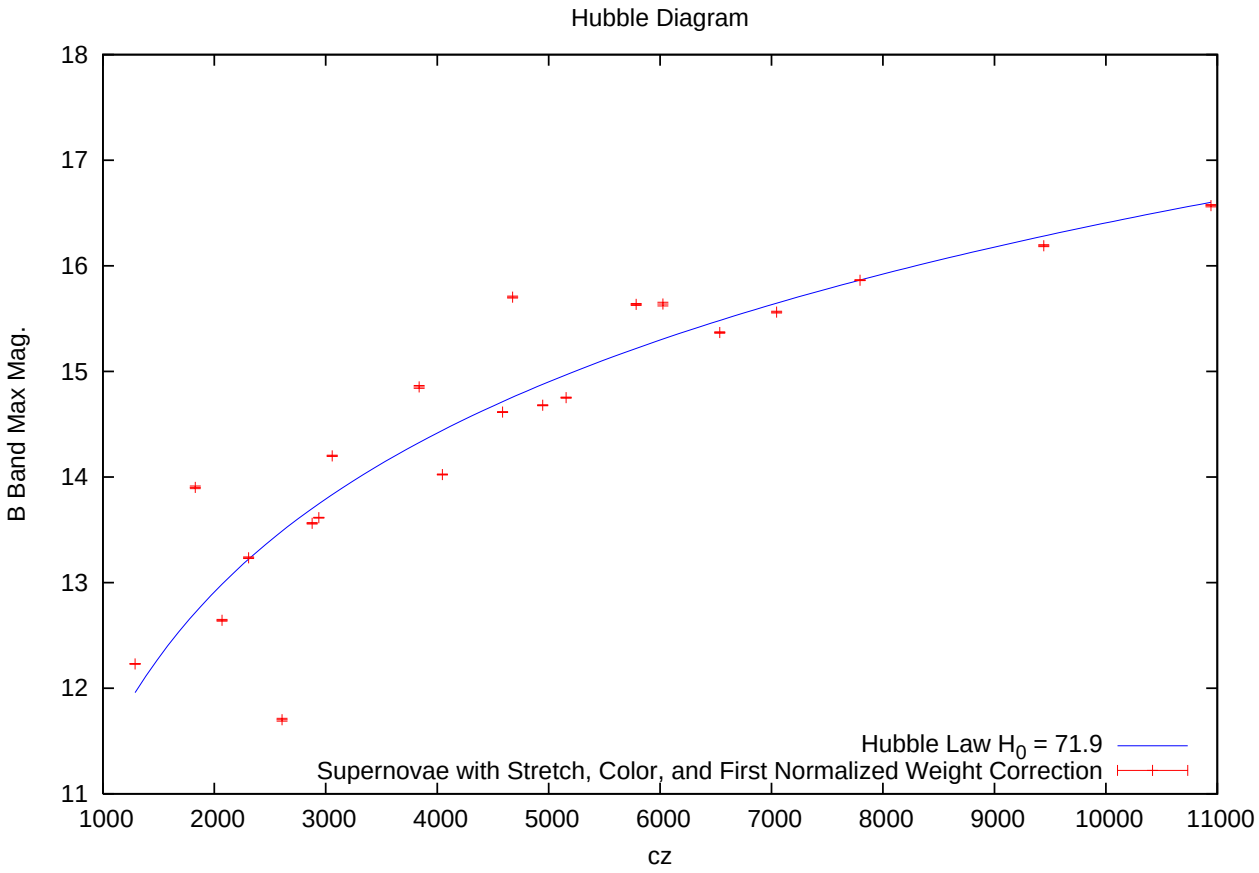

Fig. 19.— Hubble diagram of color, stretch, and first normalized weight corrected supernovae.

8. Conclusion

We find that using only the first five eigenvectors we are able to represent 95.8% of diversity within the supernova sample. It is no longer necessary to make qualitative judgments such as "SN1991T-like" when classifying supernovae; using the PCA components supernovae can be quantitatively classified into five types.

The first eigenvector has a non-zero slope which allows it to account for color. However, it also contains spectral features indicating a correlation between absorption lines and color. This suggests that color variation is not purely due to Cardelli like dust, but is partially intrinsic. We explored this possibility by warping Hsiao's template using Cardelli's law to attempt to match the supernovae and found that in many cases this does not adequately fit the spectra. We then plotted the normalized weights of the supernovae against each other along with a vector representing the normalized weights we calculated for an average spectrum warped by Cardelli dust and found that very few of the supernovae fell along this vector. We therefore conclude that color variation is primarily intrinsic.

We attempt to correlate the normalized weights with dispersion around the Hubble line. When a cut is not applied, we are able to improve the dispersion around the Hubble line by using either just the first normalized weight, or by using color, stretch, and the first normalized weight. If a 2σ cut is applied, we are unable to improve the dispersion using the normalized weights. However, the method of PCA requires only a single spectrum near maximum. Using this single spectrum we are able to improve the dispersion by 13% compared to applying no corrections. In contrast, using a color and stretch correction improves upon the normalized weights method by 6%, but requires a full, multiband lightcurve.

We've shown that PCA is useful in classifying type Ia supernovae in a quantitative manner and have used our results to argue that color excess in type Ia supernovae is intrinsic. We have also shown that PCA shows promise for reducing dispersion around the Hubble line. There are a few refinements one could do to improve this work in the future. On the data side having more supernovae would improve the quality of the components. Likewise, it has been suggested that SN1991bg does not fall on a continuum of type Ia supernovae and so removing it and other supernovae like SN1991bg before hand would likely improve the usefulness of the components for comparing and correcting more average type Ia supernovae.

We attempted to flux correct the supernovae, but the method we employed did not always improve the color. Exploring different methods of correction could improve the quality of the spectra used in the final PCA and would therefore improve the components.

Our analysis could be improved in a few ways. First, when applying the Cardelli law to Hsiao's template, we fixed R_V. Allowing this to float would provide a more complete test of whether any type of Cardelli dust can account for reddening. Second, we encountered problems with the Hubble diagrams and the dispersion corrections. This is partially due to the fact that

many of the supernovae have peculiar velocities that we did not correct for. One could correct for these by account for Virgo infall, the pull of the Great Attractor, and other local effects, or one could use higher redshift supernovae where peculiar velocity becomes unimportant. Further, the method we used to calculate the weight corrections for dispersion did not take advantage of the fact that the eigenvectors are orthonormal. It is possible to do this and get a result where the dispersion is always lowered. This method will be persued in future analysis.

9. Acknowledgments

Many people helped in the process of writing this thesis, without them it would have never been completed. I would like to thank Saul Perlmutter for allowing me to work with his group, The Supernova Cosmology Project, for the past two and a half years and for giving me an exciting and informative look into the day to day workings of a observational cosmology group. Working with Professor Perlmutter has made it clear to me that research physics is my future. I would also like to thank Nao Suzuki, who guided me when I first joined the SCP and who was always free to answer any questions I had about cosmology or my thesis. I am grateful to Mark Strovink who suggested a few ways to improve upon the methods laid out in this thesis, and am also grateful for the time David Rubin spent explaining Hubble diagrams, intrinsic dispersion, and how to get SALT2 to work. Lastly, I'd like to thank the entire SCP for their support, having so many knowledgeable people around me made writing this thesis much easier.

REFERENCES

Astier, P., Guy, J., Regnault, N., Pain, R., Aubourg, E., Balam, D., Basa, S., Carlberg, R., Fabbro, S., Fouchez, D., Hook, I., Howell, D., Lafoux, H., Neill, J., Palanque-Delabrouille, N., Perrett, K., Pritchet, C., Rich, J., Sullivan, M., Taillet, R., Aldering, G., Antilogus, P., Arsenijevic, V., Balland, C., Baumont, S., Bronder, J., Courtois, H., Ellis, R., Filiol, M., Goncalves, A., Goobar, A., Guide, D., Hardin, D., Lusset, V., Lidman, C., McMahon, R., Mouchet, M., Mourao, A., Perlmutter, S., Ripoche, P., Tao, C., & Walton, N. 2006, A&A, 447, 31

Branch, D., Baron, E., & Jeffery, D. J. 2001, ArXiv Astrophysics e-prints

Branch, D. & Tammann, G. A. 1992, ARA&A, 30, 359

Cardelli, J. A., Clayton, G. C., & Mathis, J. S. 1989, ApJ, 345, 245

Conley, A., Sullivan, M., Hsiao, E. Y., Guy, J., Astier, P., Balam, D., Balland, C., Basa, S., Carlberg, R. G., Fouchez, D., Hardin, D., Howell, D. A., Hook, I. M., Pain, R., Perrett, K., Pritchet, C. J., & Regnault, N. 2008, ArXiv e-prints, 803

Filippenko, A. V. 1997, ARA&A, 35, 309

Filippenko, A. V., Richmond, M. W., Branch, D., Gaskell, M., Herbst, W., Ford, C. H., Treffers, R. R., Matheson, T., Ho, L. C., Dey, A., Sargent, W. L. W., Small, T. A., & van Breugel, W. J. M. 1992, AJ, 104, 1543

Fixsen, D. J., Cheng, E. S., Gales, J. M., Mather, J. C., Shafer, R. A., & Wright, E. L. 1996, ApJ, 473, 576

Gomez, G., Lopez, R., & Sanchez, F. 1996, AJ, 112, 2094

Guy, J., Astier, P., Baumont, S., Hardin, D., Pain, R., Regnault, N., Basa, S., Carlberg, R. G., Conley, A., Fabbro, S., Fouchez, D., Hook, I. M., Howell, D. A., Perrett, K., Pritchet, C. J., Rich, J., Sullivan, M., Antilogus, P., Aubourg, E., Bazin, G., Bronder, J., Filiol, M., Palanque-Delabrouille, N., Ripoche, P., & Ruhlmann-Kleider, V. 2007, A&A, 466, 11

Hamuy, M., Maza, J., Phillips, M. M., Suntzeff, N. B., Wischnjewsky, M., Smith, R. C., Antezana, R., Wells, L. A., Gonzalez, L. E., Gigoux, P., Navarrete, M., Barrientos, F., Lamontagne, R., della Valle, M., Elias, J. E., Phillips, A. C., Odewahn, S. C., Baldwin, J. A., Walker, A. R., Williams, T., Sturch, C. R., Baganoff, F. K., Chaboyer, B. C., Schommer, R. A., Tirado, H., Hernandez, M., Ugarte, P., Guhathakurta, P., Howell, S. B., Szkody, P., Schmidtke, P. C., & Roth, J. 1993, AJ, 106, 2392

Hamuy, M., Phillips, M. M., Maza, J., Suntzeff, N. B., Schommer, R. A., & Aviles, R. 1995, AJ, 109, 1

Hinshaw, G., Weiland, J. L., Hill, R. S., Odegard, N., Larson, D., Bennett, C. L., Dunkley, J., Gold, B., Greason, M. R., Jarosik, N., Komatsu, E., Nolta, M. R., Page, L., Spergel, D. N., Wollack, E., Halpern, M., Kogut, A., Limon, M., Meyer, S. S., Tucker, G. S., & Wright, E. L. 2008, ArXiv e-prints

Hsiao, E. Y., Conley, A., Howell, D. A., Sullivan, M., Pritchet, C. J., Carlberg, R. G., Nugent, P. E., & Phillips, M. M. 2007, ApJ, 663, 1187

Jha, S., Kirshner, R. P., Challis, P., Garnavich, P. M., Matheson, T., Soderberg, A. M., Graves, G. J. M., Hicken, M., Alves, J. F., Arce, H. G., Balog, Z., Barmby, P., Barton, E. J., Berlind, P., Bragg, A. E., Briceño, C., Brown, W. R., Buckley, J. H., Caldwell, N., Calkins, M. L., Carter, B. J., Concannon, K. D., Donnelly, R. H., Eriksen, K. A., Fabricant, D. G., Falco, E. E., Fiore, F., Garcia, M. R., Gómez, M., Grogin, N. A., Groner, T., Groot, P. J., Haisch, Jr., K. E., Hartmann, L., Hergenrother, C. W., Holman, M. J., Huchra, J. P., Jayawardhana, R., Jerius, D., Kannappan, S. J., Kim, D.-W., Kleyna, J. T., Kochanek, C. S., Koranyi, D. M., Krockenberger, M., Lada, C. J., Luhman, K. L., Luu, J. X., Macri, L. M., Mader, J. A., Mahdavi, A., Marengo, M., Marsden, B. G., McLeod, B. A., McNamara, B. R., Megeath, S. T., Moraru, D., Mossman, A. E., Muench, A. A., Muñoz, J. A., Muzerolle, J., Naranjo, O., Nelson-Patel, K., Pahre, M. A., Patten, B. M., Peters, J., Peters, W., Raymond, J. C., Rines, K., Schild, R. E., Sobczak, G. J., Spahr, T. B., Stauffer, J. R., Stefanik, R. P., Szentgyorgyi, A. H., Tollestrup, E. V., Väisänen, P., Vikhlinin, A., Wang, Z., Willner, S. P., Wolk, S. J., Zajac, J. M., Zhao, P., & Stanek, K. Z. 2006, AJ, 131, 527

Knop, R. & The Supernovae Cosmology Project. 2003, astro-ph/0309368

Kowal, C. T. 1968, AJ, 73, 1021

Kowalski, M., Rubin, D., Aldering, G., Agostinho, R. J., Amadon, A., Amanullah, R., Balland, C., Barbary, K., Blanc, G., Challis, P. J., Conley, A., Connolly, N. V., Covarrubias, R., Dawson, K. S., Deustua, S. E., Ellis, R., Fabbro, S., Fadeyev, V., Fan, X., Farris, B., Folatelli, G., Frye, B. L., Garavini, G., Gates, E. L., Germany, L., Goldhaber, G., Goldman, B., Goobar, A., Groom, D. E., Haissinski, J., Hardin, D., Hook, I., Kent, S., Kim, A. G., Knop, R. A., Lidman, C., Linder, E. V., Mendez, J., Meyers, J., Miller, G. J., Moniez, M., Mourao, A. M., Newberg, H., Nobili, S., Nugent, P. E., Pain, R., Perdereau, O., Perlmutter, S., Phillips, M. M., Prasad, V., Quimby, R., Regnault, N., Rich, J., Rubenstein, E. P., Ruiz-Lapuente, P., Santos, F. D., Schaefer, B. E., Schommer, R. A., Smith, R. C., Soderberg, A. M., Spadafora, A. L., Strolger, L. G., Strovink, M., Suntzeff, N. B., Suzuki, N., Thomas, R. C., Walton, N. A., Wang, L., & Wood-Vasey, W. M. 2008, ArXiv e-prints

Matheson, T., Kirshner, R. P., Challis, P., Jha, S., Garnavich, P. M., Berlind, P., Calkins, M. L., Blondin, S., Balog, Z., Bragg, A. E., Caldwell, N., Dendy Concannon, K., Falco, E. E., Graves, G. J. M., Huchra, J. P., Kuraszkiewicz, J., Mader, J. A., Mahdavi, A., Phelps, M., Rines, K., Song, I., & Wilkes, B. J. 2008, AJ, 135, 1598

Minkowski, R. 1941, PASP, 53, 224

Nugent, P., Kim, A., & Perlmutter, S. 2002, PASP, 114, 803

Nugent, P., Phillips, M., Baron, E., Branch, D., & Hauschildt, P. 1995, ApJ, 455, L147+

Perlmutter, S., Aldering, G., Goldhaber, G., Knop, R. A., Nugent, P., Castro, P. G., Deustua, S., Fabbro, S., Goobar, A., Groom, D. E., Hook, I. M., Kim, A. G., Kim, M. Y., Lee, J. C., Nunes, N. J., Pain, R., Pennypacker, C. R., Quimby, R., Lidman, C., Ellis, R. S., Irwin, M., McMahon, R. G., Ruiz-Lapuente, P., Walton, N., Schaefer, B., Boyle, B. J., Filippenko, A. V., Matheson, T., Fruchter, A. S., Panagia, N., Newberg, H. J. M., Couch, W. J., & The Supernova Cosmology Project. 1999, ApJ, 517, 565

Perlmutter, S., Gabi, S., Goldhaber, G., Goobar, A., Groom, D. E., Hook, I. M., Kim, A. G., Kim, M. Y., Lee, J. C., Pain, R., Pennypacker, C. R., Small, I. A., Ellis, R. S., McMahon, R. G., Boyle, B. J., Bunclark, P. S., Carter, D., Irwin, M. J., Glazebrook, K., Newberg, H. J. M., Filippenko, A. V., Matheson, T., Dopita, M., Couch, W. J., & The Supernova Cosmology Project. 1997, ApJ, 483, 565

Perlmutter, S. & Schmidt, B. P. 2003, in Lecture Notes in Physics, Berlin Springer Verlag, Vol. 598, Supernovae and Gamma-Ray Bursters, ed. K. Weiler, 195–217

Person, K. 1901, Philosophical Magazine

Phillips, M. M. 1993, ApJ, 413, L105

Riess, A. G., Filippenko, A. V., Challis, P., Clocchiatti, A., Diercks, A., Garnavich, P. M., Gilliland, R. L., Hogan, C. J., Jha, S., Kirshner, R. P., Leibundgut, B., Phillips, M. M., Reiss, D., Schmidt, B. P., Schommer, R. A., Smith, R. C., Spyromilio, J., Stubbs, C., Suntzeff, N. B., & Tonry, J. 1998, AJ, 116, 1009

Riess, A. G., Li, W., Stetson, P. B., Filippenko, A. V., Greenhill, L., & Jha, S. 2005, in Bulletin of the American Astronomical Society, Vol. 37, Bulletin of the American Astronomical Society, 1460

Riess, A. G., Press, W. H., & Kirshner, R. P. 1996a, ApJ, 473, 88

—. 1996b, ApJ, 473, 588

Sullivan, M., Ellis, R. S., Aldering, G., Amanullah, R., Astier, P., Blanc, G., Burns, M. S., Conley, A., Deustua, S. E., Doi, M., Fabbro, S., Folatelli, G., Fruchter, A. S., Garavini, G., Gibbons, R., Goldhaber, G., Goobar, A., Groom, D. E., Hardin, D., Hook, I., Howell, D. A., Irwin, M., Kim, A. G., Knop, R. A., Lidman, C., McMahon, R., Mendez, J., Nobili, S., Nugent, P. E., Pain, R., Panagia, N., Pennypacker, C. R., Perlmutter, S., Quimby, R., Raux, J., Regnault, N., Ruiz-Lapuente, P., Schaefer, B., Schahmaneche, K., Spadafora, A. L., Walton, N. A., Wang, L., Wood-Vasey, W. M., & Yasuda, N. 2003, MNRAS, 340, 1057

Suzuki, N. 2005, ApJ*submitted*, astro-ph/0503248

Suzuki, N., Tytler, D., Kirkman, D., O'Meara, J. M., & Lubin, D. 2005, ApJ, 618, 592

Turatto, M., Benetti, S., Cappellaro, E., Danziger, I. J., Della Valle, M., Gouiffes, C., Mazzali, P. A., & Patat, F. 1996, MNRAS, 283, 1

Vaughan, T. E., Branch, D., Miller, D. L., & Perlmutter, S. 1995, ApJ, 439, 558

Appendix: A

With the exception of SN1991T and SN1991bg, we provide four figures for each supernova used in this analysis. The first figure shows a blue spectrum, and possibly a red spectrum. If there is only a blue spectrum, then we applied no flux correction to the raw data, and only re-binned it and trimmed the edges off before using it in our analysis. If we show a red and a blue spectrum, then the red spectrum represents the data before flux calibration, and the blue spectrum shows the data we finally used after flux calibration.

The second figure shows a step in our flux calibration process. We fit a light curve with SALT2 and used SALT2 to generate an artificial spectrum for the supernova. We then re-binned both the supernova's spectrum and the SALT2 spectrum to 500 Å bins. We compared these, and plotted a point for each bin which represents the number we'd have to multiple the data bin by to match the SALT2 bin. If a pink line is shown, then this is the function we used for the flux calibration. If no line is shown, then no flux calibration was performed.

The third figure shows the light curve fit by SALT2. The x scale of this plot is adjusted to only include the portion that SALT2 fit. While other points exist they are not included in the fit and so are not plotted.

The fourth figure shows the supernova spectrum, and the best fit using a χ^2 fit of Hsiao's template warped with a Cardelli law. These plots were created to give an indication of the inability of a single parameter warp to account for all of a supernova's features.

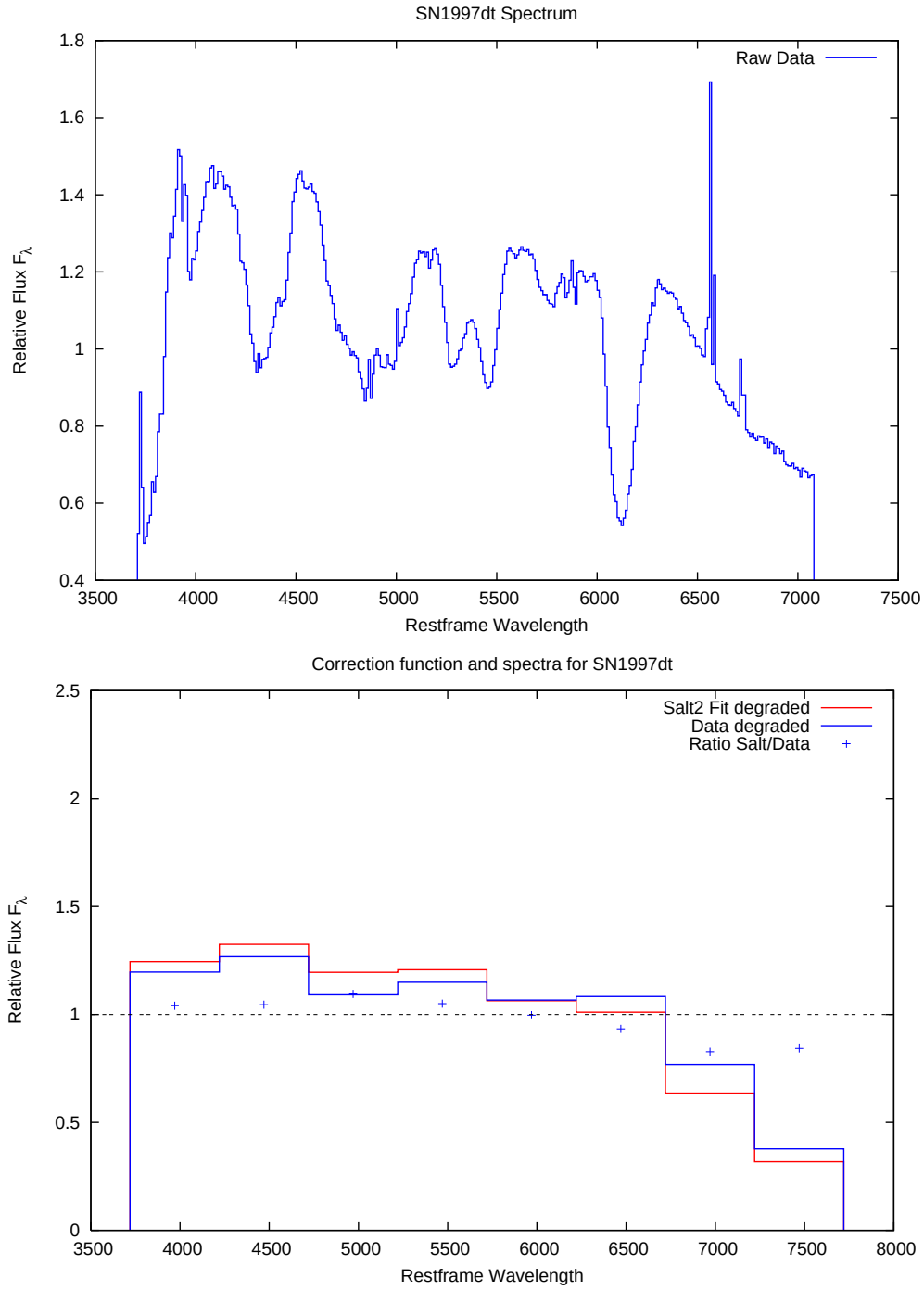

Fig. 20.— SN1997dt spectrum before and after warping, as well as the correction function used to warp.

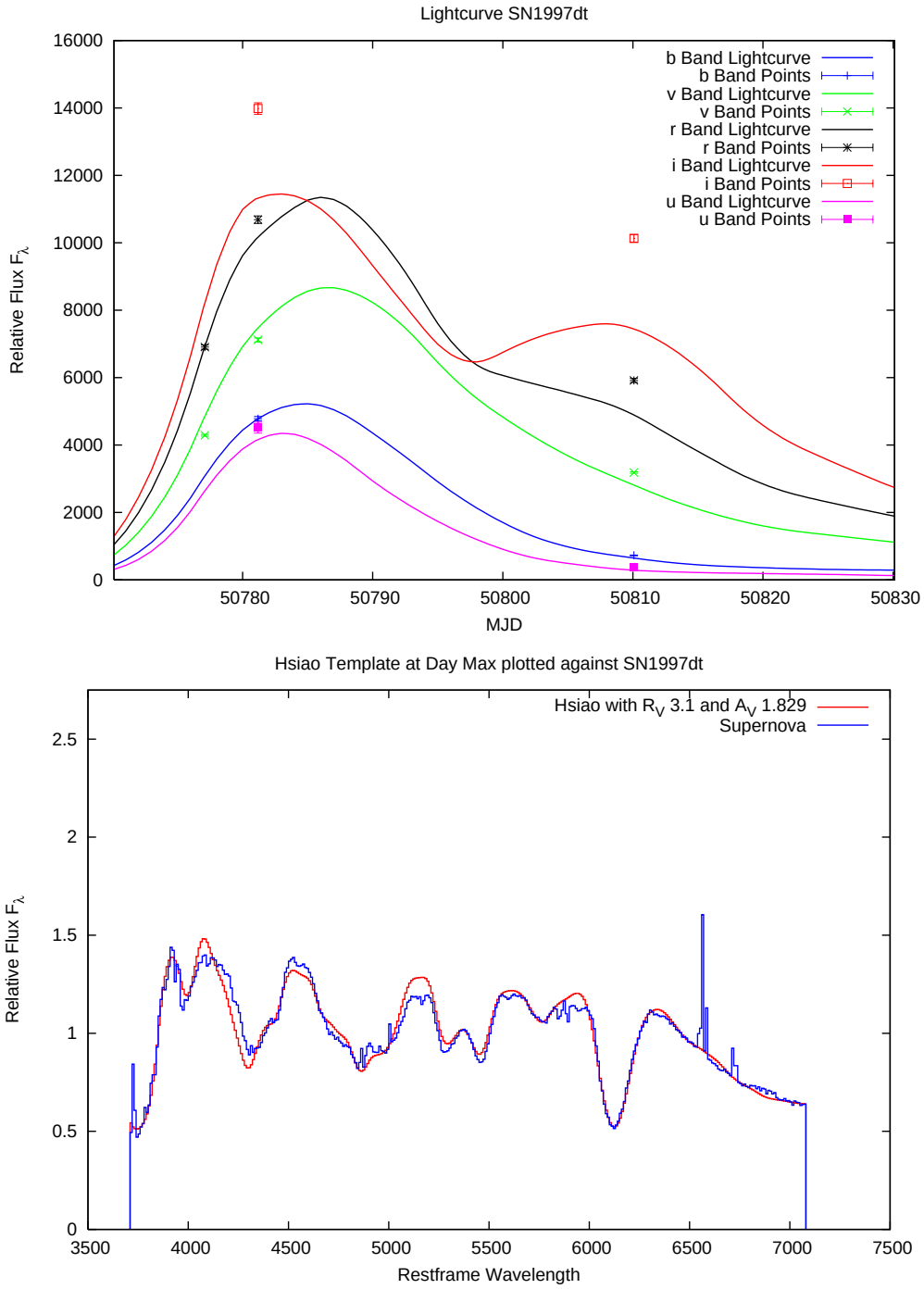

Fig. 21.— SN1997dt light curve fit, as well as the best fit for Hsiao template warped using the Cardelli law to match the spectrum.

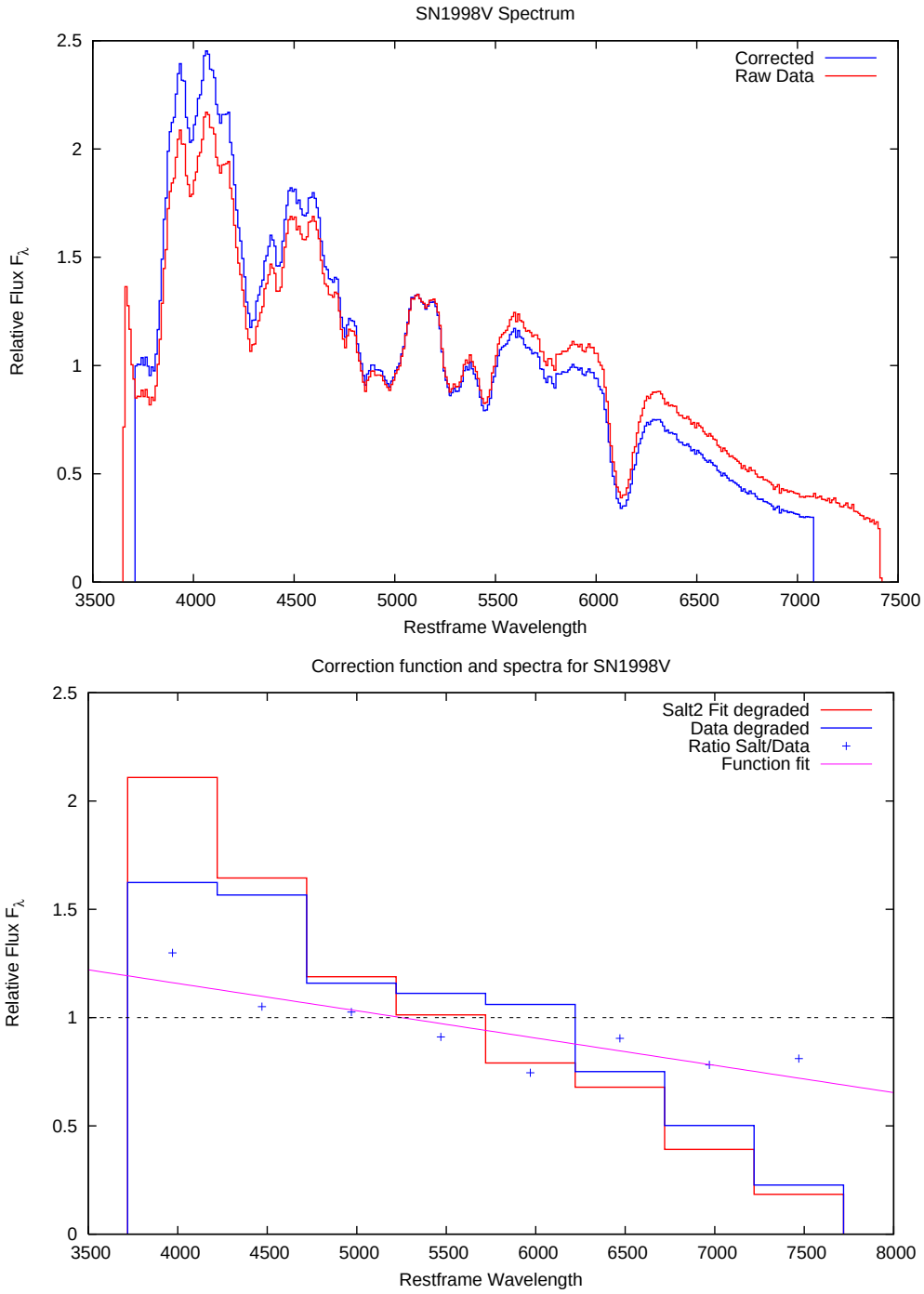

Fig. 22.— SN1998V spectrum before and after warping, as well as the correction function used to warp.

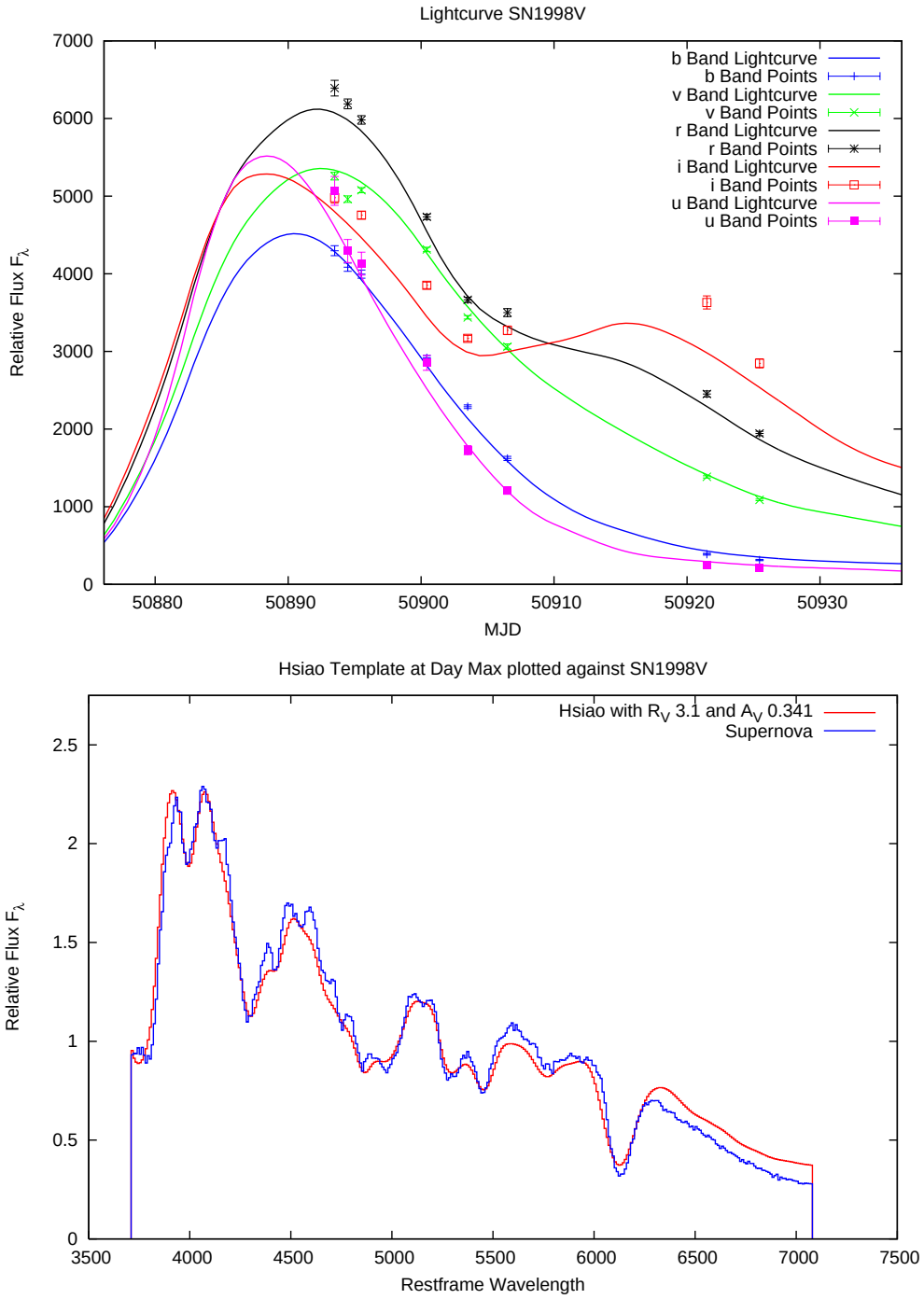

Fig. 23.— SN1998V light curve fit, as well as the best fit for Hsiao template warped using the Cardelli law to match the spectrum.

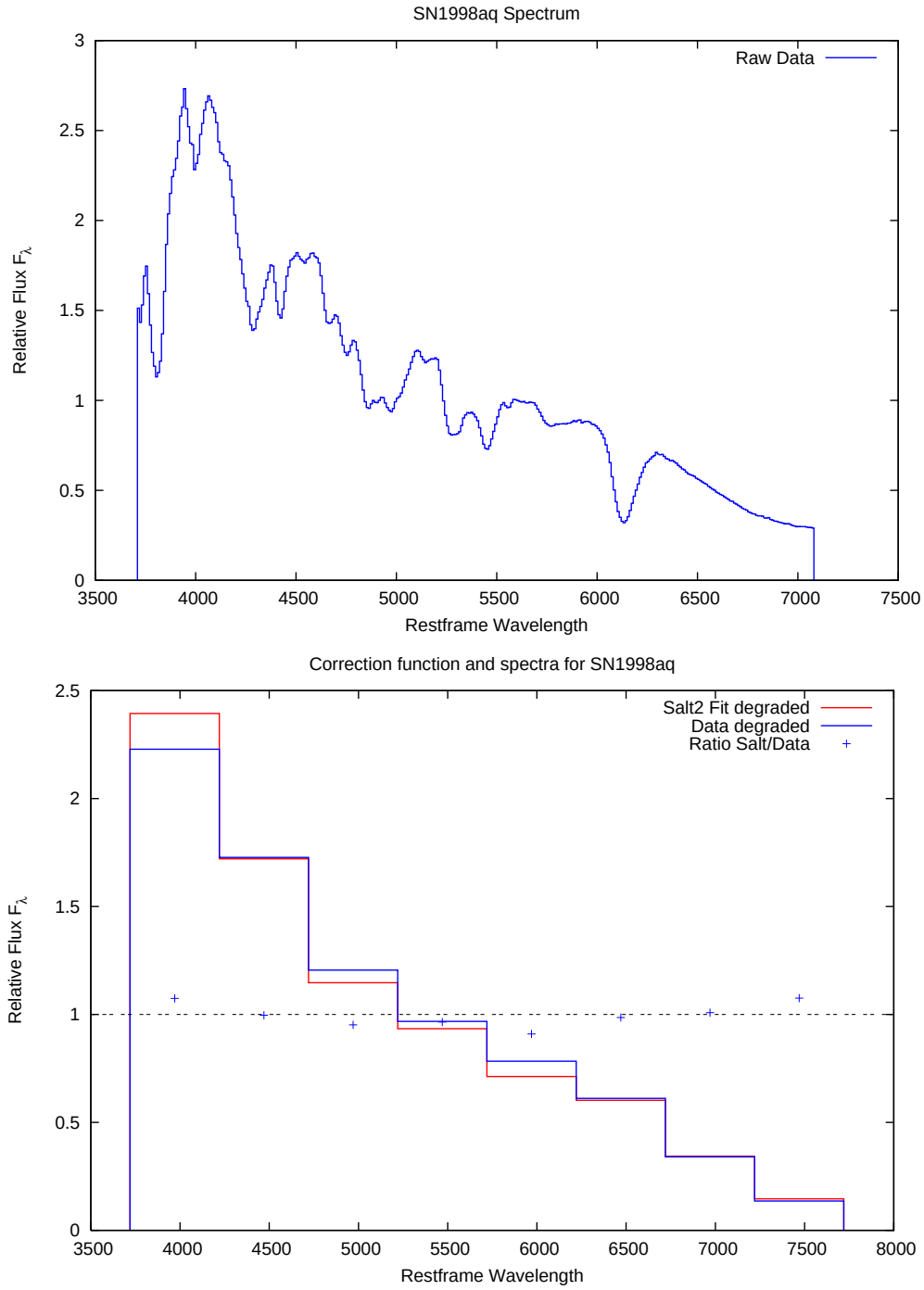

Fig. 24.— SN1998aq spectrum before and after warping, as well as the correction function used to warp.

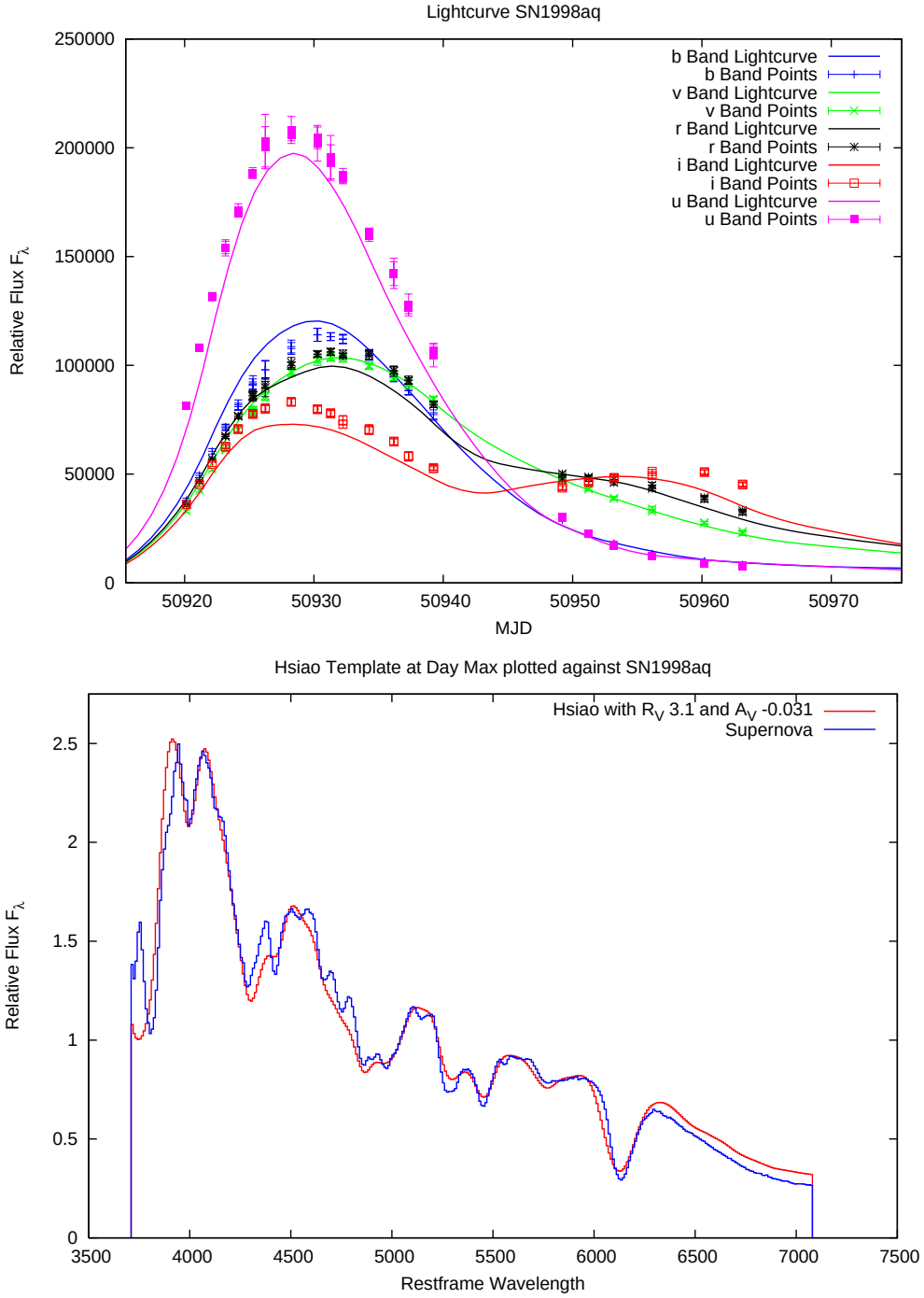

Fig. 25.— SN1998aq light curve fit, as well as the best fit for Hsiao template warped using the Cardelli law to match the spectrum.

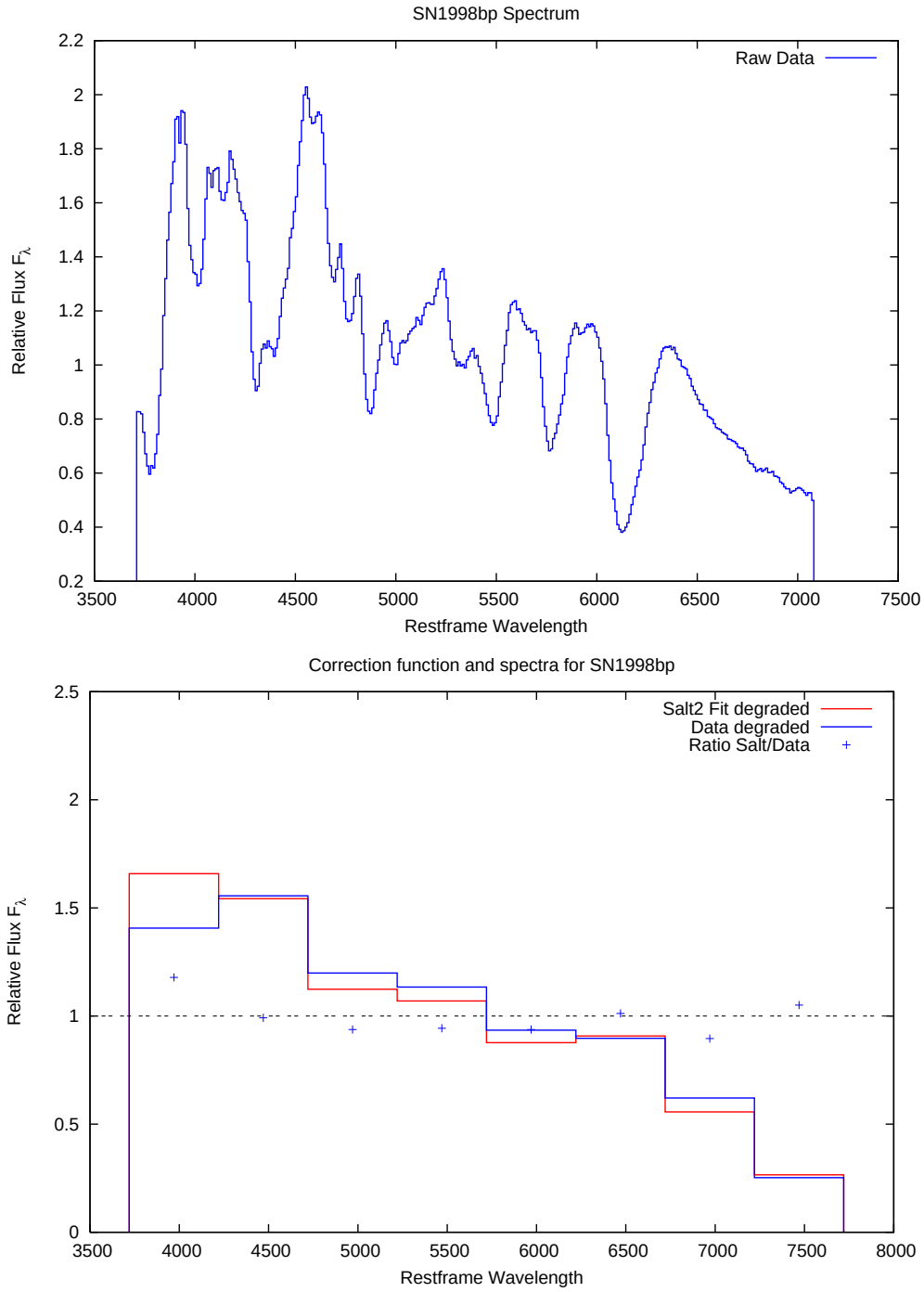

Fig. 26.— SN1998bp spectrum before and after warping, as well as the correction function used to warp.

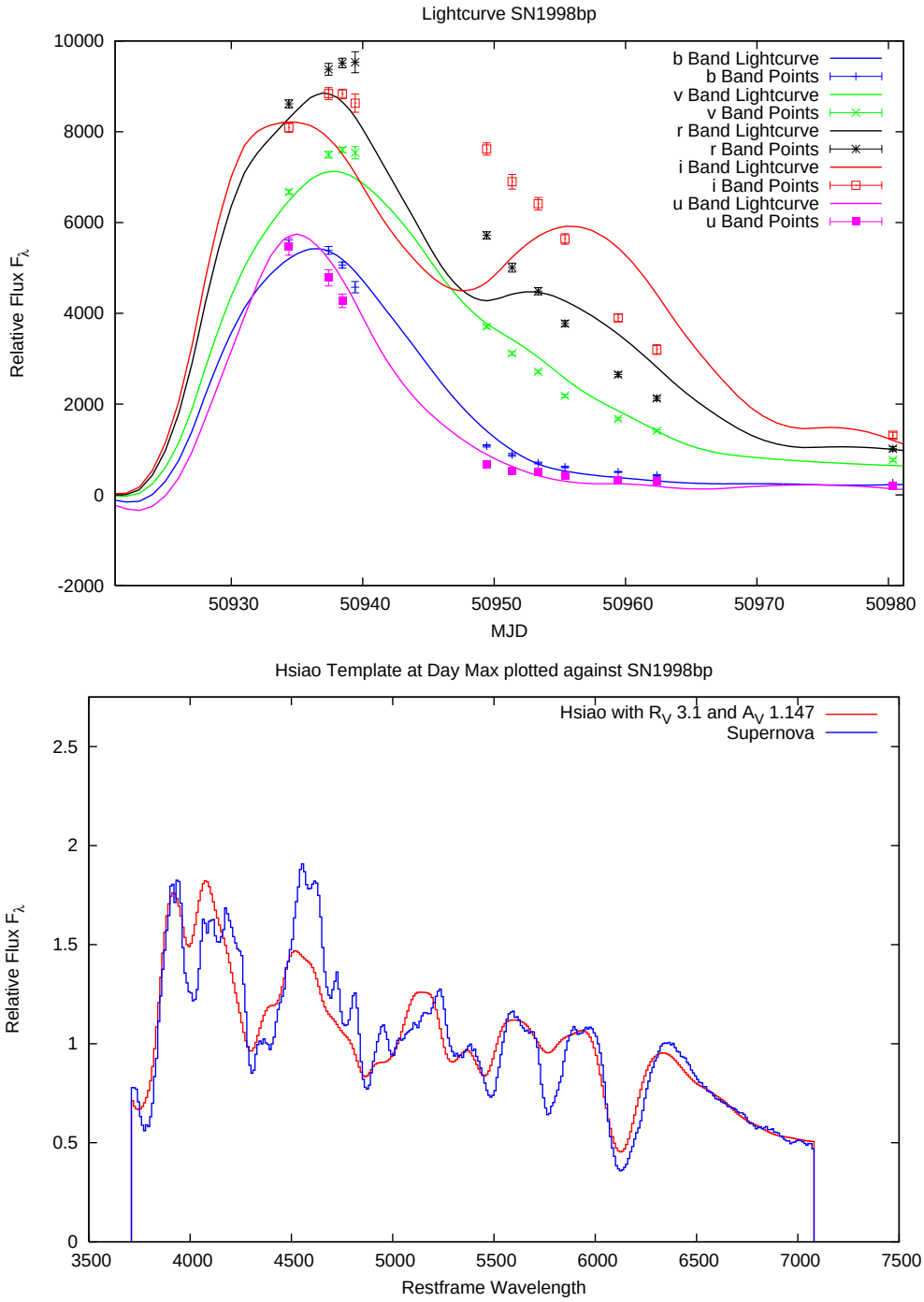

Fig. 27.— SN1998bp light curve fit, as well as the best fit for Hsiao template warped using the Cardelli law to match the spectrum.

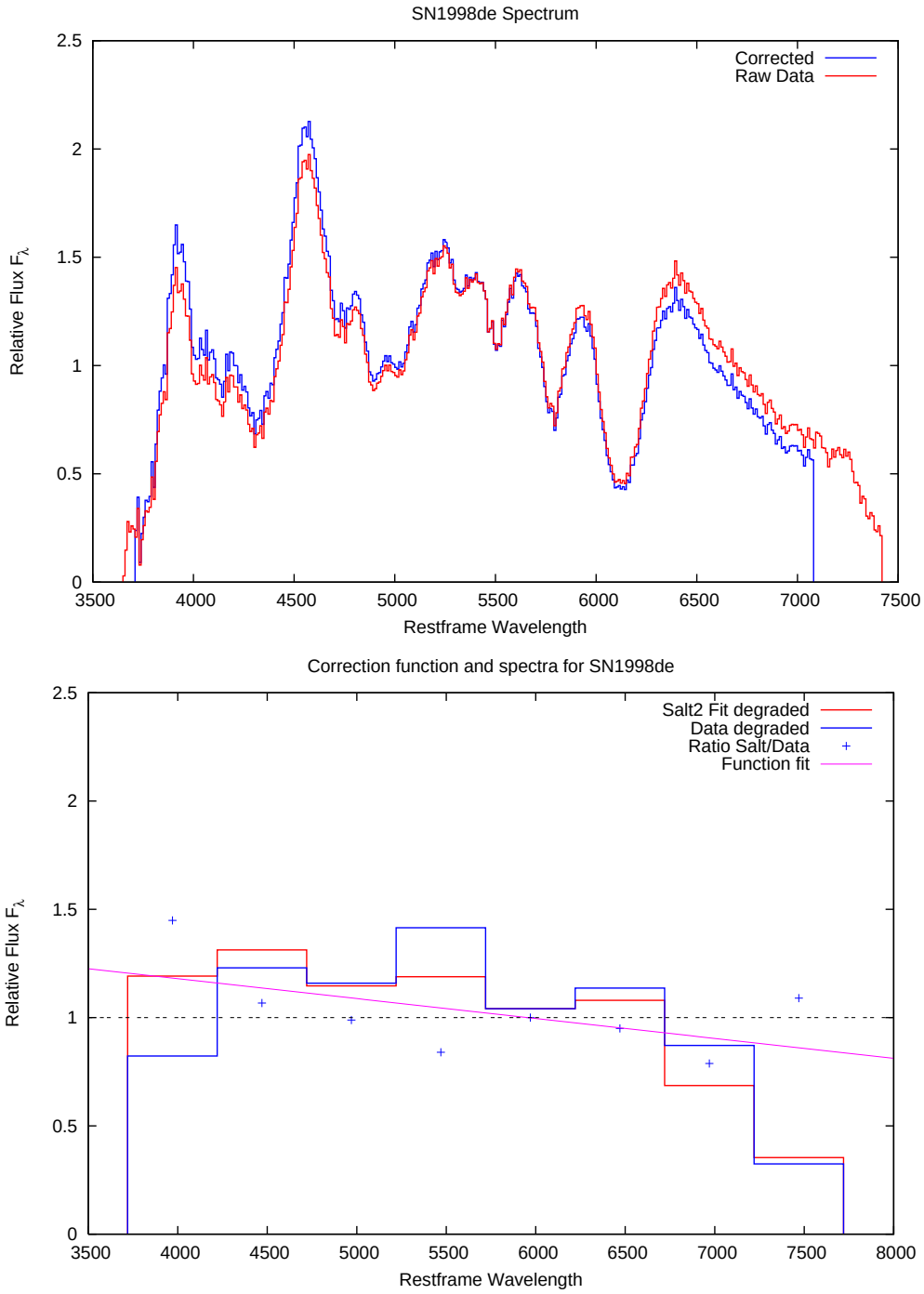

Fig. 28.— SN1998de spectrum before and after warping, as well as the correction function used to warp.

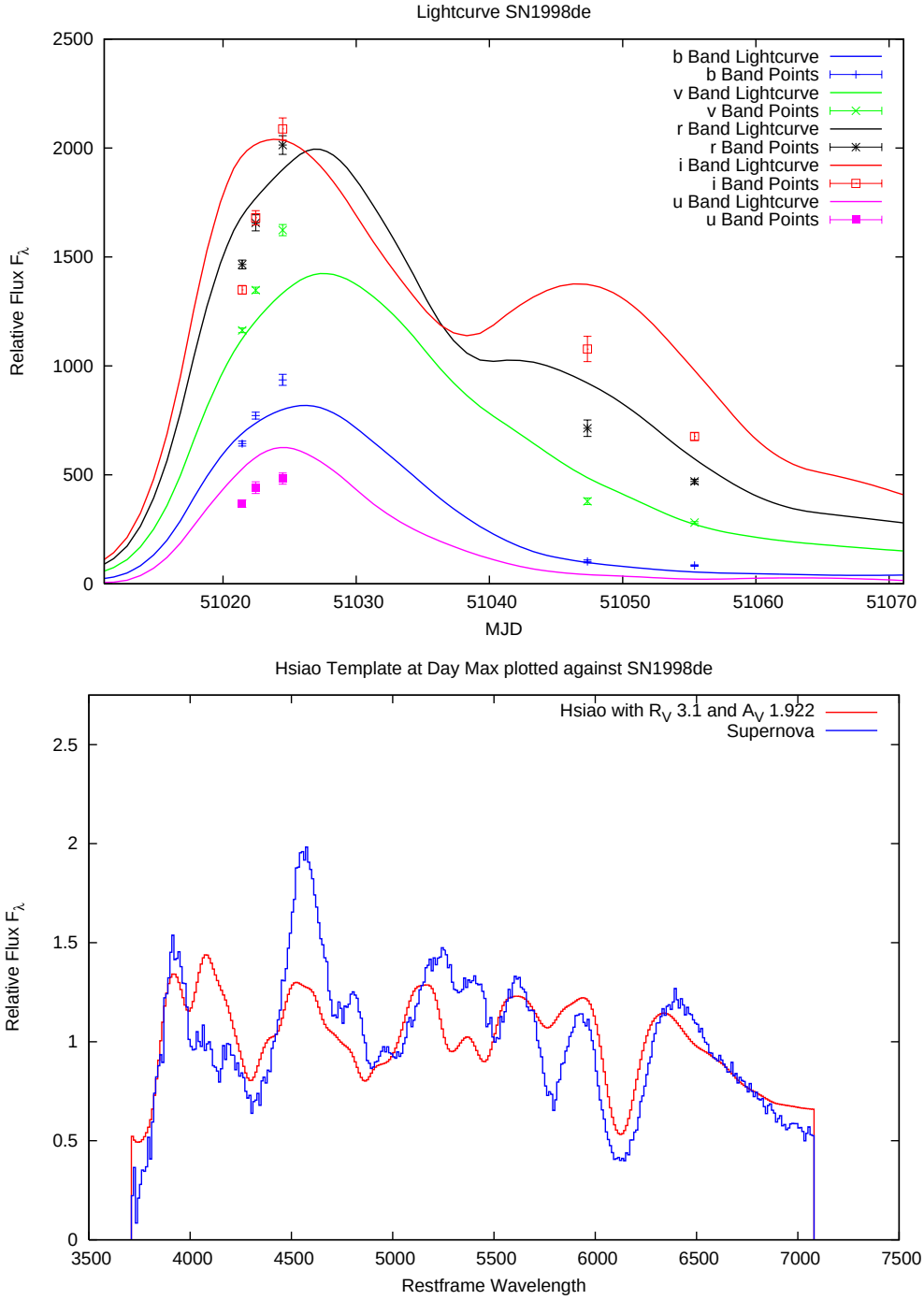

Fig. 29.— SN1998de light curve fit, as well as the best fit for Hsiao template warped using the Cardelli law to match the spectrum.

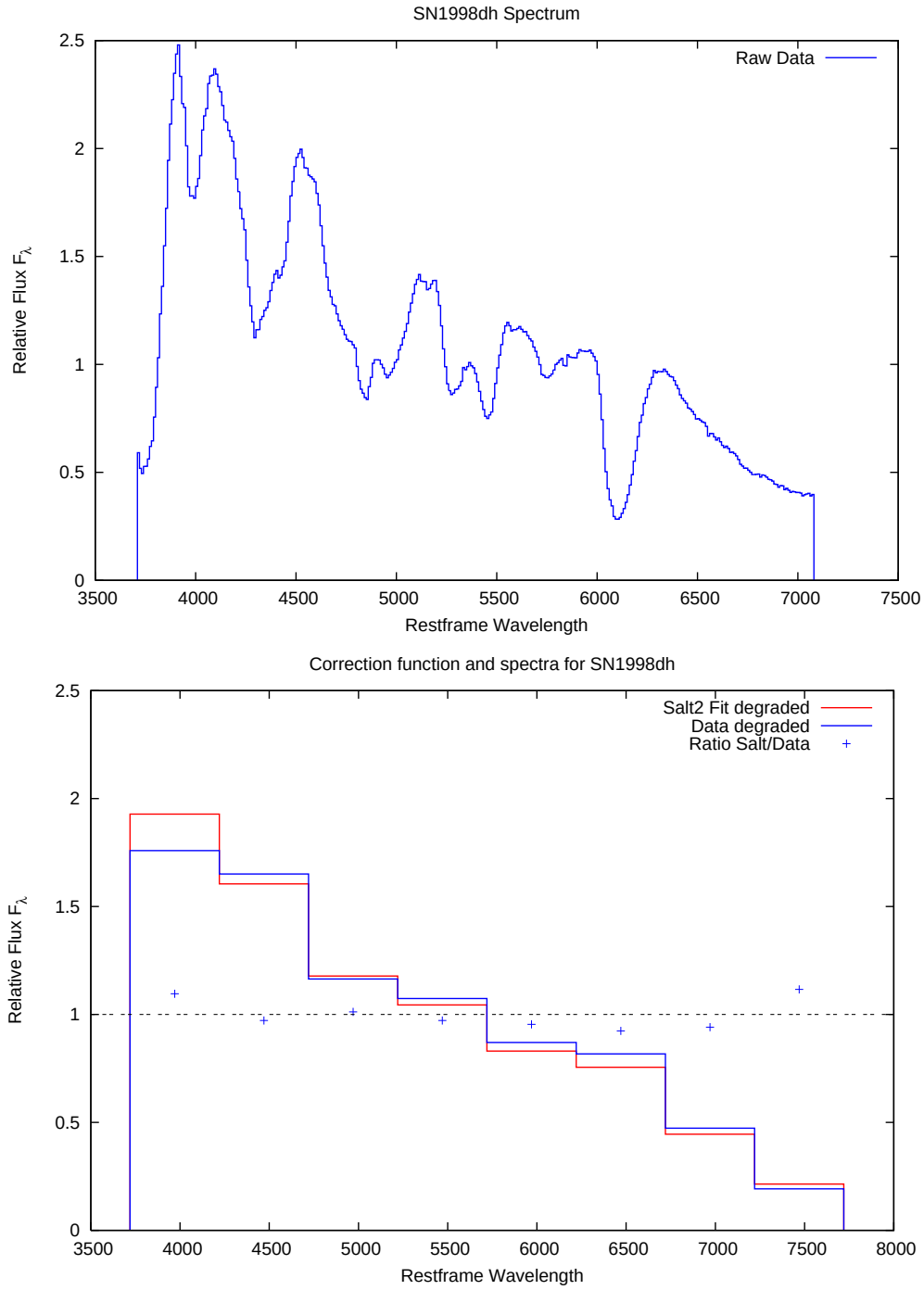

Fig. 30.— SN1998dh spectrum before and after warping, as well as the correction function used to warp.

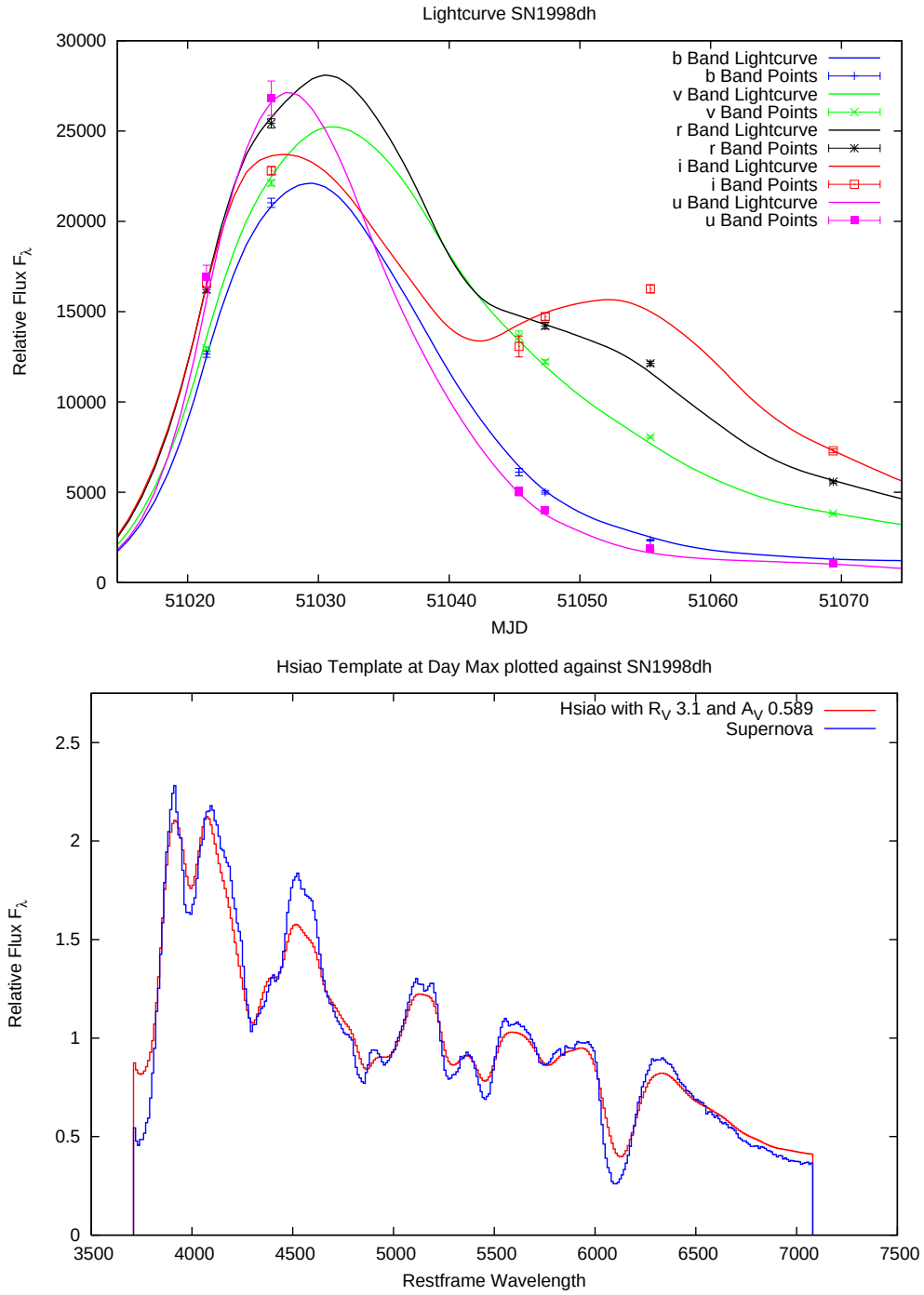

Fig. 31.— SN1998dh light curve fit, as well as the best fit for Hsiao template warped using the Cardelli law to match the spectrum.

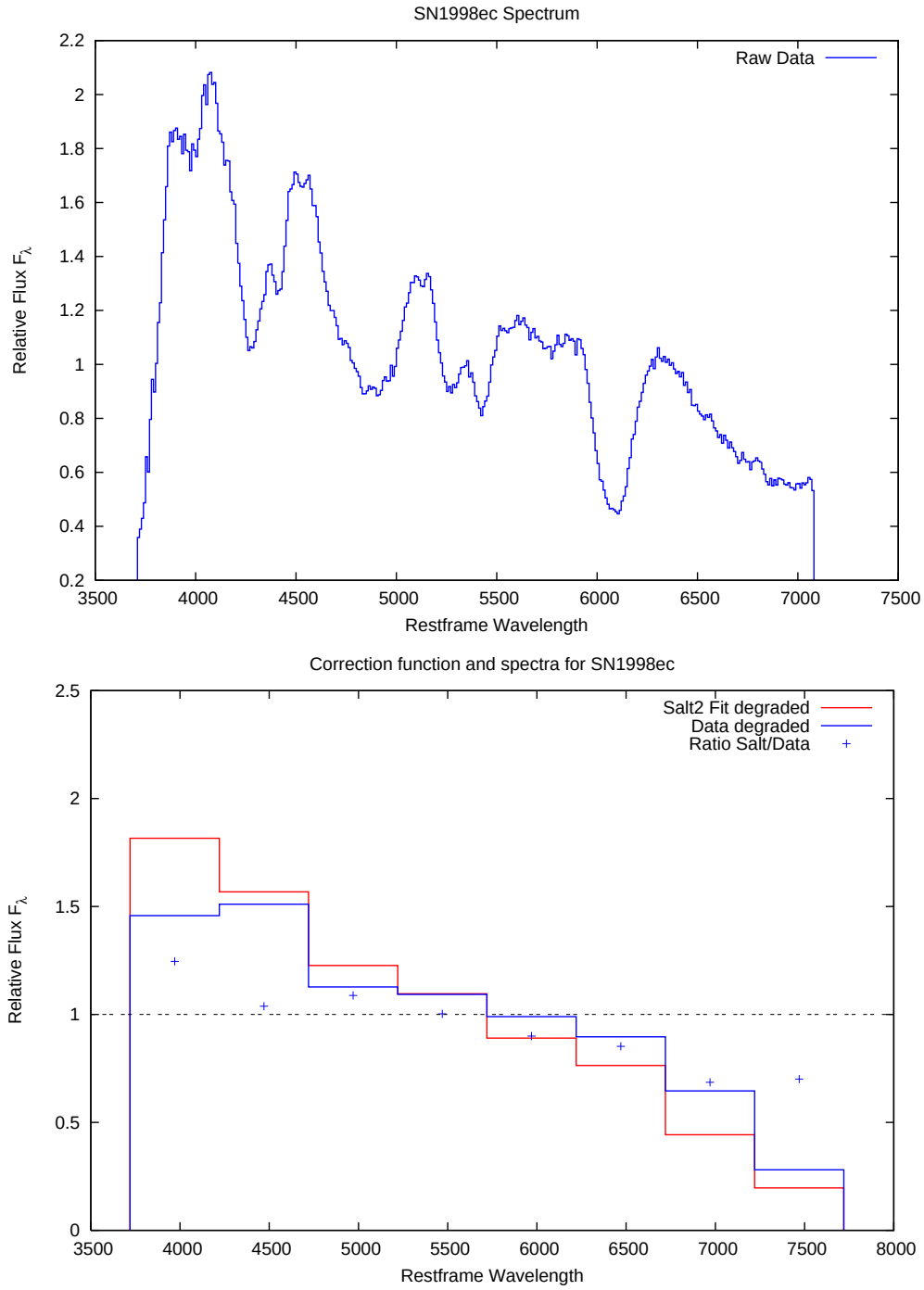

Fig. 32.— SN1998ec spectrum before and after warping, as well as the correction function used to warp.

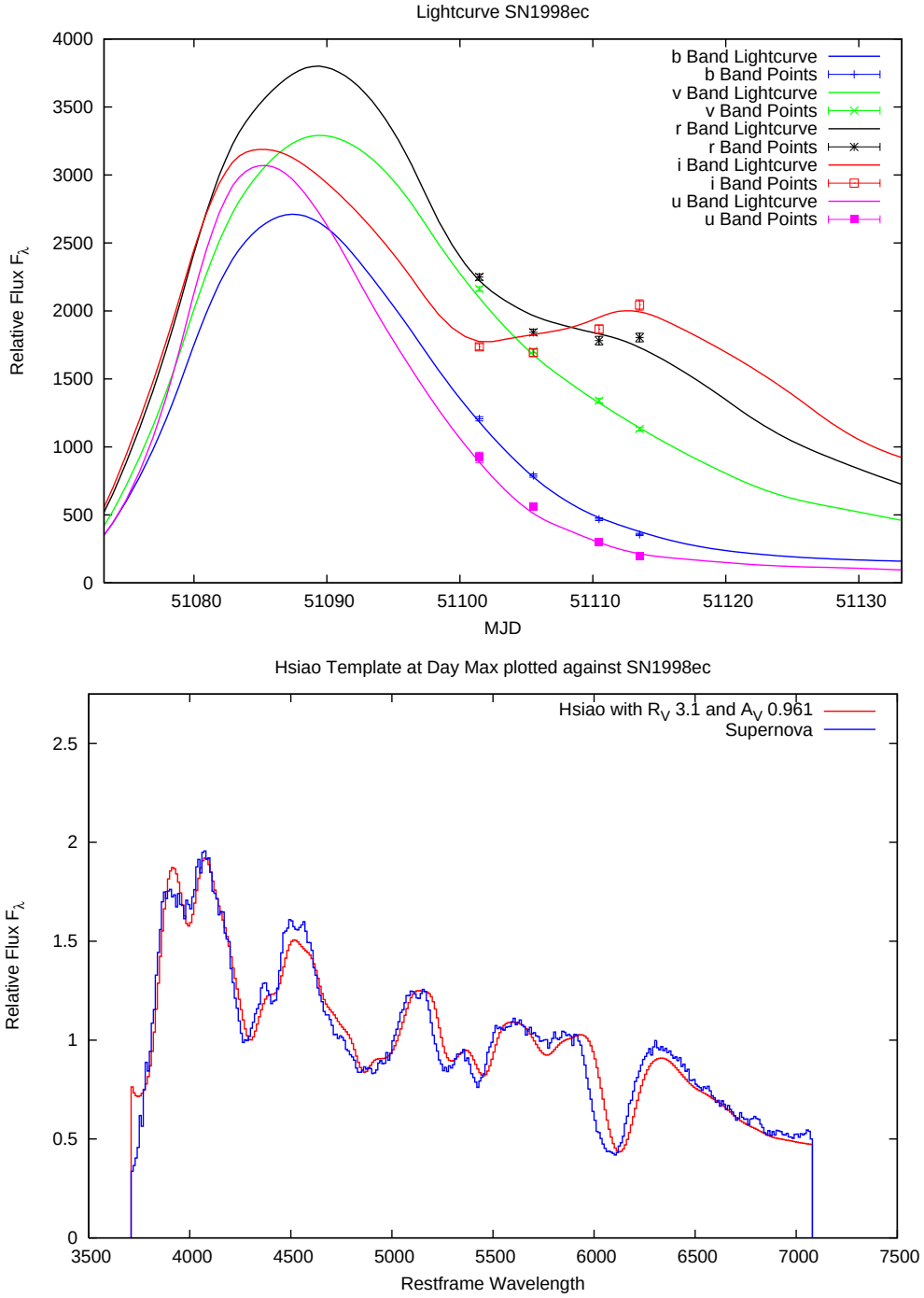

Fig. 33.— SN1998ec light curve fit, as well as the best fit for Hsiao template warped using the Cardelli law to match the spectrum.

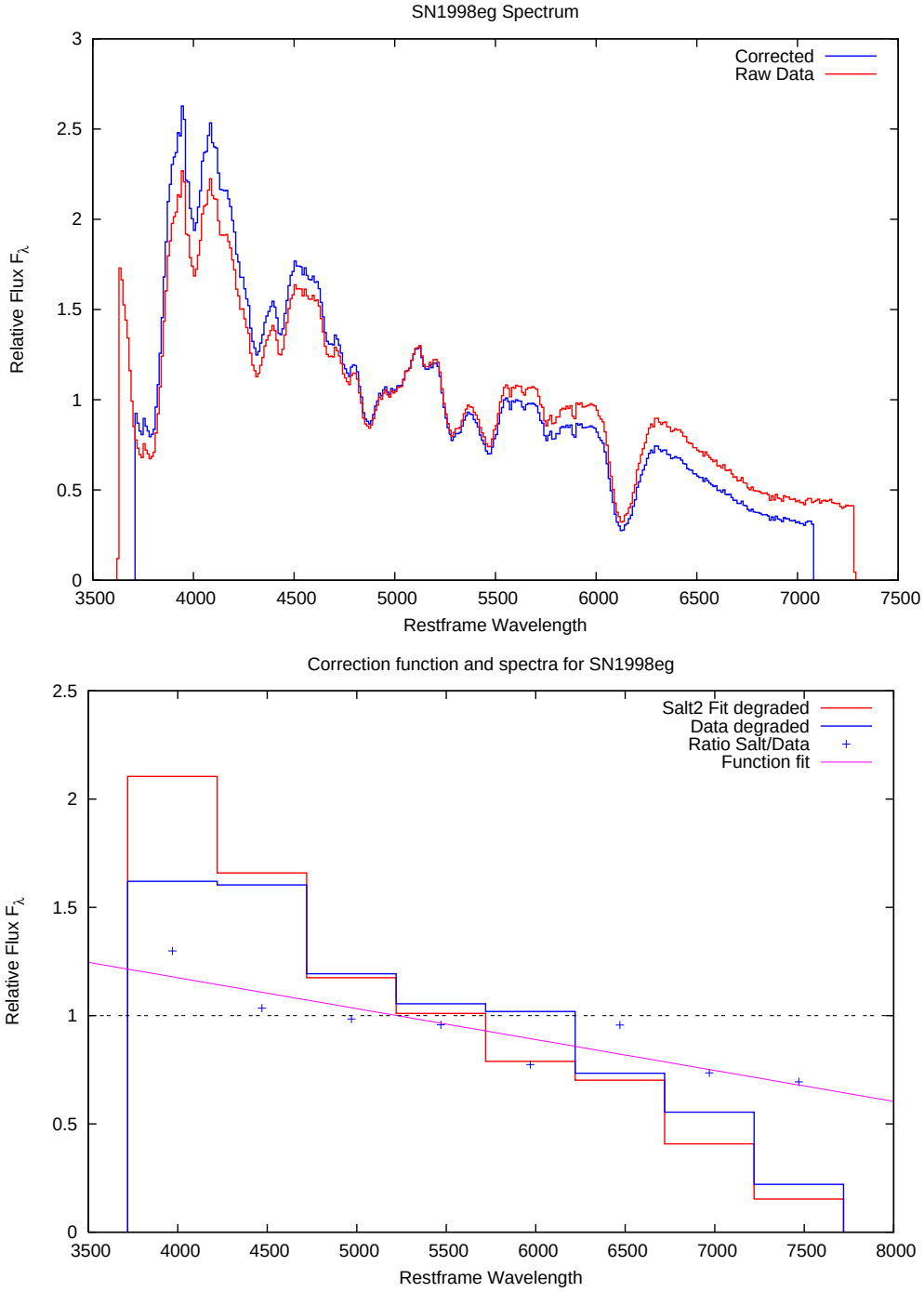

Fig. 34.— SN1998eg spectrum before and after warping, as well as the correction function used to warp.

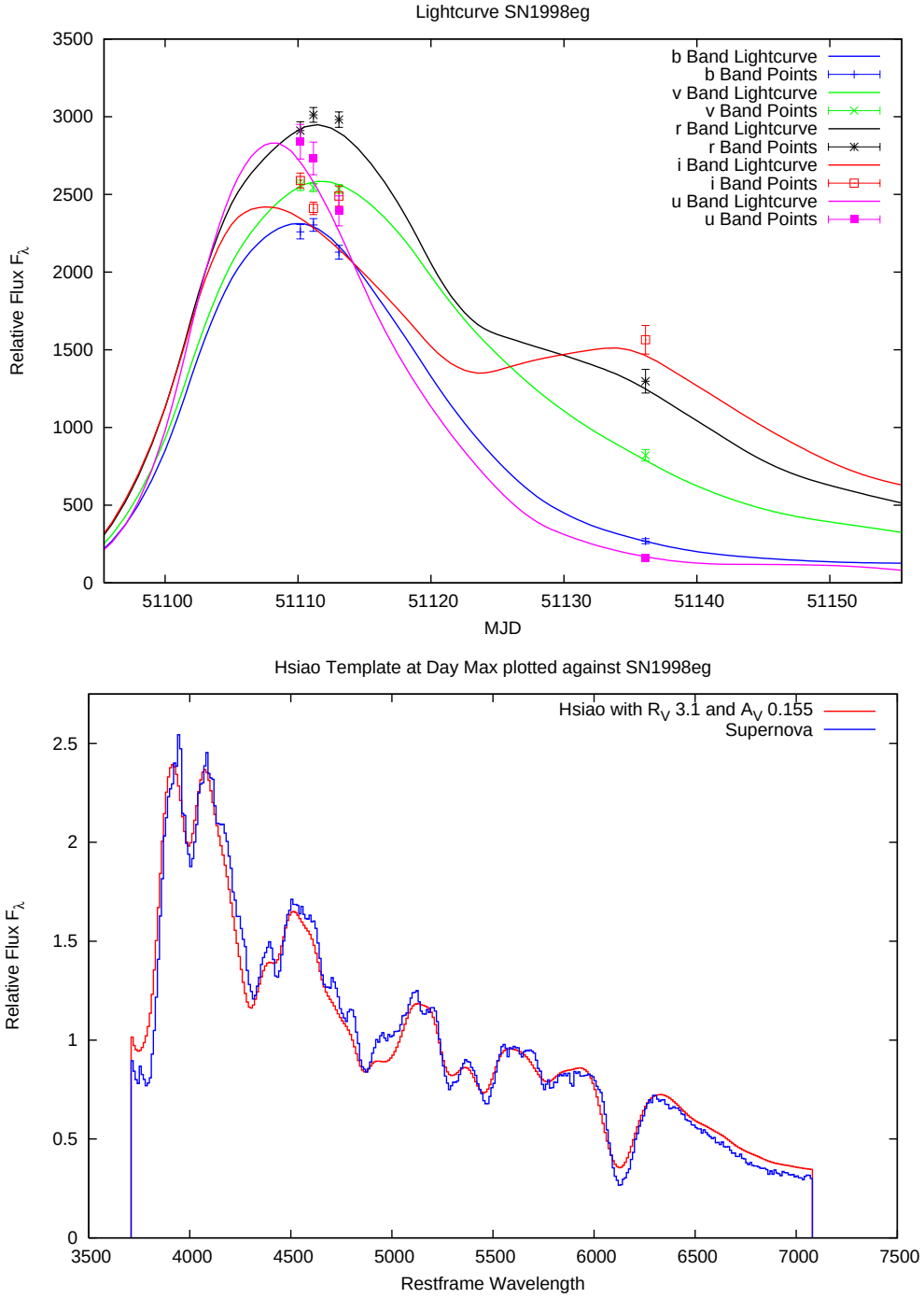

Fig. 35.— SN1998eg light curve fit, as well as the best fit for Hsiao template warped using the Cardelli law to match the spectrum.

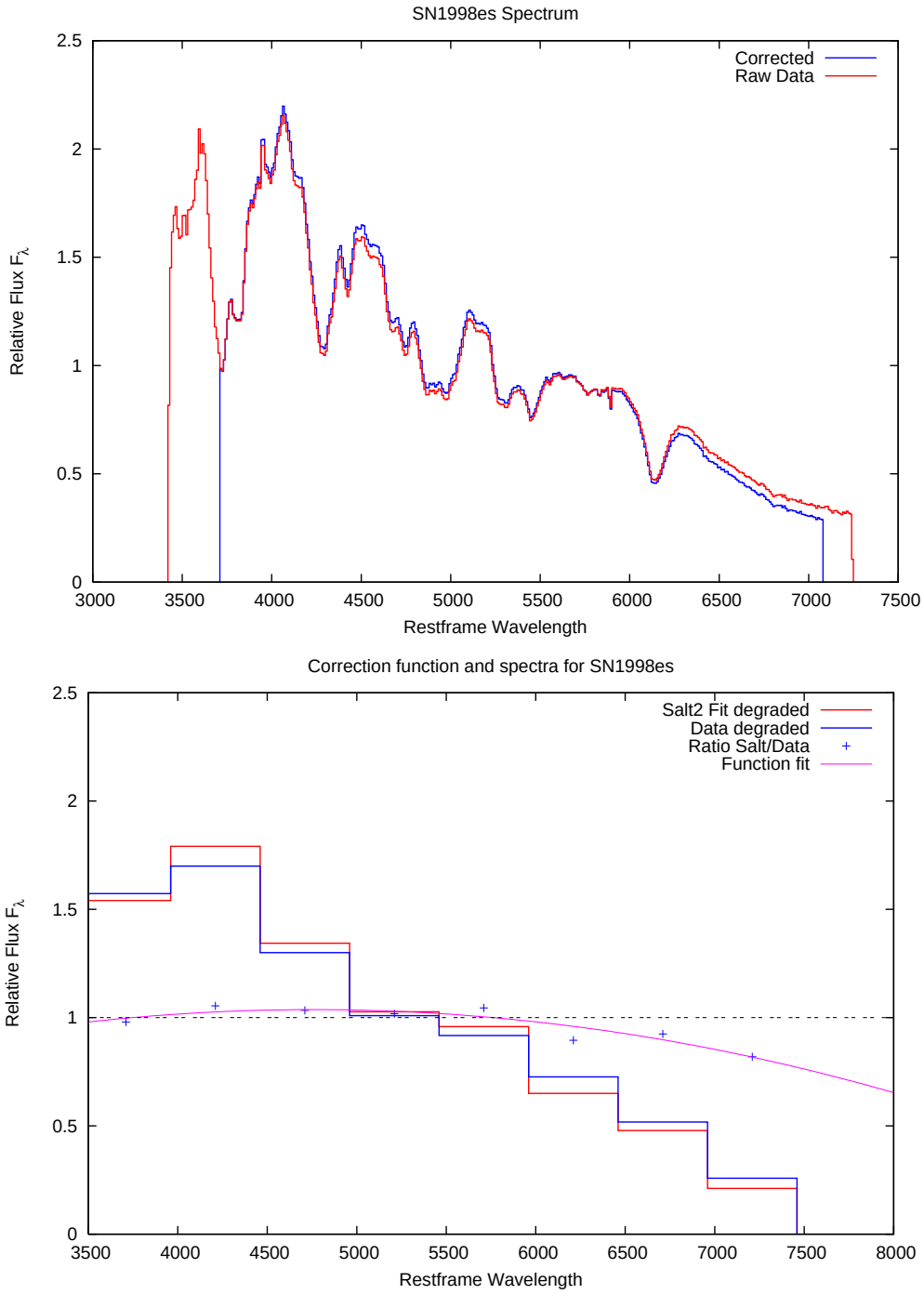

Fig. 36.— SN1998es spectrum before and after warping, as well as the correction function used to warp.

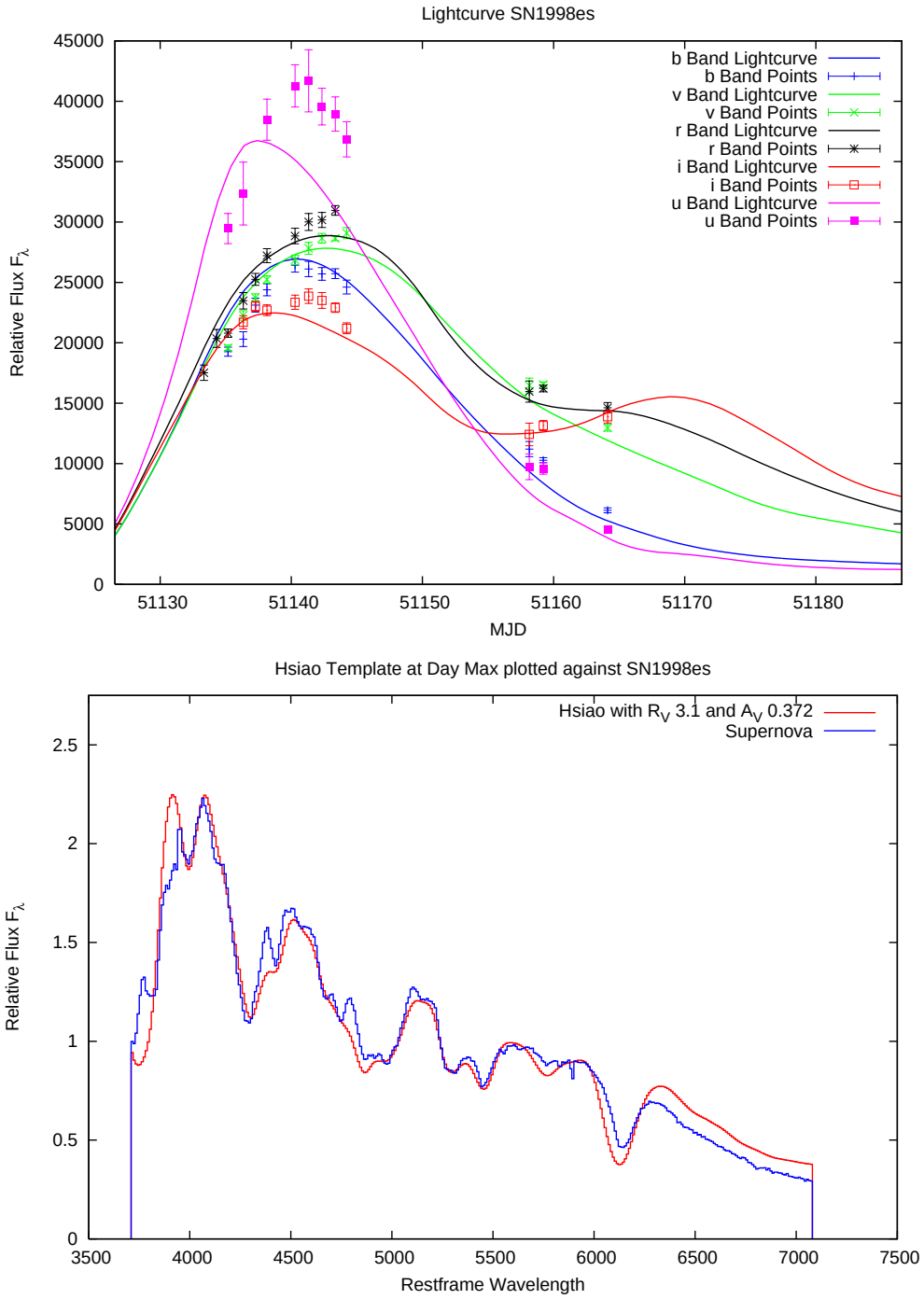

Fig. 37.— SN1998es light curve fit, as well as the best fit for Hsiao template warped using the Cardelli law to match the spectrum.

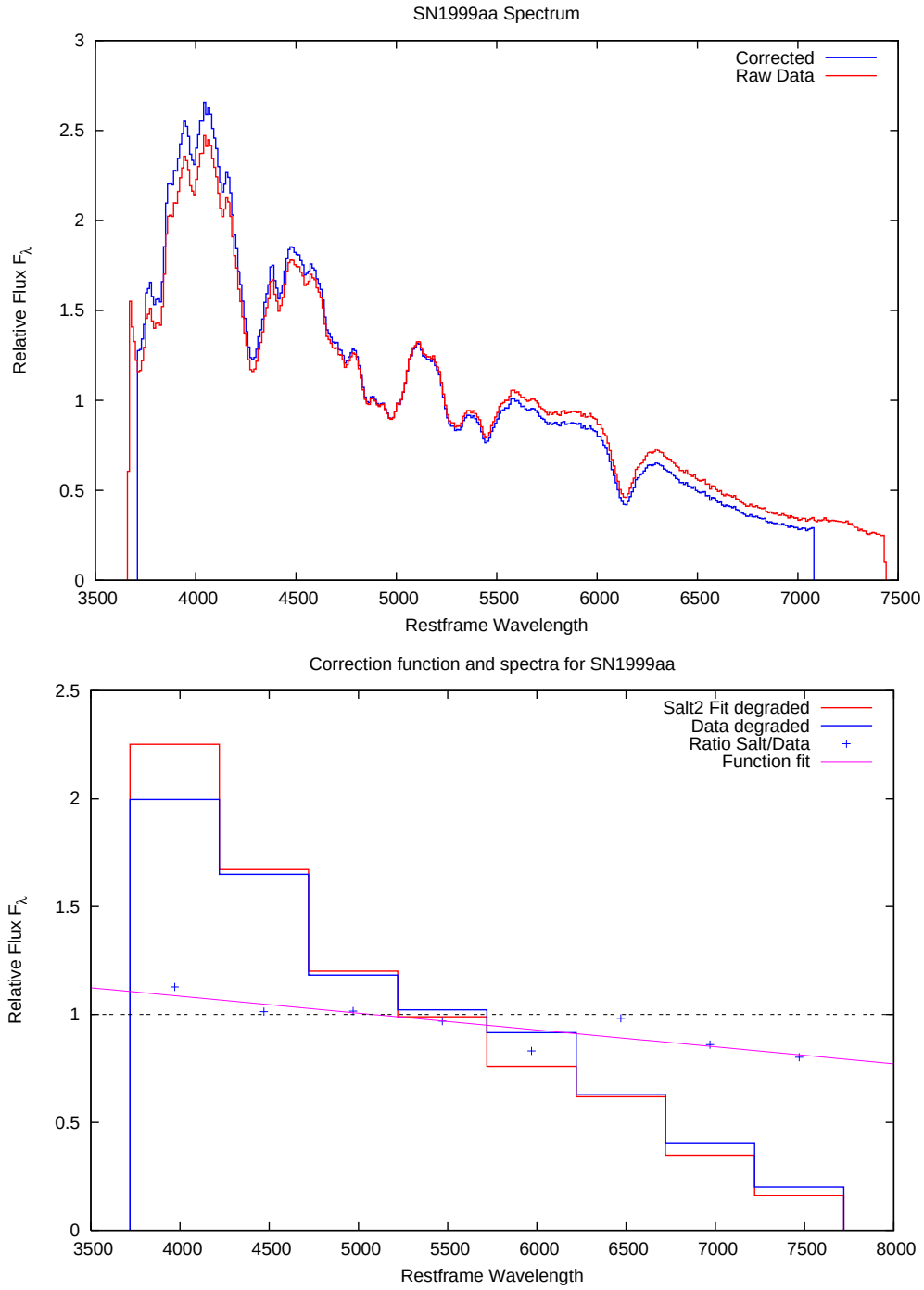

Fig. 38.— SN1999aa spectrum before and after warping, as well as the correction function used to warp.

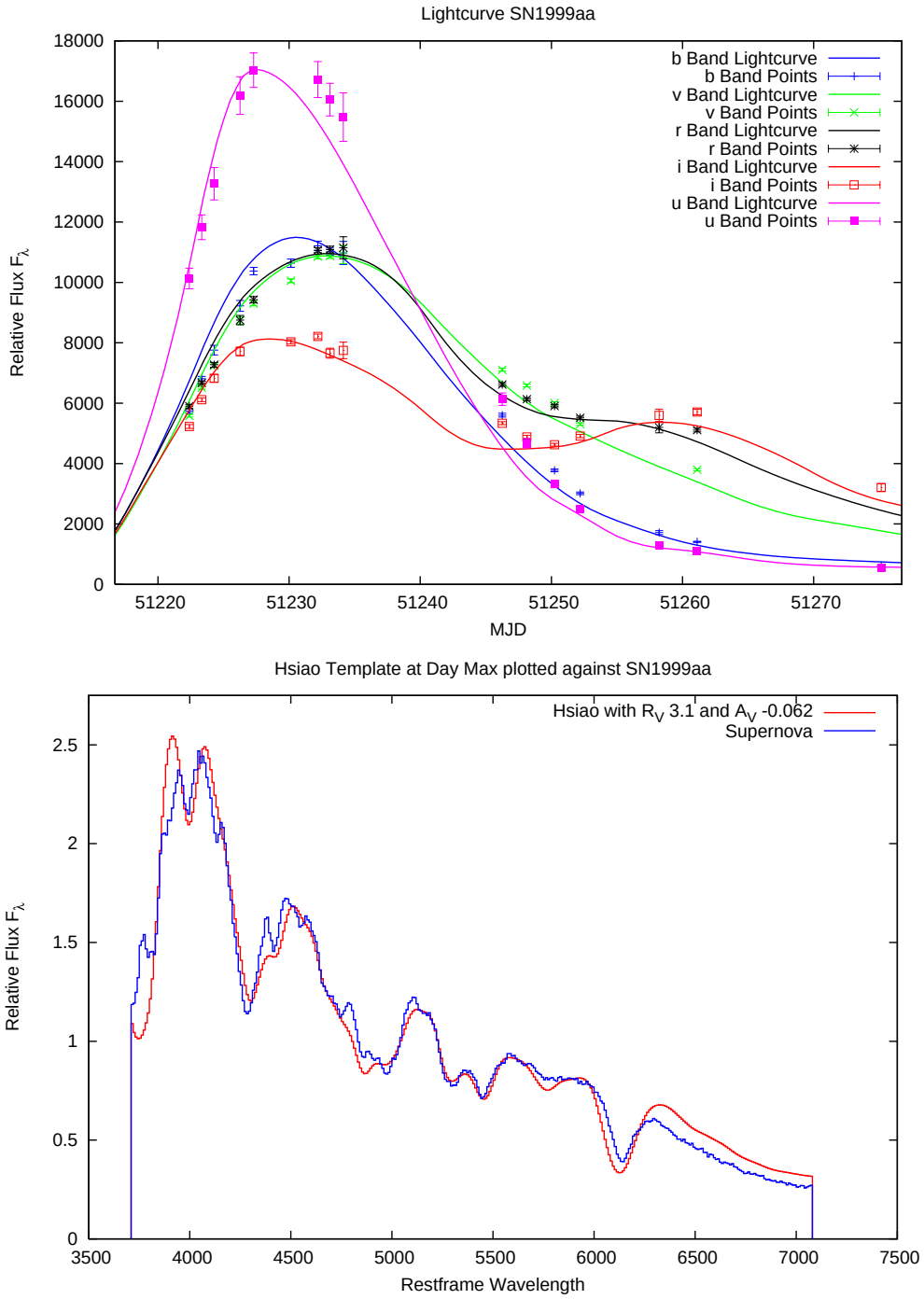

Fig. 39.— SN1999aa light curve fit, as well as the best fit for Hsiao template warped using the Cardelli law to match the spectrum.

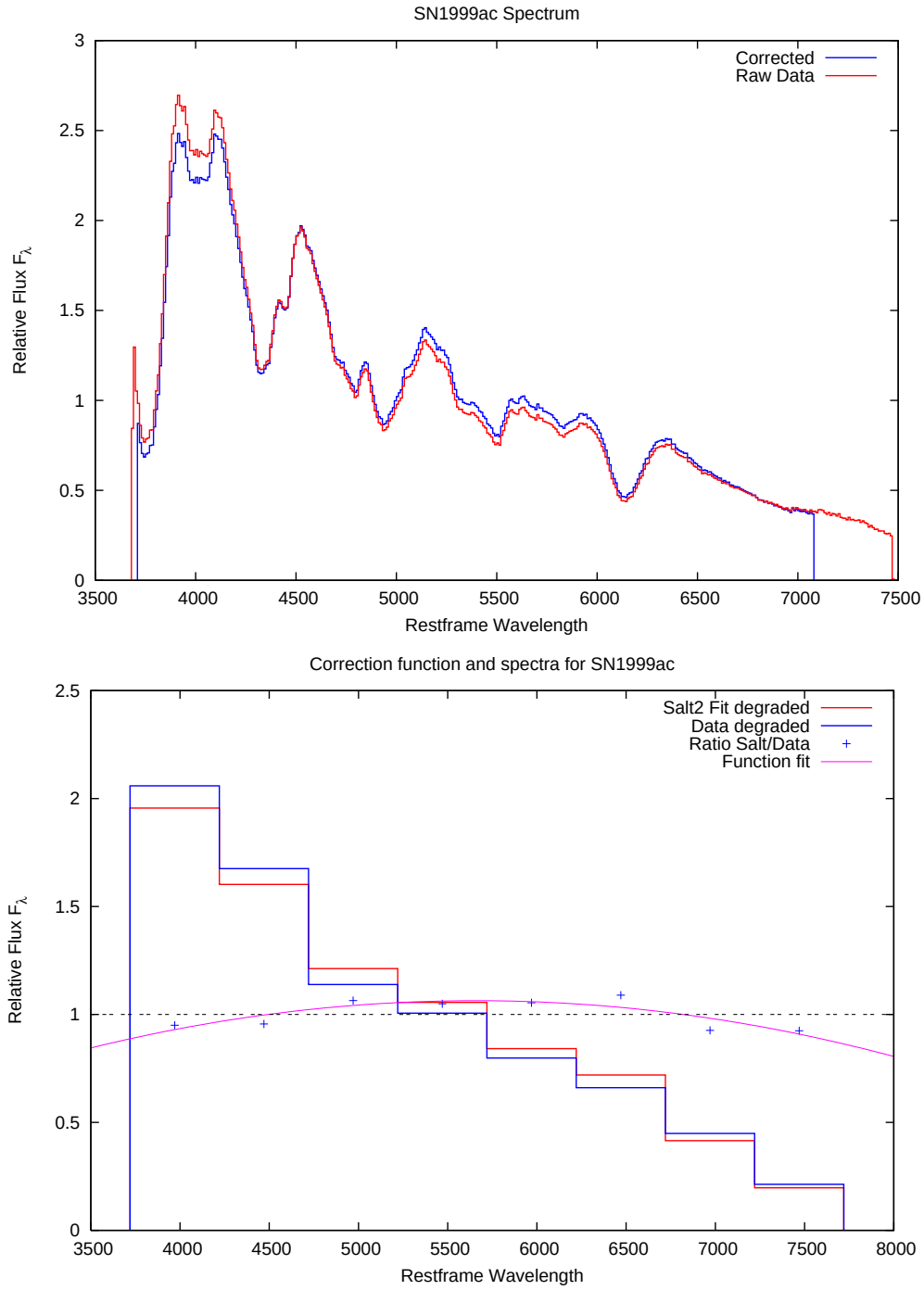

Fig. 40.— SN1999ac spectrum before and after warping, as well as the correction function used to warp.

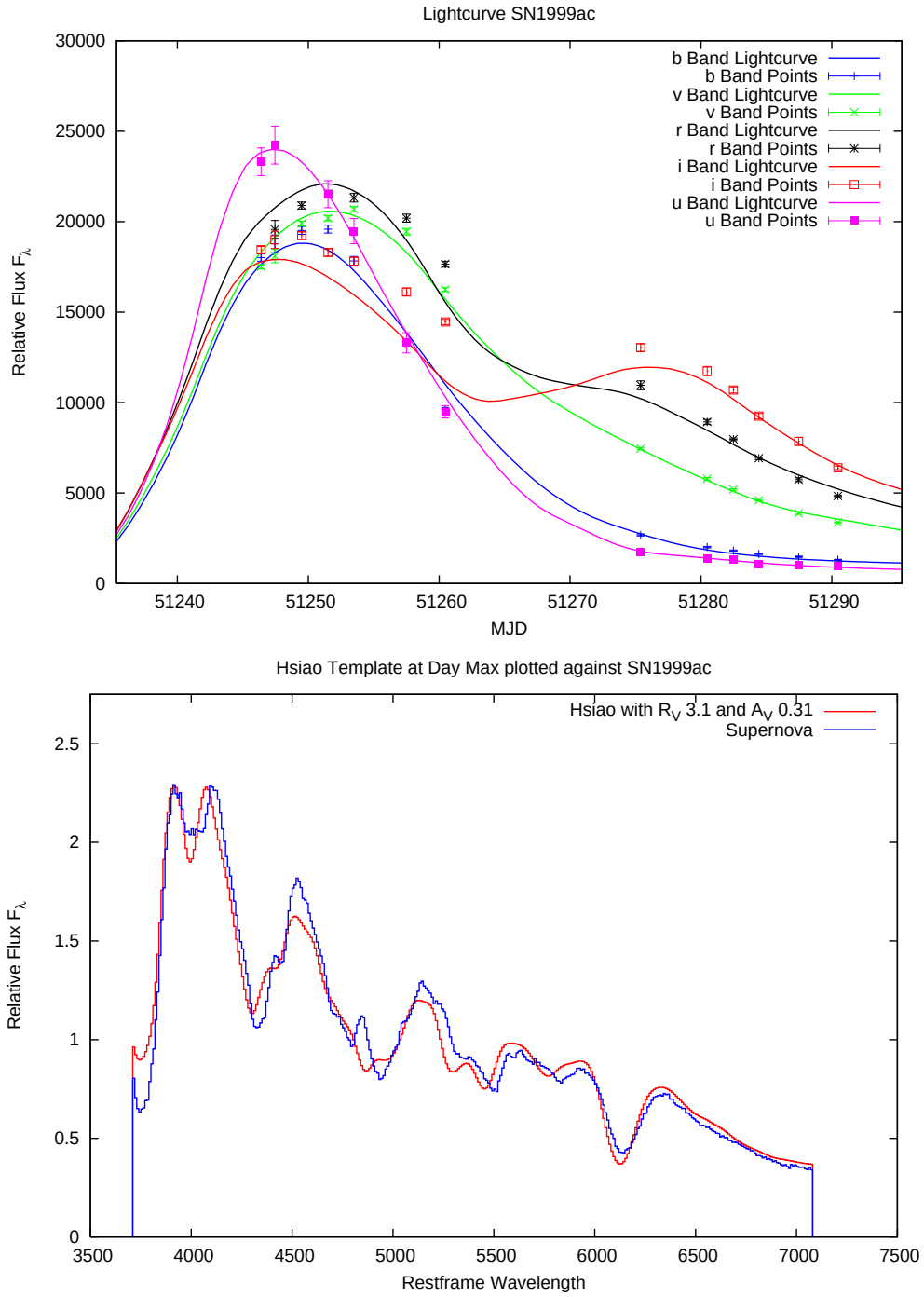

Fig. 41.— SN1999ac light curve fit, as well as the best fit for Hsiao template warped using the Cardelli law to match the spectrum.

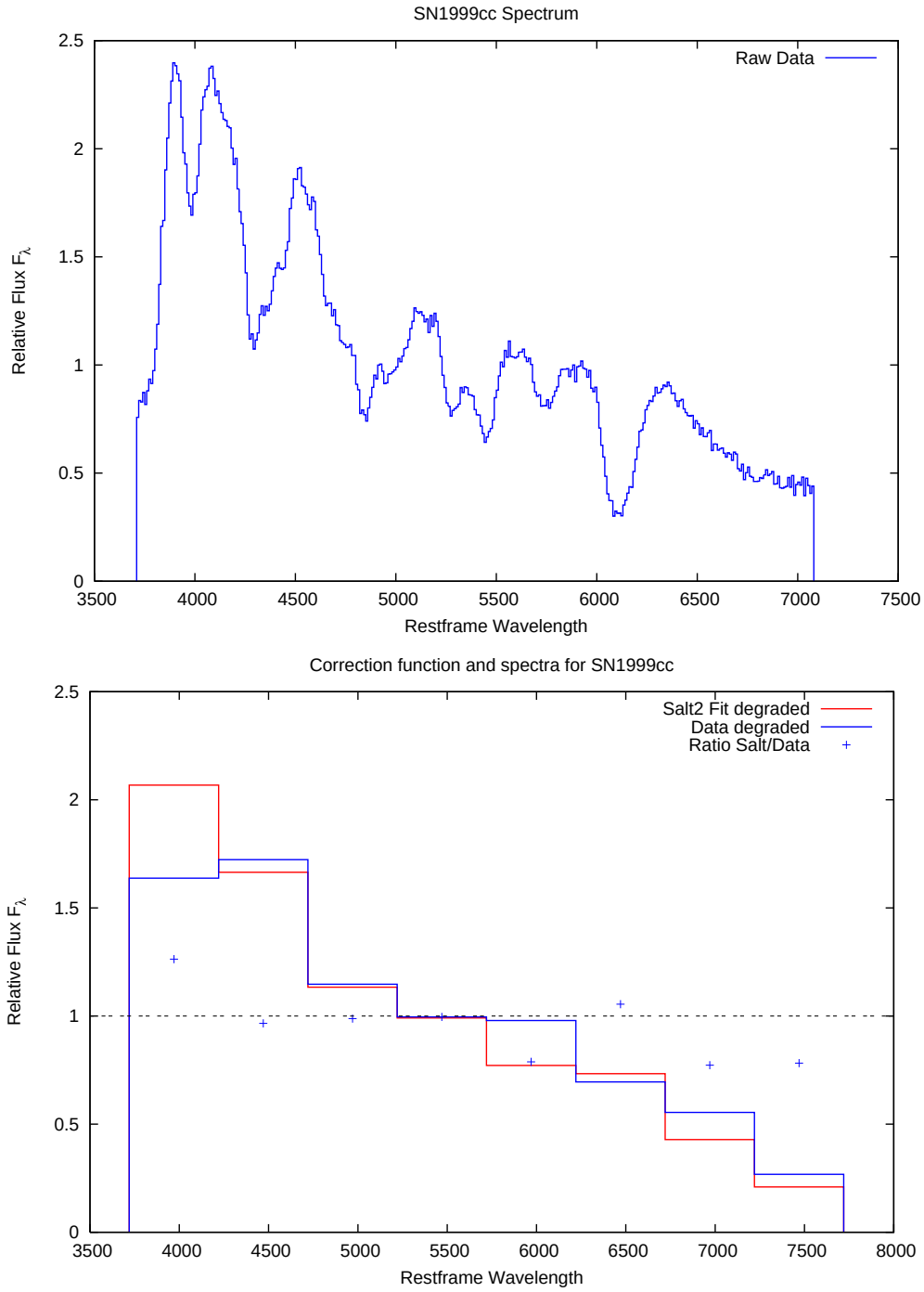

Fig. 42.— SN1999cc spectrum before and after warping, as well as the correction function used to warp.

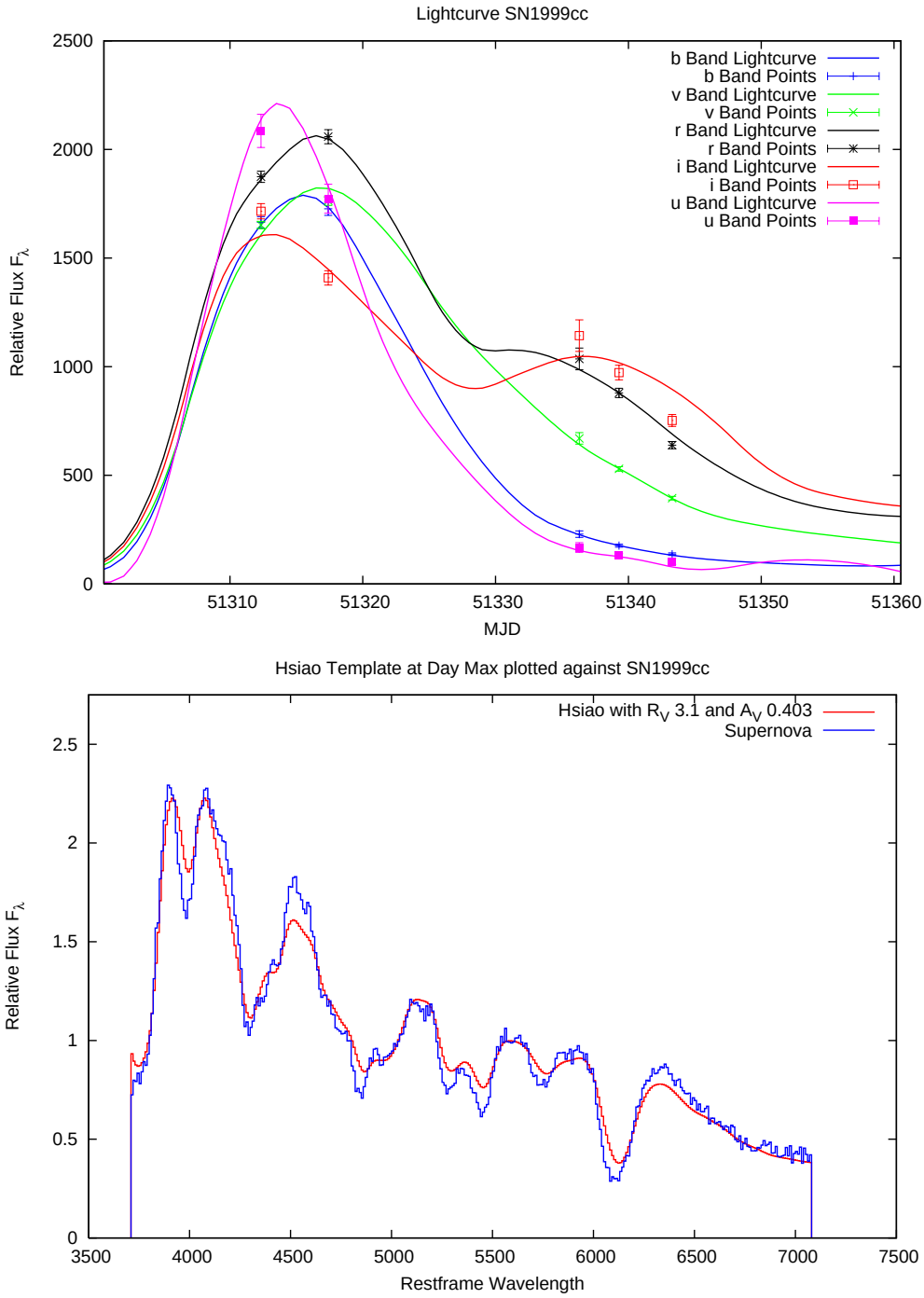

Fig. 43.— SN1999cc light curve fit, as well as the best fit for Hsiao template warped using the Cardelli law to match the spectrum.

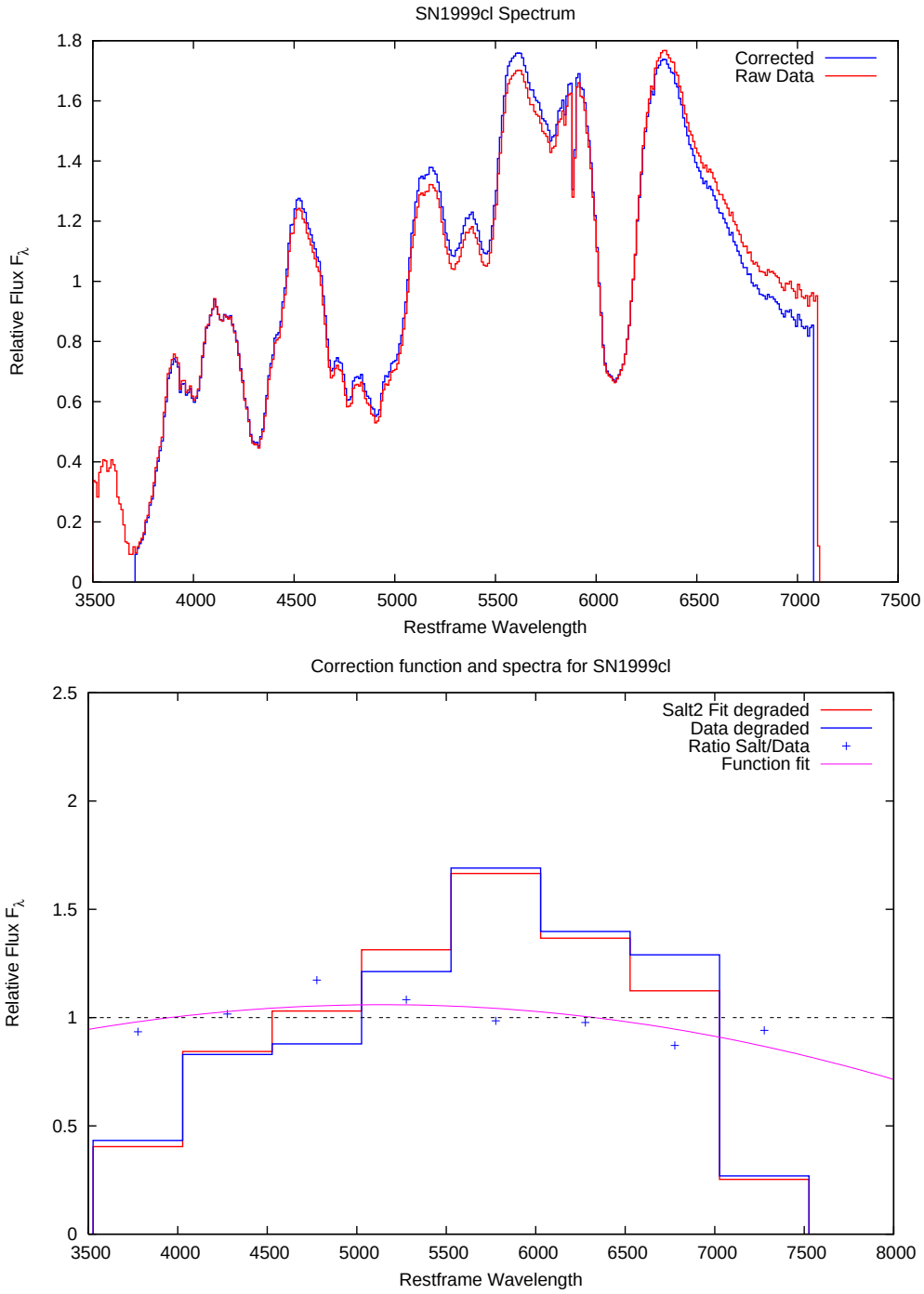

Fig. 44.— SN1999cl spectrum before and after warping, as well as the correction function used to warp.

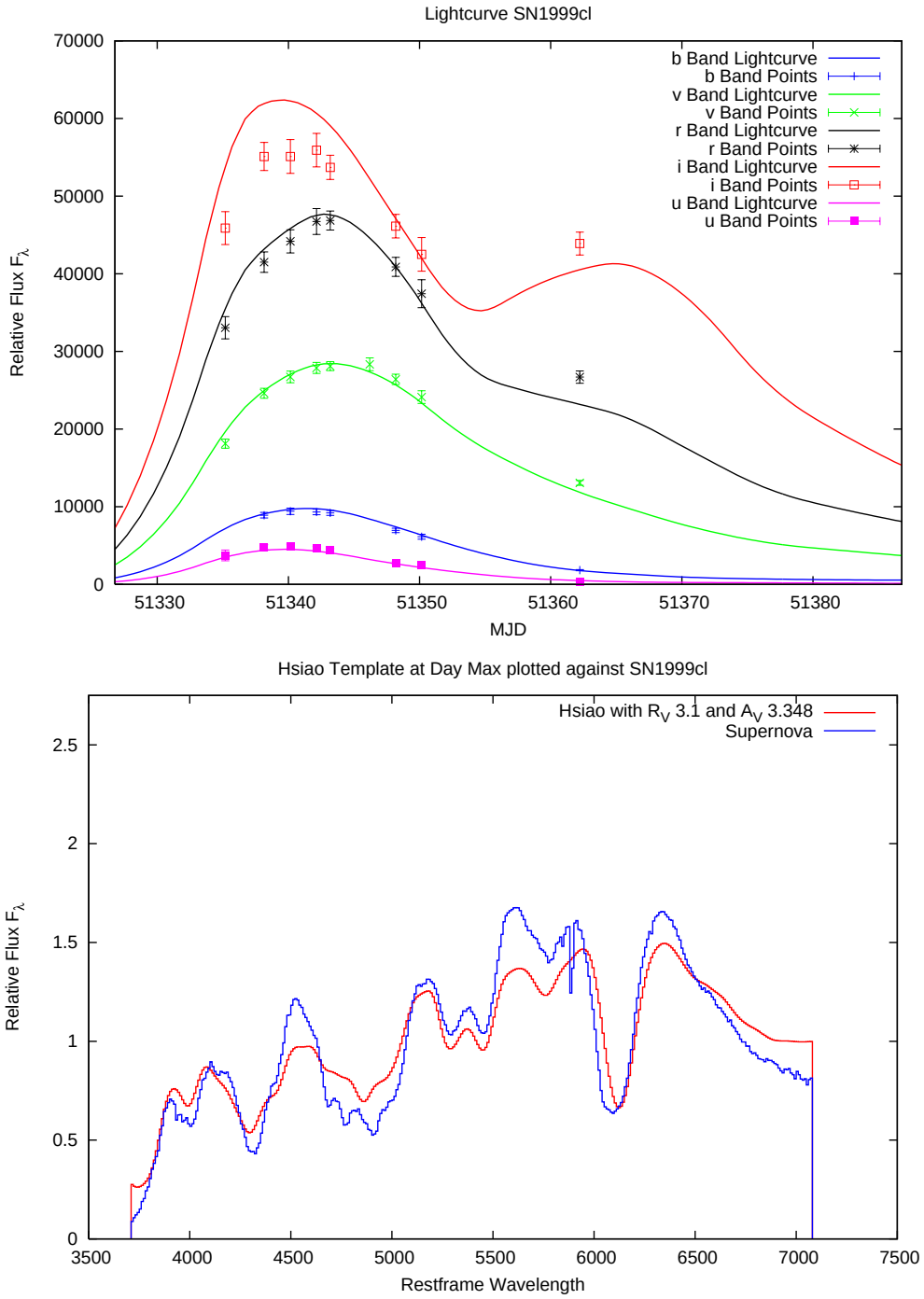

Fig. 45.— SN1999cl light curve fit, as well as the best fit for Hsiao template warped using the Cardelli law to match the spectrum.

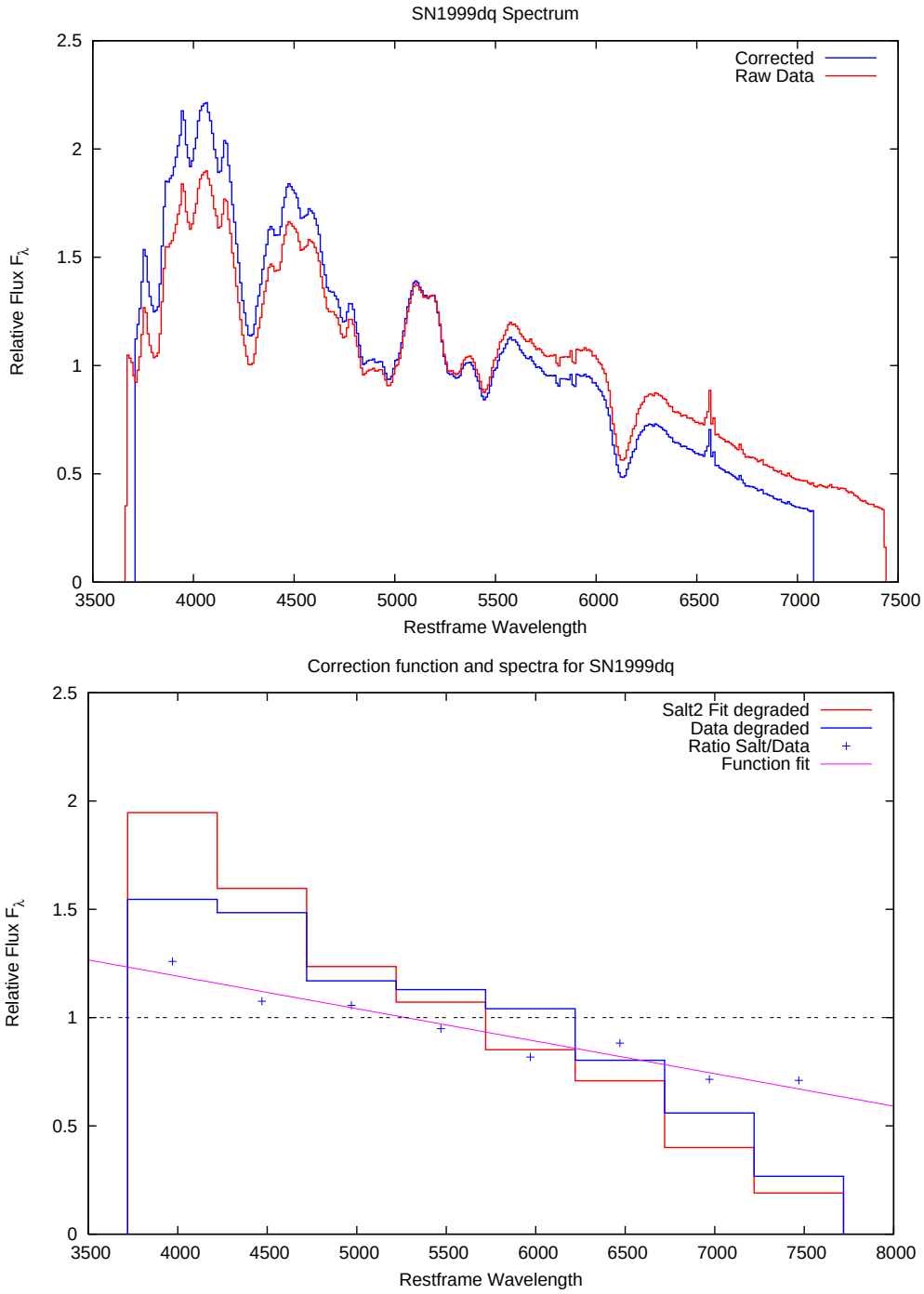

Fig. 46.— SN1999dq spectrum before and after warping, as well as the correction function used to warp.

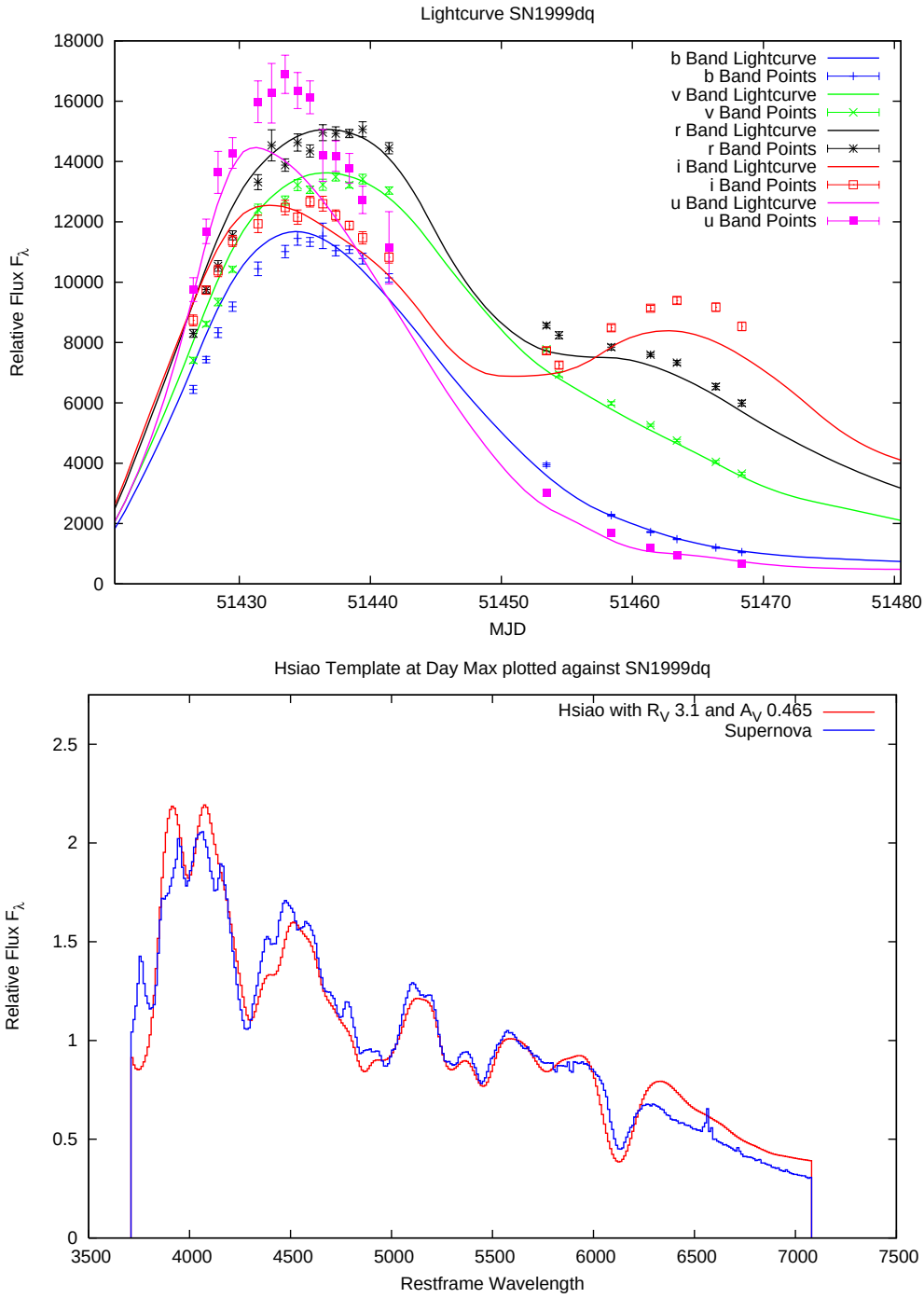

Fig. 47.— SN1999dq light curve fit, as well as the best fit for Hsiao template warped using the Cardelli law to match the spectrum.

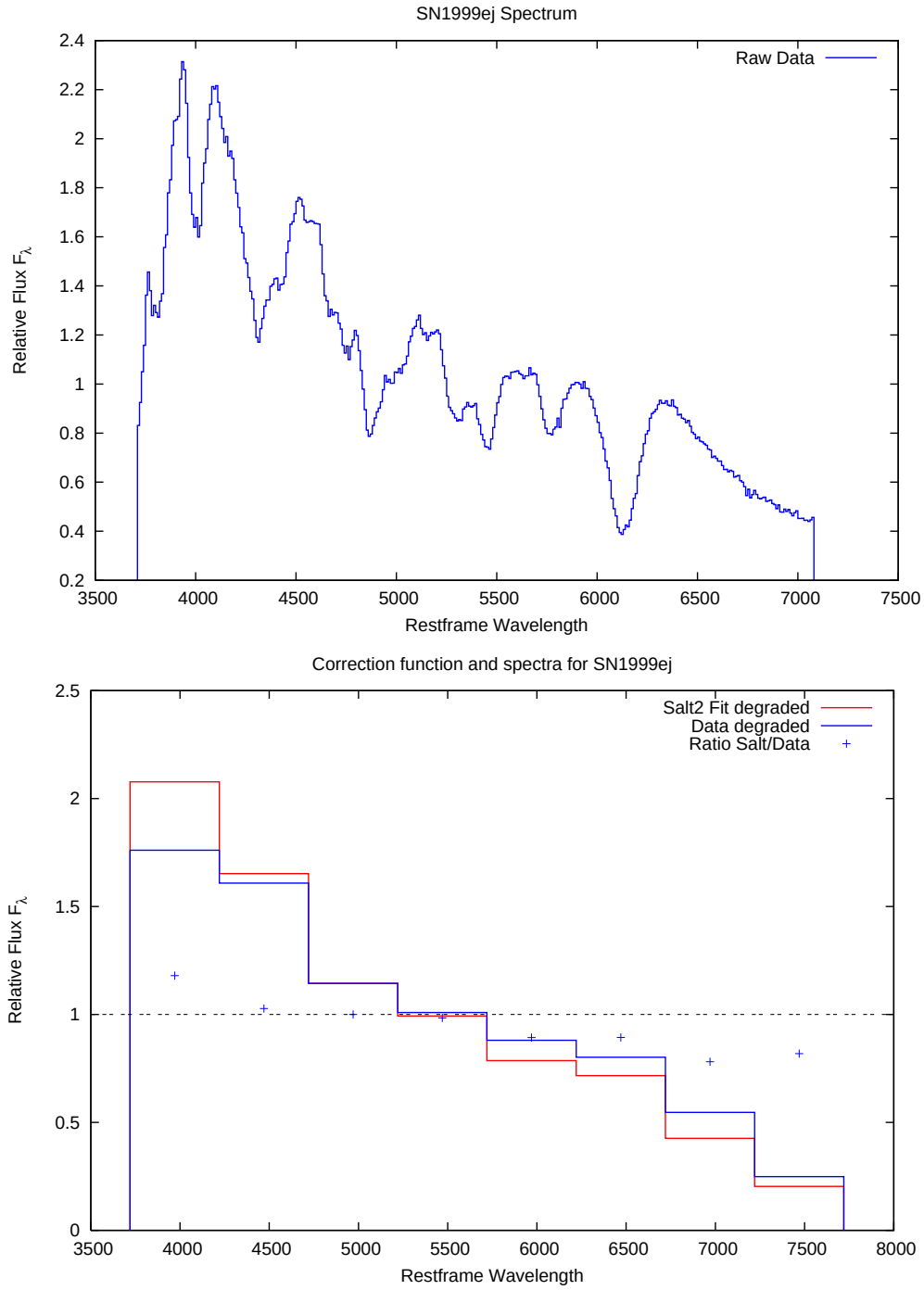

Fig. 48.— SN1999ej spectrum before and after warping, as well as the correction function used to warp.

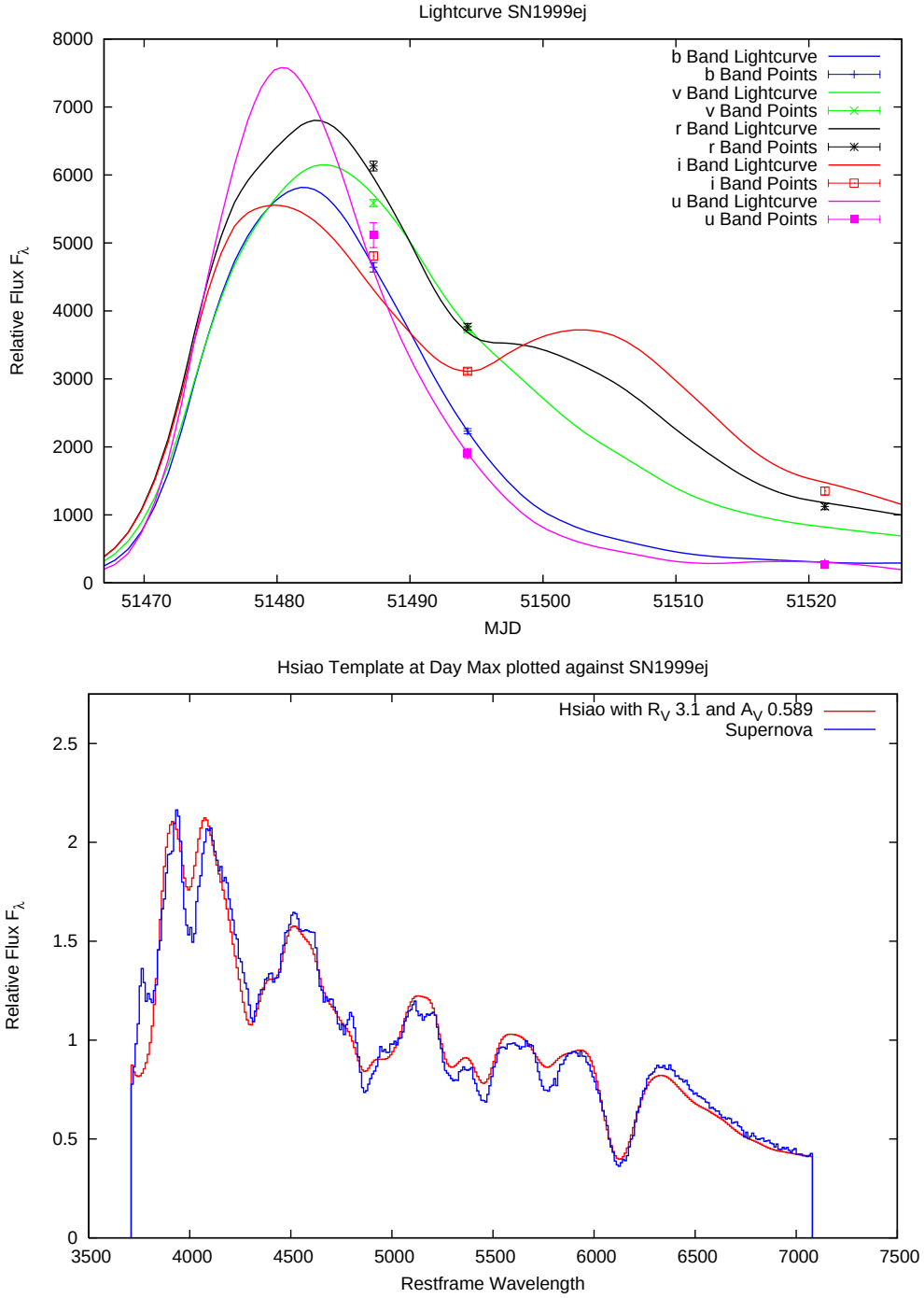

Fig. 49.— SN1999ej light curve fit, as well as the best fit for Hsiao template warped using the Cardelli law to match the spectrum.

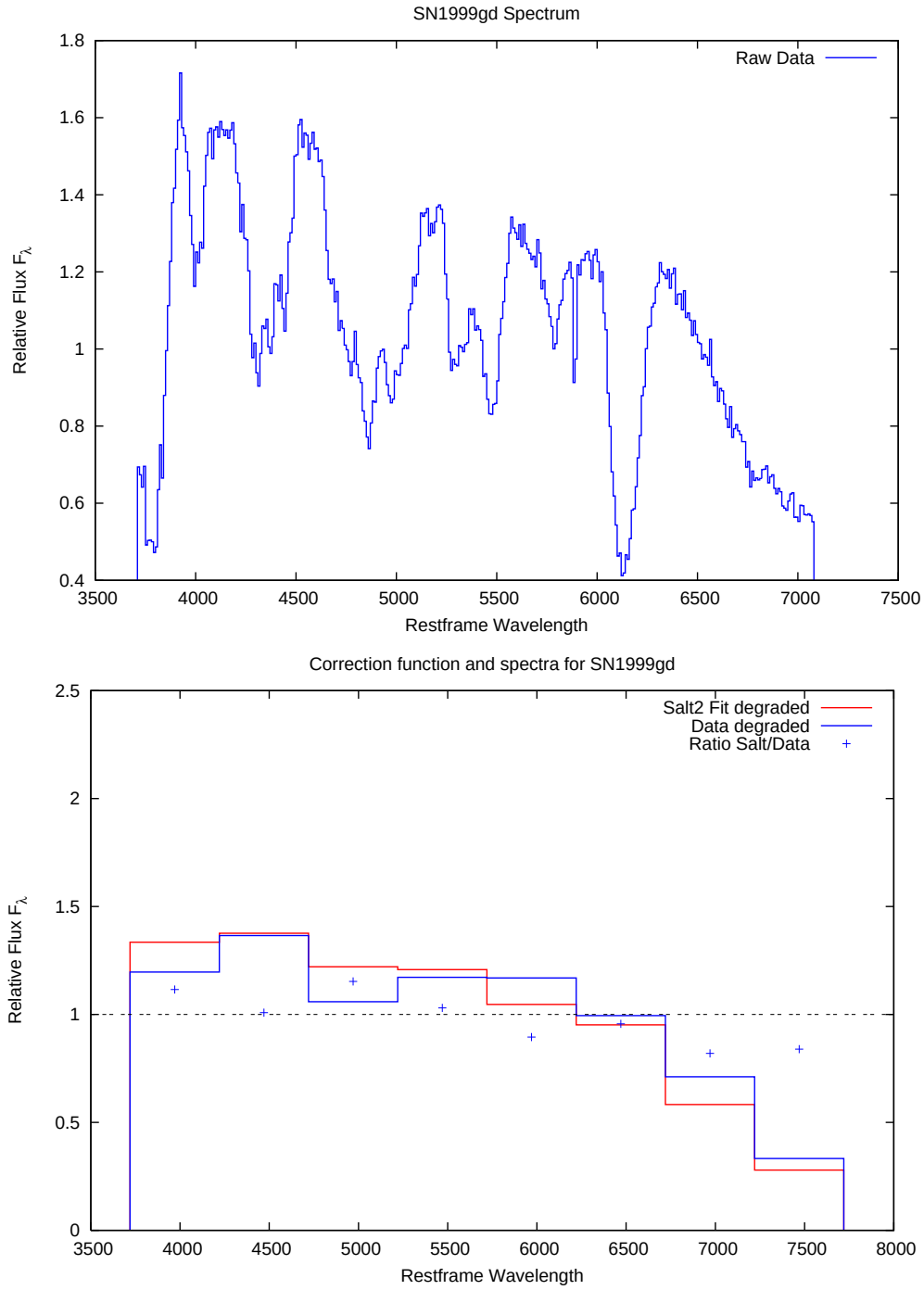

Fig. 50.— SN1999gd spectrum before and after warping, as well as the correction function used to warp.

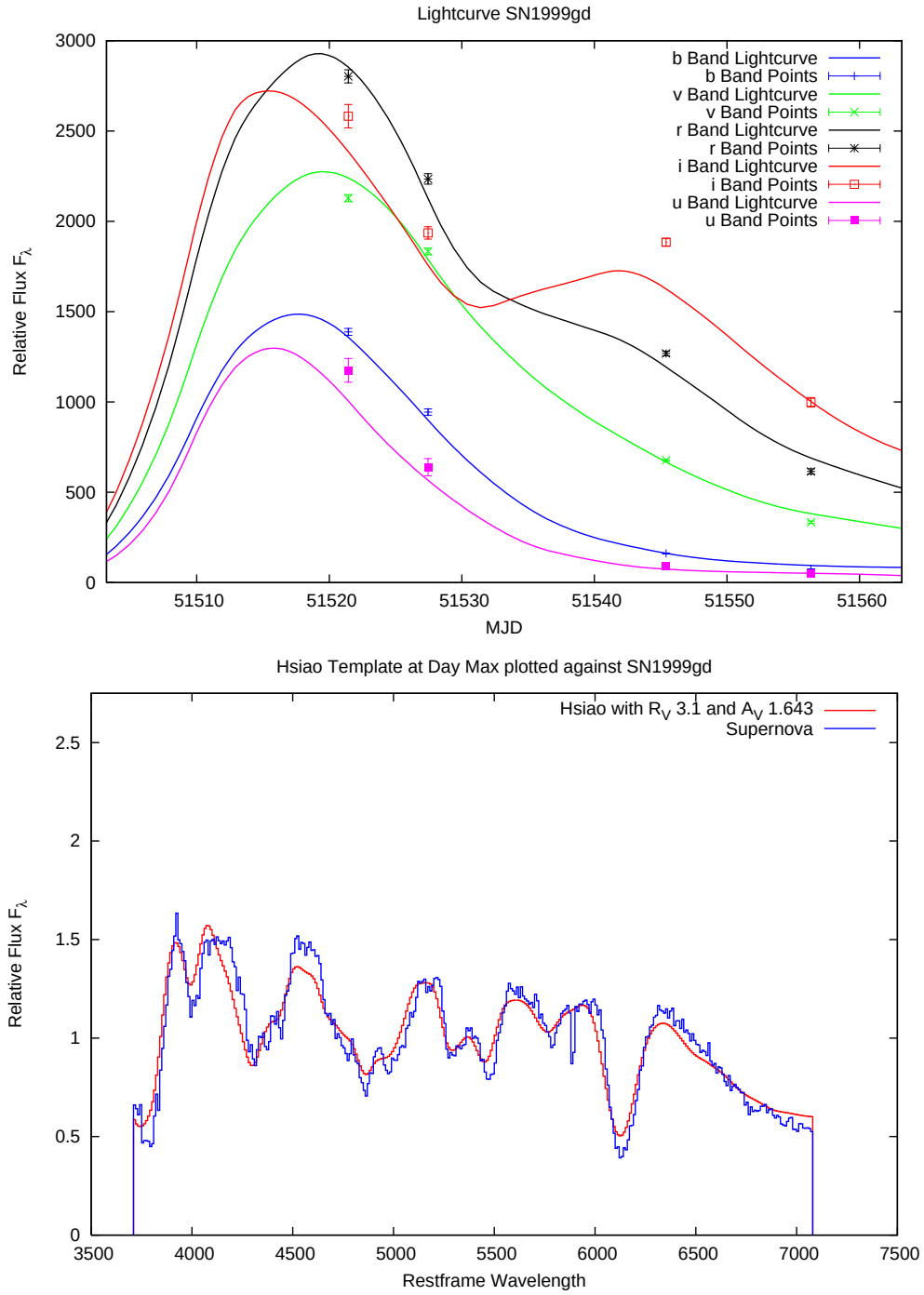

Fig. 51.— SN1999gd light curve fit, as well as the best fit for Hsiao template warped using the Cardelli law to match the spectrum.

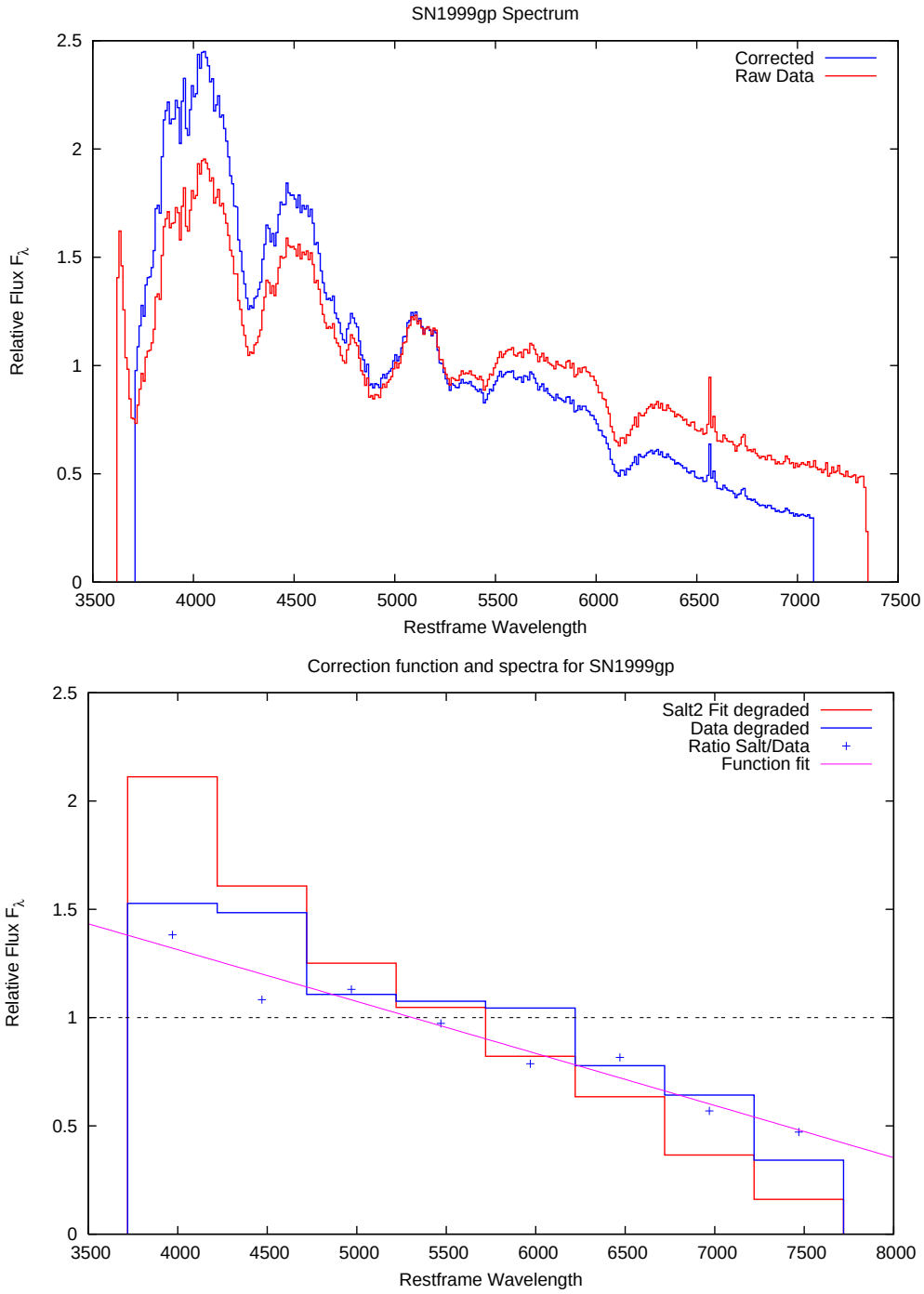

Fig. 52.— SN1999gp spectrum before and after warping, as well as the correction function used to warp.

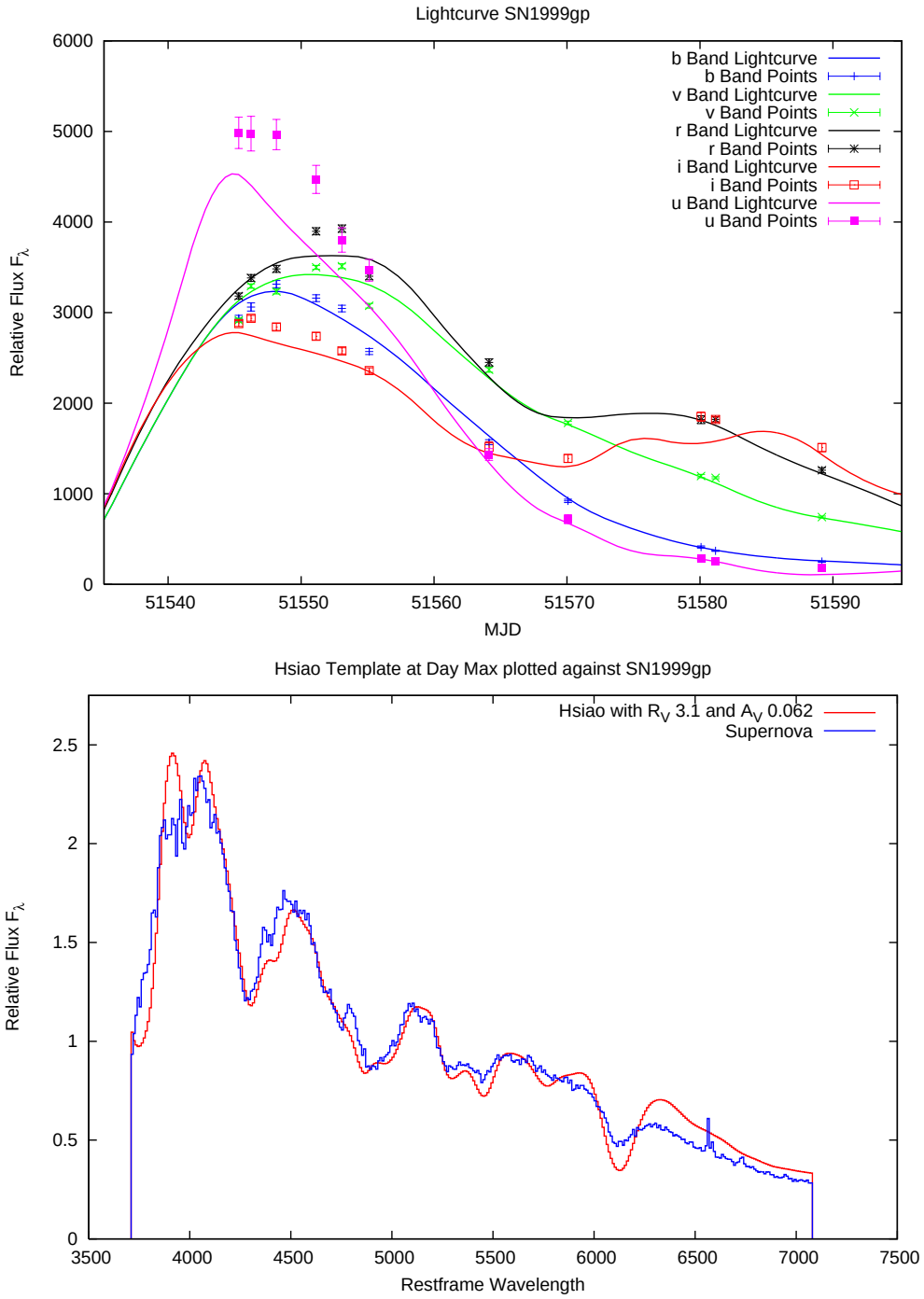

Fig. 53.— SN1999gp light curve fit, as well as the best fit for Hsiao template warped using the Cardelli law to match the spectrum.

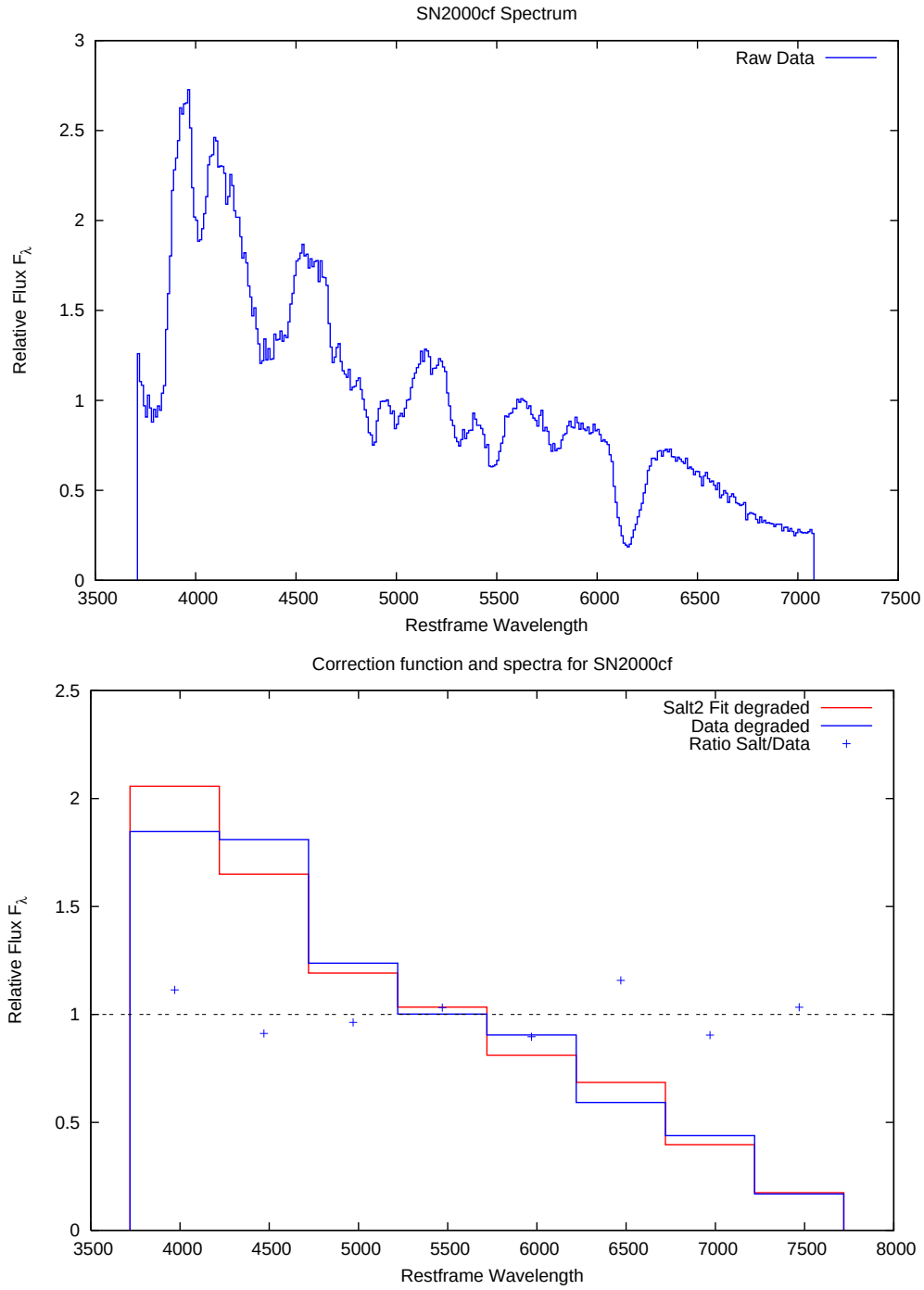

Fig. 54.— SN2000cf spectrum before and after warping, as well as the correction function used to warp.

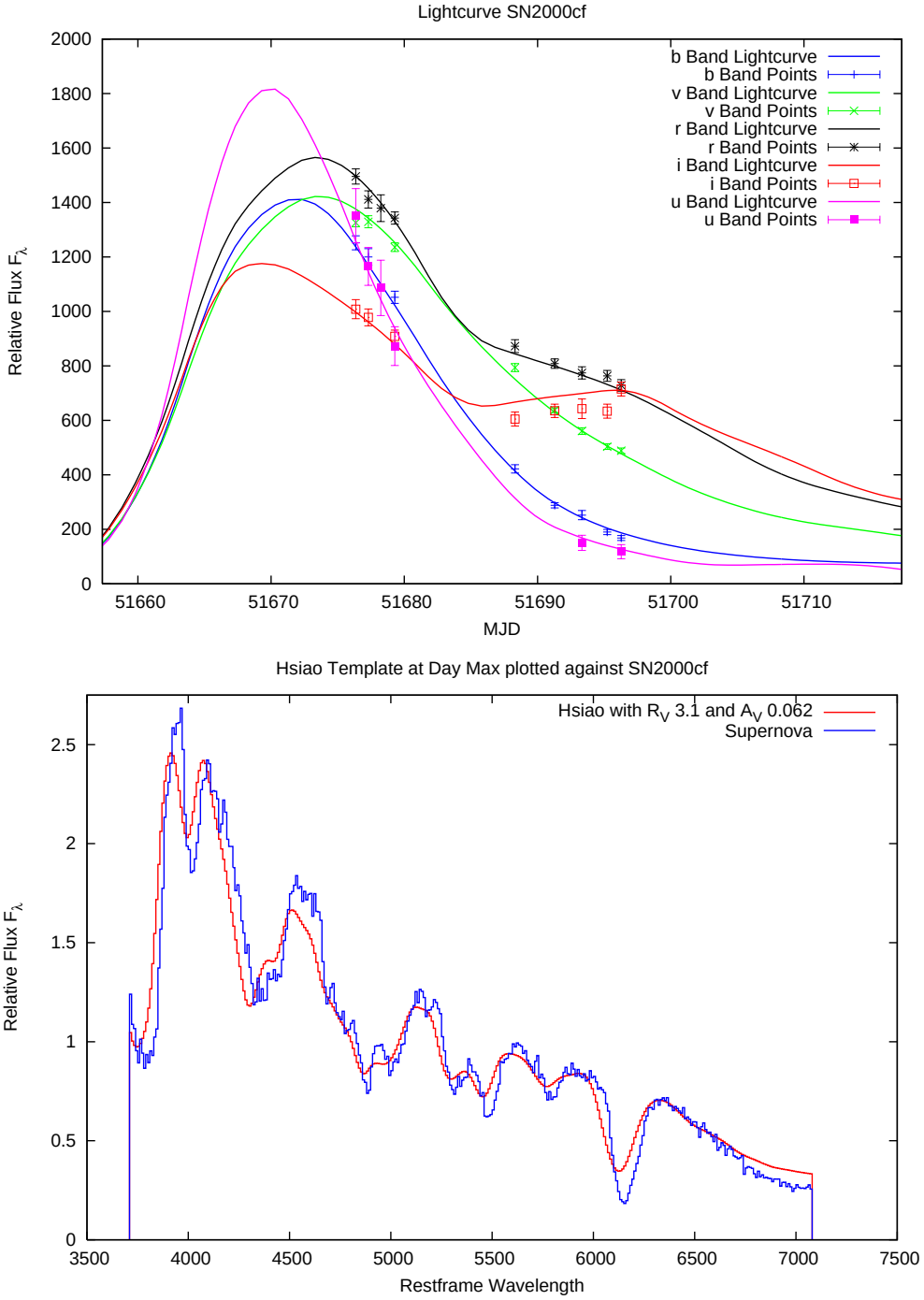

Fig. 55.— SN2000cf light curve fit, as well as the best fit for Hsiao template warped using the Cardelli law to match the spectrum.

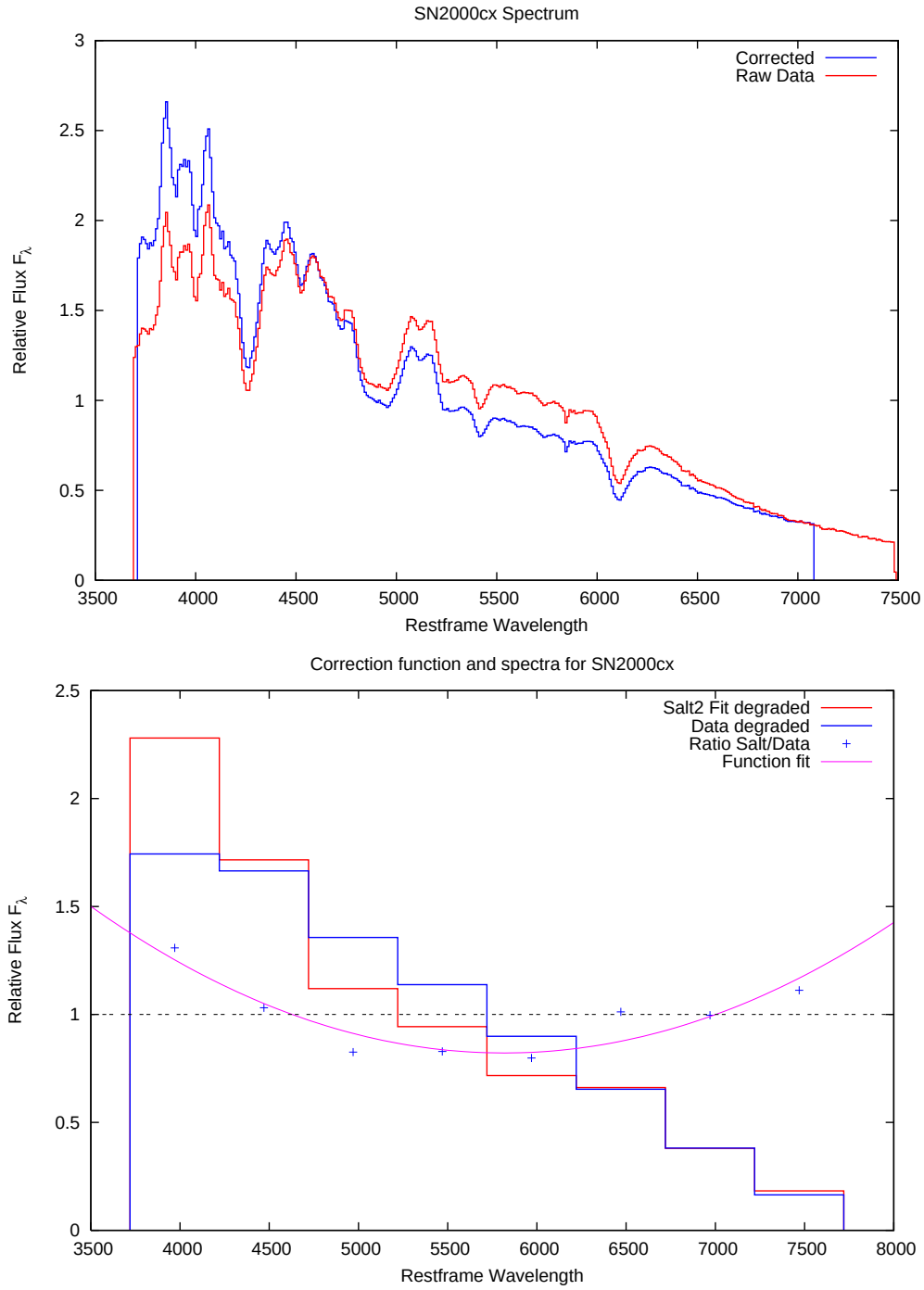

Fig. 56.— SN2000cx spectrum before and after warping, as well as the correction function used to warp.

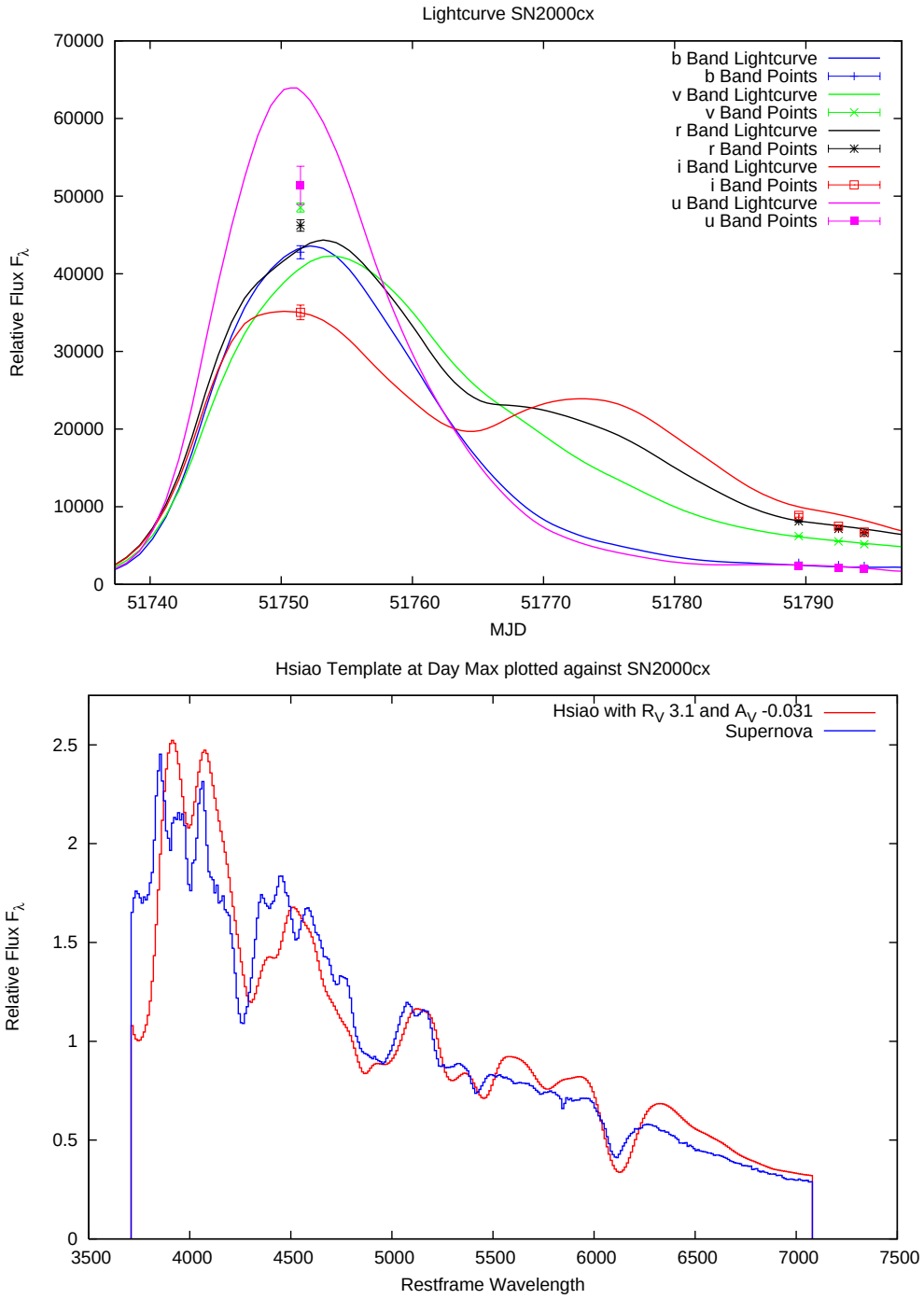

Fig. 57.— SN2000cx light curve fit, as well as the best fit for Hsiao template warped using the Cardelli law to match the spectrum.

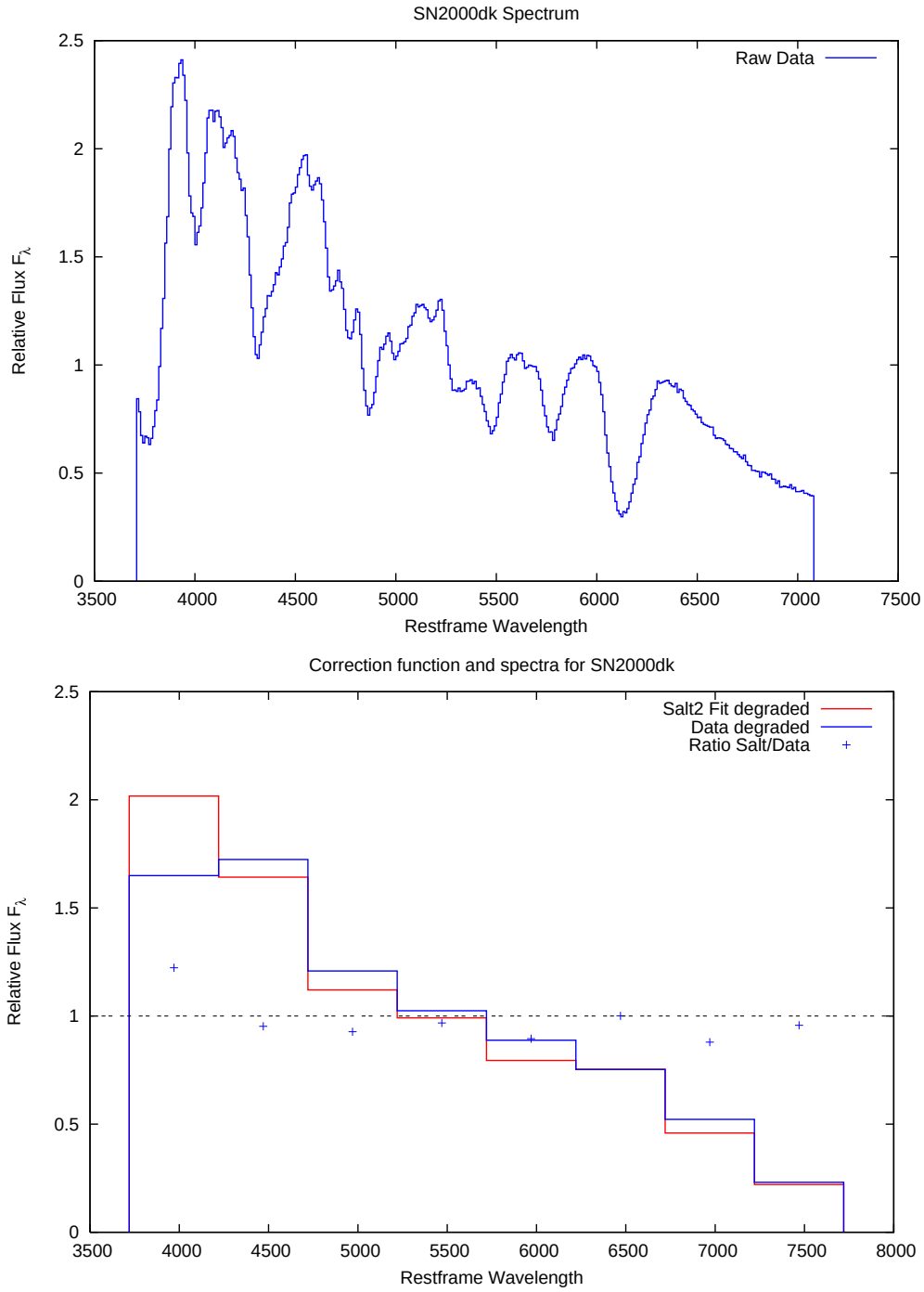

Fig. 58.— SN2000dk spectrum before and after warping, as well as the correction function used to warp.

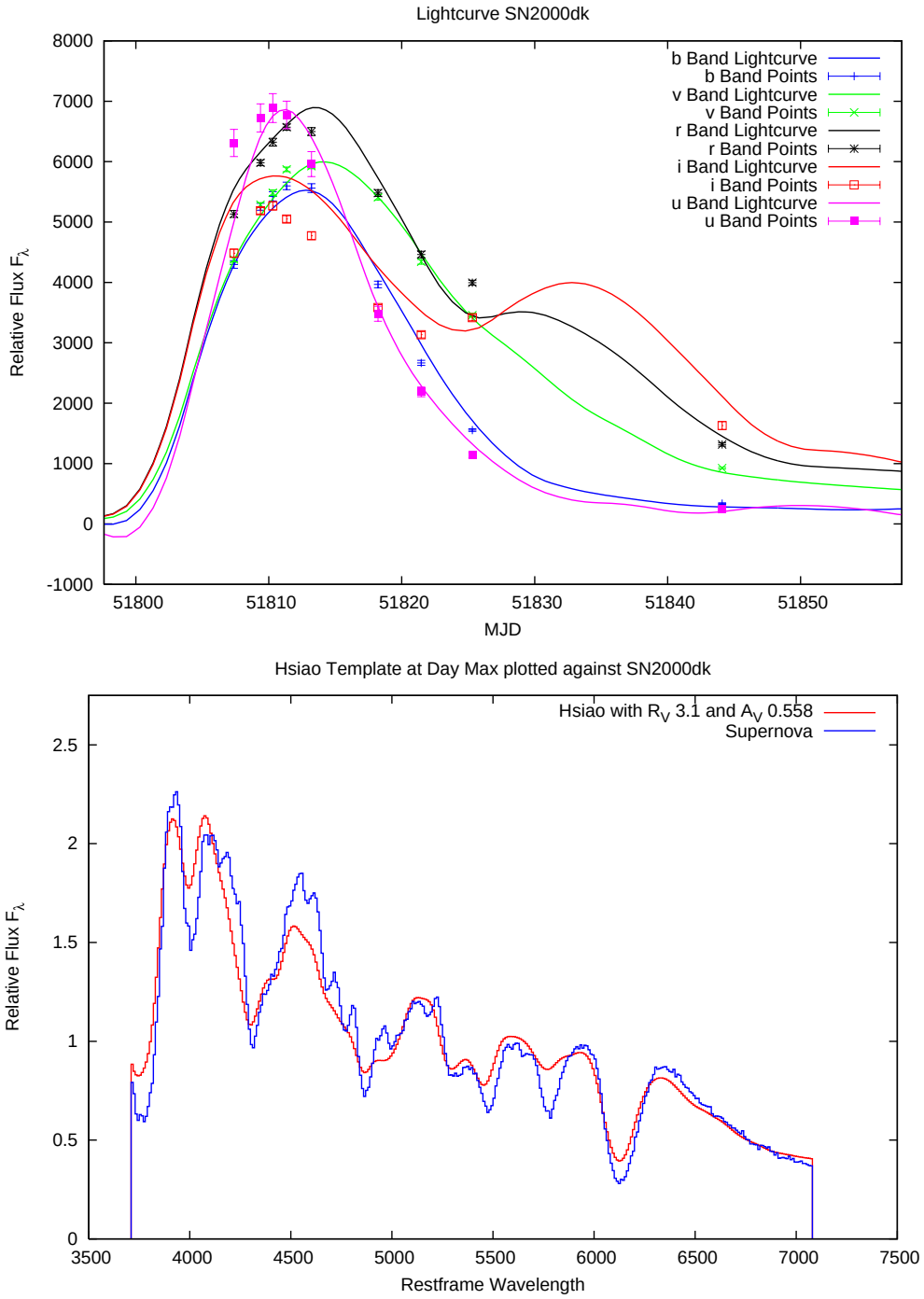

Fig. 59.— SN2000dk light curve fit, as well as the best fit for Hsiao template warped using the Cardelli law to match the spectrum.

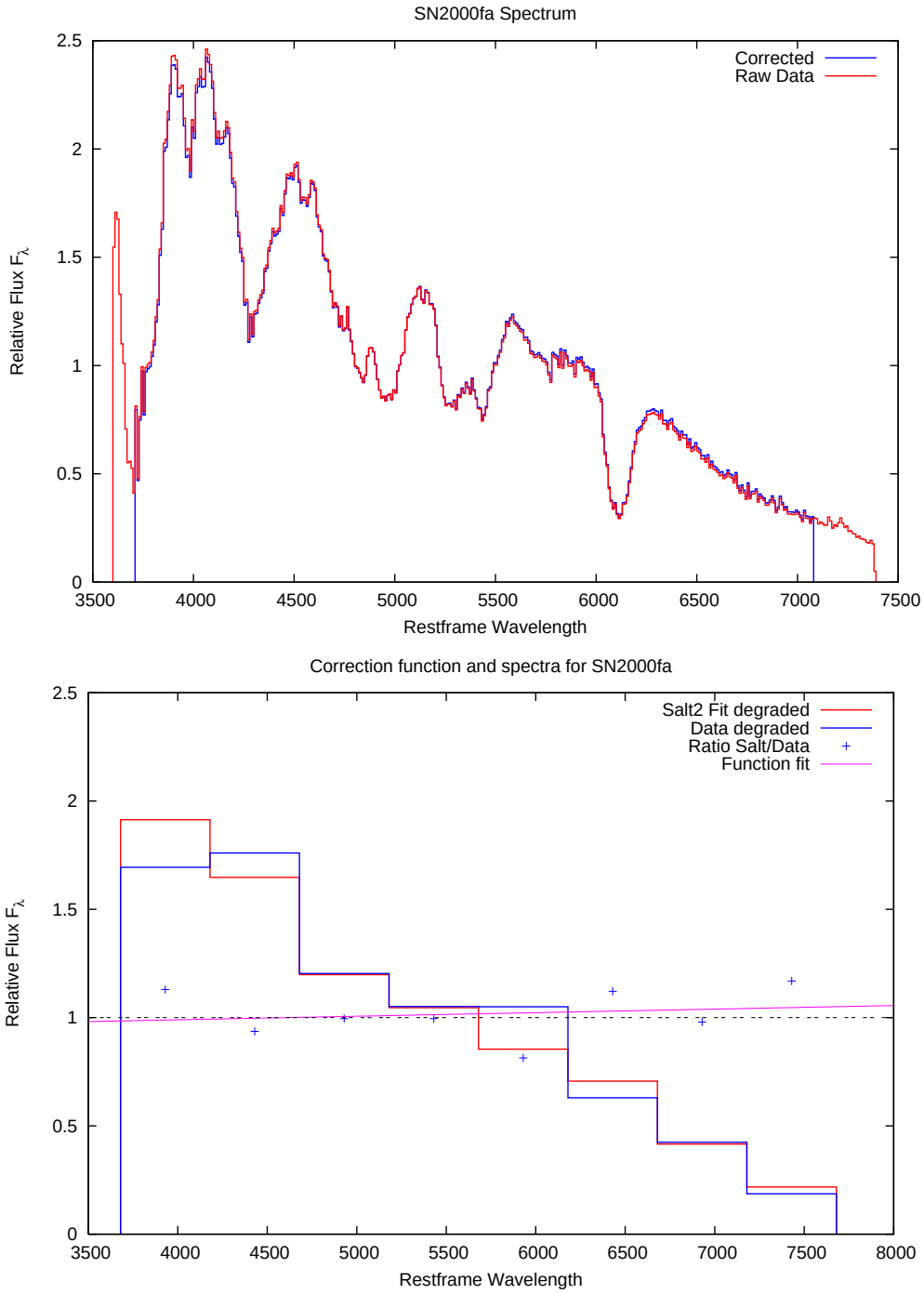

Fig. 60.— SN2000fa spectrum before and after warping, as well as the correction function used to warp.

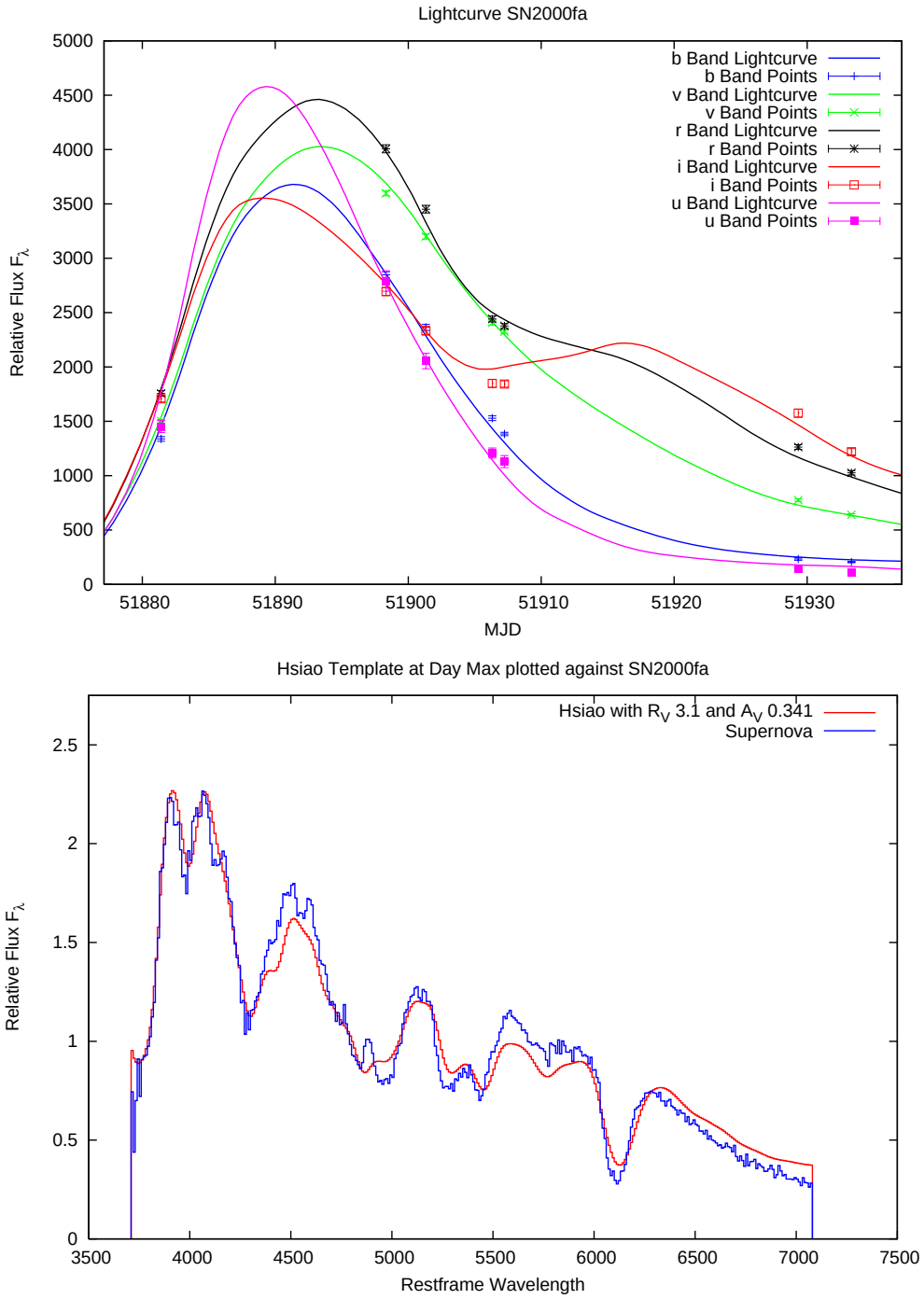

Fig. 61.— SN2000fa light curve fit, as well as the best fit for Hsiao template warped using the Cardelli law to match the spectrum.

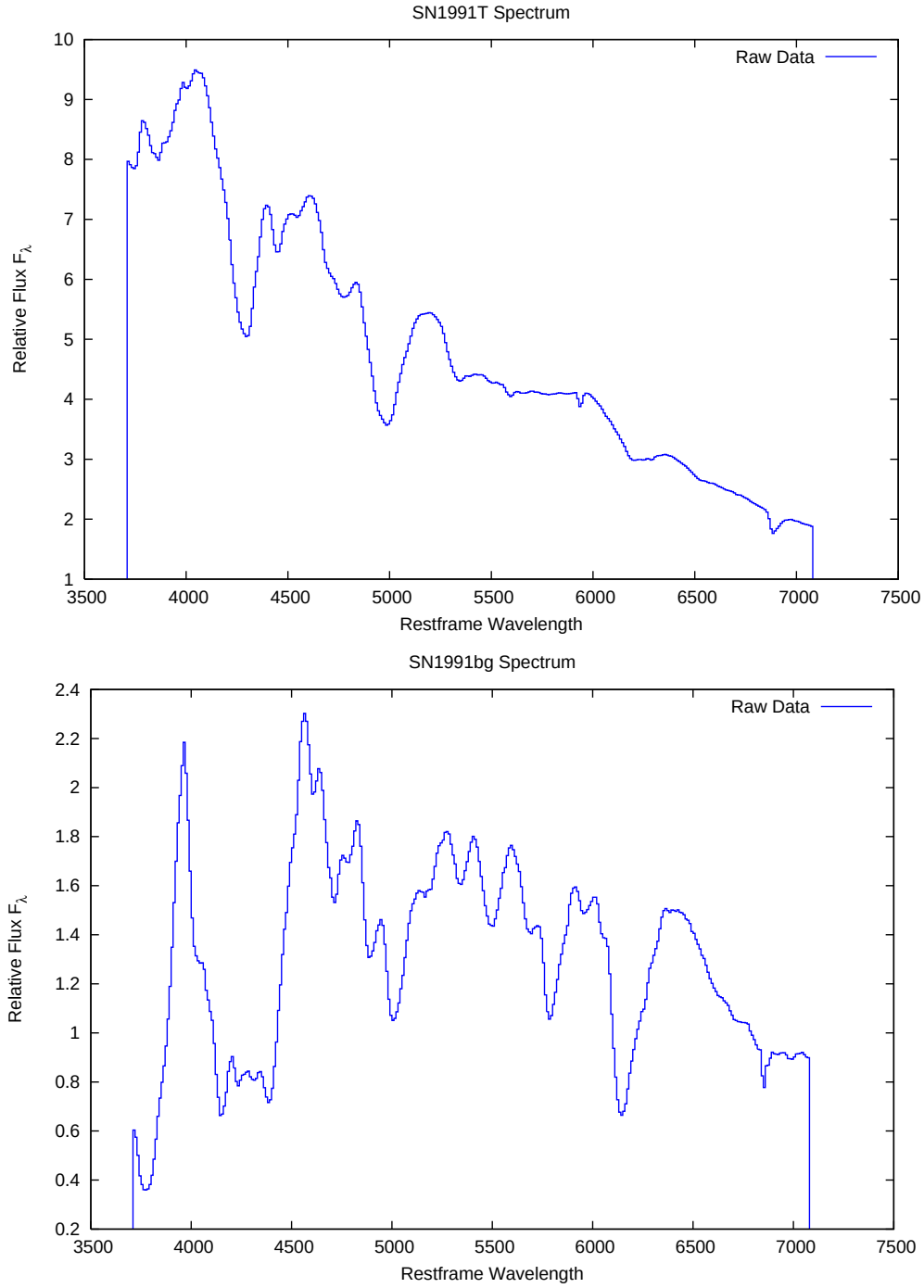

Fig. 62.— SN1991T Spectrum and SN1991bg Spectrum.